NASA TECHNICAL MEMORANDUM

NASA TM X-73,140

NASA TM X-73,140

SIMULATION AND MODELING OF THE DEEP SPACE RECEIVER INTERACTION WITH CHANNEL DECODING PERFORMANCE

Harry W. Jones, Jr.

Ames Research Center
Moffett Field, California 94035

July 1976

1. Report No.	2. Government Accession No.	3. Recipient's Catalog No.
NASA TM X-73,140		

4. Title and Subtitle	5. Report Date
SIMULATION AND MODELING OF THE DEEP SPACE RECEIVER INTERACTION WITH CHANNEL DECODING PERFORMANCE	6. Performing Organization Code
7. Author(s)	8. Performing Organization Report No.
Harry W. Jones, Jr.	A-6620
	10. Work Unit No. 650-60-10
9. Performing Organization Name and Address	11. Contract or Grant No.
Ames Research Center Moffett Field, California 94035	
	13. Type of Report and Period Covered
12. Sponsoring Agency Name and Address	Technical Memorandum
National Aeronautics and Space Administration Washington, D. C. 20546	14. Sponsoring Agency Code

15. Supplementary Notes

16. Abstract

Computer models were developed in an attempt to reproduce the sequential decoder computation curve of Deep Space Network (DSN) ground station receivers, by simulation of the binary data output of the gaussian channel with the carrier phaselock loop and the subcarrier demodulator assembly. Simulations were run at bit rates equal to the powers of 2 from 8 to 2048, and agreement with DSN data was generally good above 32 bits per second. Simulation results at data rates of 8, 16, and 32 bits per second did not closely match experimental data. This simulation provides a more accurate prediction of DSN computation lengths than either current mathematical models or simulations without both the subcarrier demodulator and carrier loop.

17. Key Words (Suggested by Author(s))	18. Distribution Statement
Sequential decoding, Deep space network, Phaselock loop	Unlimited STAR Category - 17

19. Security Classif. (of this report)	20. Security Classif. (of this page)	21. No. of Pages	22. Price*
Unclassified	Unclassified	81	$4.75

*For sale by the National Technical Information Service, Springfield, Virginia 22161

SIMULATION AND MODELING OF THE DEEP SPACE RECEIVER INTERACTION WITH CHANNEL DECODING PERFORMANCE

Harry W. Jones, Jr.

Ames Research Center

ABSTRACT

Computer models were developed in an attempt to reproduce the sequential decoder computation curve of Deep Space Network (DSN) ground station receivers, by simulation of the binary data output of the gaussian channel with the carrier phaselock loop and the subcarrier demodulator assembly. Simulations were run at bit rates equal to the powers of 2 from 8 to 2048, and agreement with DSN data was generally good above 32 bits per second. Simulation results at data rates of 8, 16, and 32 bits per second did not closely match experimental data. This simulation provides a more accurate prediction of DSN computation lengths than either current mathematical models or simulations without both the subcarrier demodulator and carrier loop.

INTRODUCTION

The performance of sequential decoders and the behavior of the deep space network carrier loop have been extensively investigated, but no satisfactory mathematical model of sequential decoding performance exists for medium (10 to 10^3 bps) data rates (Layland). The experimental data have noise bursts, due primarily to carrier tracking errors (Hofman and Lumb). The noise bursts increase the probability that a large number of computations will be required to decode a data frame. Since the carrier phaselock loop has been well described

(Viterbi, Farnworth, Edelson, JPL), it was decided to attempt to reproduce the data by simulating the channel and carrier phaselock loop.

The experimental data were collected at two NASA deep space communications facilities. An alternating 1,0 symbol sequence was used to PSK modulate a 32,768 Hz square-wave subcarrier which phase modulated an S-band carrier. Data rates ranged from 16 to 4096 symbols per second in binary steps. Signal strength and modulation index were set for various combinations of $P_C/N_0 2B_{1o}$ and normalized symbol signal-to-noise ratio (E_s/N_0). The standard Deep Space Network configuration of S-band receiver with 12 Hz threshold carrier loop bandwidth, Subcarrier Demodulator Assembly (SDA), and Symbol Synchronizer Assembly (SSA) were used. The raw data were digital magnetic tape recordings of the SSA outputs, quantized to 256 levels. These data were used as inputs to a program at Ames Research Center that simulates the Pioneer 10/11 rate 1/2, k=32 sequential decoder, and an optimum rate 1/2, k=7 Viterbi decoder. Frame length was 384 symbols; tail length was 48 symbols; and an upper limit of 10^5 computations per frame was set.

The experimental data were used to generate a power budget for each test (Table I). The error probability corresponds to an E_s/N_0 at the decoder input (E_s/N_0). The modulation index and the E_s/N_0 were used in computer programs based on Linsey's work (Linsey 1964, Linsey 1968) to compute the E_s/N_0 loss due to the carrier loop (R_X). The losses due to the subcarrier loop (SDA) and bit synchronizer (SSA) were taken from JPL 810-5. The computed E_s/N_0 is in fair agreement with measured values.

The basic simulation (mode 1) produces eight-level quantized data corresponding to an alternate 1,0 symbol sequence input to a gaussian noise channel (Jacobs). Mode 2 adds a simulation of the carrier phaselock loop to the channel simulation, by reducing E_s/N_o according to the current phase error. Mode 3 similarly adds a simulation of the subcarrier demodulator to the channel, and Mode 4 combines channel, carrier, and subcarrier simulations. The mode numbers follow a slash in the graphs of the appendices, so that SIM 20-3/1 is a mode 1 simulation. As in mode 4, modes 5 and 7 use the carrier and subcarrier simulations, but in mode 5 the subcarrier loop depends on the current carrier tracking error, rather than the average error, and in mode 7 the subcarrier loop depends both on the current state of the carrier loop and the recent channel noise. Mode 6 is like mode 3 in that only the channel and subcarrier are simulated, but in mode 6 the subcarrier loop depends on the current channel noise. The computation curve simulations of the modes with added dependencies (modes 5, 6, and 7) are not consistently different from the simulations of the corresponding modes with no dependencies.

Carrier Phase Lock Loop Simulation

The carrier phase lock loop simulation is based on the analysis by Viterbi, Farnsworth, and Edelson and on the DSN phase lock loop specification (JPL). The exact DSN parameters are used to completely determine the simulation. The limiter suppression factor is included. The simulation block diagram and parameter computations are given in Fig. 1.

The values of the average cosine of the phase error (cos ϕ) given by the simulation are plotted in Fig. 2. The measurements agree closely with theory (Linsey 1964)(Viterbi, p. 111) especially for high $P_c/N_0 2B_{LO}$ or for a linearized ($\sin\phi = \phi$) simulation. The variance of the phase error ($\sigma^2\phi$) determines the loop signal-to-noise ratio in the linear loop model (Viterbi, p. 35, 93).

$$\frac{P_c}{N_0\ 2B_L} = \frac{1}{2\ \sigma^2\phi}$$

Again, the measurements plotted in Fig. 3 agree closely with theory at high $P_c/N_0 2B_{LO}$ or when the loop is linearized. The minimum $P_c/N_0 2B_L$ is -8.16 dB corresponding to a maximum $\sigma^2\phi$ and equal to $\pi^2/3$, the variance of a uniform distribution of ϕ in the interval $-\pi, \pi$. The data for low $P_c/N_0 2B_L$ is highly variable because of poor loop tracking and consequent high dependence of the phase reference on the particular random noise sequence input to the simulation. (The DSN experimental $P_c/N_0 2B_{LO}$ is in the range 6 to 26 dB.) All the receiver simulations use the nonlinear loop model.

Carrier Phase Lock Loop Simulation Results

When the carrier phase lock loop simulation was combined with the channel simulation two problems were observed. The program run time was excessively long and speed was increased by an average factor of 25 by reducing the noise spectral width (and the noise sample rate) from the receiver IF bandwidth to a noise bandwidth of several times the carrier loop bandwidth. The

distribution of the simulated output data in the eight different quantization bins differed greatly from the experimental data. For best performance the quantization bin widths should be 0.5 σ, where σ is the noise variance (Heller and Jacobs). The actual receiver bin width is nominally fixed at 0.5 σ for a E_s/N_0 corresponding to 9% error rate, and would be larger in terms of σ for smaller error rate. Since the data bin widths vary widely from the nominal values, the simulation bin widths were made equal to the data bin widths for each simulation.

All the simulations of the channel and phase lock loop, except three runs for which no mode 1 (channel only) simulations were made, are given in Appendix A.

The probability of error (PE) for the data and for the simulations are given in Table II. The Linsey loss (R_x) produced by the simulation is easily computed. The simulation PE corresponds to a given E_s/N_0 on the PSK error curve. The difference between this measured E_s/N_0 and the simulation input E_s/N_0 is the Linsey loss. Except at 8 bps, the data and simulation values agree closely. The 8 bps simulations designated R below have R_x adjusted to the simulation value.

The sequential decoding computation curves of the appendices are approximately straight lines of negative slope k on log-log graphs. This is the Pareto distribution (Wozencraft and Jacobs, p. 440).

Probability (number of computations is greater than L) = $P_0 L^{-k}$

If the slopes of the data, the Gaussian simulation, and the phase lock loop simulation are measured at the largest L where all the curves are available, a numerical rating of the simulation can be made; namely,

$$\text{Rating} = \frac{k_{\text{simulation}} - k_{\text{Gaussian}}}{k_{\text{data}} - k_{\text{Gaussian}}}$$

The rating is the fraction of the difference between the data and Gaussian slopes that is reproduced by the simulation. A rating of 1.0 would correspond to a perfect simulation, a rating of 0 would correspond to a simulation no better than Gaussian. The ratings agree fairly well with subjective evaluations of the full curves. Ratings for all the carrier phase lock loop simulations are given in Fig. 4. The simulations are good at medium rates and poor at high and low rates.

This performance is what would be expected from theoretical considerations. The noise equivalent bandwidth, B_L, of the phase lock loop is directly obtainable from the loop parameters (Viterbi, p. 36) (JPL spec.). If the bandpass is assumed to be rectangular, the low frequency noise components are overemphasized and the correlation time of the phase reference is increased. For a rectangular bandpass of width $2B_L$, the phase autocorrelation is of the (sin x)/x form, with the first zero crossing at $t = 1/(2B_L)$. Using this as an overestimate of the correlation time, the maximum number of symbols correlated is $2(\text{rate})/2B_L$. This number is given in Table III. At the high rates, the number of pulses correlated is high but the carrier tracking loss is very small. At the low rates the carrier loss is high, but the

phase error is uncorrelated between pulses. In both cases, the simulation does not produce error bursts that would cause the decoding computation curve to depart from the Gaussian noise curve. In the middle range of rates, losses are large and the number of pulses correlated is significant. Here the data deviate most from a Gaussian noise curve, and the simulations are reasonably close to the data.

It seems apparent that, although the carrier phase lock loop accounts for the largest deviations from Gaussian noise behavior, it isn't fully responsible for all such deviations. The table also gives the losses and number of symbols correlated for the subcarrier demodulator and for the symbol synchronizer. The correlations were computed in the same way as carrier correlation (subcarrier B_L from 810-5, p. 2-76)(synchronizer B_L from 810-5, p. 2-93,4). All correlations are significant compared to the frame length of 384 symbols, but the subcarrier losses are larger. It was decided to add a subcarrier demodulator simulation to the receiver simulation.

Subcarrier Phase Lock Loop Simulation

The subcarrier loop simulation is similar to the carrier simulation, but it uses a soft limiter instead of a hard limiter, and it also includes a loss due to data errors (since the data controls subcarrier phase and a data estimate is used to recover the subcarrier). The subcarrier loop is a linear loop since the subcarrier is a square wave. The simulation is based on the analysis of Edelson and Brockman (1967, 1968). The simulation block diagram and computations are given in Fig. 5.

The E_s/N_0 loss produced by the simulation is in close agreement with theoretical values derived from loop parameters, but, over a 25 dB range of input E_s/N_0, the simulation loss differs by as much as .1 dB from the values given in 810-5, Rev. D. The simulation is much closer to 810-5 at values of E_s/N_0 near 0 dB. Table IV lists the power budget (Table I) input SDA losses, originally taken from 810-5, Rev. C, and the simulation SDA losses.

All of the simulations of the Gaussian channel with the subcarrier demodulator are given in Appendix B, and the slope ratings are given in Fig. 6 below. The ratings are all quite low, indicating that the subcarrier demodulator (SDA) is not a major cause of the data deviation from Gaussian, especially when the deviation is large.

Simulations Using the Channel, Carrier, and Subcarrier

All the simulations made using both carrier and subcarrier loops are given in Appendix C, and the slope ratings are given in Fig. 7. The addition of the subcarrier loop improves the simulation at high rates, as shown by the average slope ratings, given in Fig. 8. This is reasonable, since the difference between the data and a Gaussian channel only simulaion is small at the high rates, and the effect of the subcarrier demodulator is also small. At medium rates the simulation is only slightly changed from the carrier only case. Appendix D, pages 1 and 2, shows carrier only (/2) and carrier and subcarrier (/4, /5, /7) simulations for two medium rate runs. The 64 bps simulations at lower $P_c/N_0 2B_{LO}$ (5-1, 40-5) differ more from the data than simulations at higher $Pc/N_0 2B_{LO}$ (40-1, 21-2). The apparent improvement

at low rates is due to the use of the Linsey loss (R_x) found by the carrier simulation, rather than the original estimate at 8 bps. None of the 8 or 16 bps simulations, with carrier or subcarrier or both, differ significantly from the Gaussian channel simulations.

There are seven cases of repeated runs in Appendix C, and in four of the five cases where probabilities in the order of 10^{-3} are plotted, the curves are noticeably different. This occurs because there are only a few frames in a group of total probability of 10^{-3}, so that large relative fluctuations occur. The number of frames of data and simulated data for each run is given in Table V. There are also some similar data runs given in Appendix D, pp. 3-6, which show random fluctuations at low probability levels. Runs 14-3 and 35-3 are quite different because the bit synchronizer lost lock during 35-3, as it did in all but four of twenty-four attempted runs at 8 bps.

The performance parameter of most interest in sequential decoding is the probability that the number of computations required is so large that the decoder time allowed per frame will be insufficient, and the frame will not be decoded. This is the deletion probability, P_{del}, which is given in Fig. 9 and 10, assuming that the maximum computation length is 10^3. Each run is represented by a line with the top point being P_{del} for the data, and the lower points being simulations. The curve is P_{del} for a Gaussian channel. For the high rates, Fig. 9, the simulations give P_{del} corresponding to an E_s/N_0 within .2 dB of the data E_s/N_0, except in three of fourteen cases where the E_s/N_0 errors are .3, .3, and .4 dB. For the low rates E_s/N_0 errors vary from .3 to 2.0 dB.

The Viterbi error rates are not simulated.

Concluding Remarks

The carrier simulation reproduces the large deviations from Gaussian channel performance found at medium bit rates. The additional simulation of the subcarrier improves the simulation's agreement with the small deviations found at the higher bit rates. The large, inconsistent deviations from Gaussian channel performance at low bit rates were not reproduced. The symbol synchronizer was not simulated, but its effects would be much smaller than those of the subcarrier demodulator.

The DSN and the experimental data should be investigated to determine the cause of non-Gaussian behavior at low rates.

The simulation could be used to find the modulation index that minimizes P_{del} given total signal power. This would be significant design information.

The tradeoff could be examined between larger thermal noise (and more errors) and lower correlation time (and easier decoding of errors) as the loop bandwidths are increased.

A mathematical model of the DSN similar to Layland's, but with greater accuracy, at high rates, could possibly be generated using the simulation results.

TABLE I - INPUT DATA

Rate (BPS)	ID	PE (%)	MI (deg)	E_S/N_O (dB)	R_x	SSA	SDA	E_S/N_O In (dB)	Exp't E_S/N_O	Unexplained Losses (dB)	$\frac{P_C}{N_O 2B_{1O}}$
2048	20-3	7.60	45.0	.10	.02	.07	.24	.43	1.12	.69	25.76
	20-1	5.35	53.0	1.15	.09	.06	.22	1.52	2.18	.66	24.39
1024	32-1	5.11	53.0	1.25	.11	.06	.26	1.68	1.88	.20	22.04
	12-11	6.74	63.5	.49	.25	.06	.27	1.07	1.4	.33	17.11
512	18-1	6.31	45.0	.70	.15	.06	.35	1.26	1.60	.34	17.56
	39-4	2.81	66.54	2.55	.27	.05	.29	3.16	3.26	.10	15.22
256	7-1	8.27	66.5	-.17	.80	.05	.17	.85	1.30	.45	9.92
	7-2	5.28	66.5	1.17	.65	.05	.16	2.03	1.80	.23	11.10
128	43-2	4.38	56.0	1.60	.58	.05	.21	2.38	2.72	.34	12.25
	21-5	8.22	40.0	-.15	.35	.08	.27	.55	.71	.16	15.47
64	5-1	6.52	66.5	.58	2.00	.04	.20*	2.82	3.80	.98	5.87
	40-5	5.14	66.5	1.25	1.70	.06	.27	3.28	3.28	.0	6.31
	40-1	4.91	53.0	1.36	.82	.05	.27	2.49	2.56	.07	10.31
	21-2	3.57	50.0	2.10	.80	.05	.24	3.19	3.11	-.08	11.94
32	38-2	4.07	42.0	1.85	.80	.05	.30	3.00	2.87	-.13	11.18
	24-2	3.76	50.0	1.95	1.15	.05	.30	3.45	3.60	.15	9.19
	22-7	3.55	40.0	2.05	.65	.05	.30	3.05	3.07	.02	11.85
16	23-5	2.98	37.0	2.45	.95	.08	.35	3.85	4.02	.19	10.55
	24-1	2.69	45.0	2.65	1.45	.08	.34	4.52	4.44	-.08	8.78
8	12-3	7.51	31.7	.15	1.60	.12	.54	2.41	3.30	.89	7.85
	14-3	2.92	45.0	2.49	2.80	.08	.44	5.82	5.86	.04	7.03
	35-5	4.55	40.0	1.53	2.22	.10	.47	4.32	3.89	-.43	7.10

*Should be .28 .20 used

TABLE II - CARRIER SIMULATION RESULTS

ID	Data Rate BPS	PE Data	PE SIM	Linsey Loss (R_X) Data	Linsey Loss (R_X) SIM
20-3	2048	7.60	7.65, 7.66	.02	.03, .03
20-1	2048	5.35	5.25	.09	.10, .09
32-1	1024	5.11	5.11, 5.10	.11	.10, .09
12-11	1024	6.74	6.72	.25	.25
7-1	256	8.27	8.40, 8.36	.80	.85, .84
7-2	256	5.28	5.41	.65	.71
5-1	64	6.52	6.45, 6.45	2.00	1.96, 1.96
40-5	64	5.14	5.48	1.70	1.88
38-2	32	4.07	3.83, 3.84	.80	.70, .70
24-2	32	3.76	3.88	1.15	1.06
12-3	8	7.51	6.50	1.60	1.16
14-3	8	2.98	1.69	2.80	1.72

TABLE III - SUBSYSTEM CORRELATIONS AND LOSSES

		CARRIER			SUBCARRIER			SYMBOL SYNC	
Rate (BPS)	ID	$2B_L$	#Correlated	Loss (R_X)	$2B_L$	#Correlated	Loss	#Correlated	Loss
2048	20-3	98	42.0	.02	3.0	1360	.24	800	.07
	20-1	93	44.0	.09	3.2	1280	.22	800	.06
1024	32-1	83	25.0	.11	2.5	820	.26	800	.06
	12-11	59	35.0	.25	2.3	890	.27	800	.06
512	18-1	62	17.0	.15	1.7	600	.35	800	.06
	39-4	50	21.0	.27	2.4	430	.29	800	.05
256	7-1	30	17.0	.80	.2	2600	.17	800	.05
	7-2	34	15.0	.65	.3	1700	.16	800	.05
128	43-2	37	6.9	.58	.15	1700	.21	800	.05
	21-5	51	5.0	.35	.14	1800	.27	800	.08
64	5-1	20.5	6.2	2.00	.15	850	.20	800	.04
	40-5	21.5	6.0	1.70	.15	850	.27	800	.06
	40-1	31.5	4.1	.82	.15	850	.27	800	.05
	21-2	37.0	3.5	.80	.15	850	.24	800	.05
32	38-2	34.0	1.9	.80	.08	800	.30	800	.05
	24-2	28.0	2.3	1.15	.08	800	.30	800	.05
	22-7	36.0	1.8	.65	.08	800	.30	800	.05
16	23-5	32.0	1.0	.95	.08	400	.35	1000	.08
	24-1	27.0	1.2	1.45	.08	400	.34	1000	.08
8	12-3	24.5	.65	1.60	.05	320	.54	1000	.12
	14-3	23.0	.69	2.80	.06	260	.44	1000	.09
	35-5	23.0	.65	2.22	.06	260	.47	1000	.10

TABLE IV - SUBCARRIER LOSS

		SDA LOSS, dB	
RATE	ID	INPUT	SIMULATION
2048	20-3	.24	.22
	20-1	.22	.21
1024	32-1	.26	.27
	12-11	.27	.28
512	18-1	.35	.34
	39-4	.29	.32
256	7-1	.17	.18
	7-2	.16	.18
128	43-2	.21	.22
	21-5	.27	.28
64	5-1	.28	.27
	40-5	.27	.27
	40-1	.27	.28
	21-2	.24	.26
32	38-2	.30	.32
	24-2	.30	.32
	22-7	.30	.32
16	23-5	.35	.38
	24-1	.34	.39
8	12-3	.54	.51
	14-3	.44	.47
	35-5	.47	.50

TABLE V - NUMBER OF FRAMES

ID	# Frames Data	# Frames Simulated
20-3	7214	5328
20-1	6958	5328
32-1	6345	5328
12-11	5248	5328
18-1	5526	5328
39-4	4896	5328
7-1	1000	5328
7-2	3484	5328
43-2	5360	5328
21-5	2317	5328
5-1	11567	2664
40-5	3111	2664
40-1	2786	2664
21-2	2200	2664
38-2	1976	2131
24-2	1934	2131
22-7	1960	2131
23-5	2131	1598
24-1	1875	1598
12-3	1150	1598
14-3	1156	1598
35-5	953	1598

Figure 1. Carrier Loop Simulation

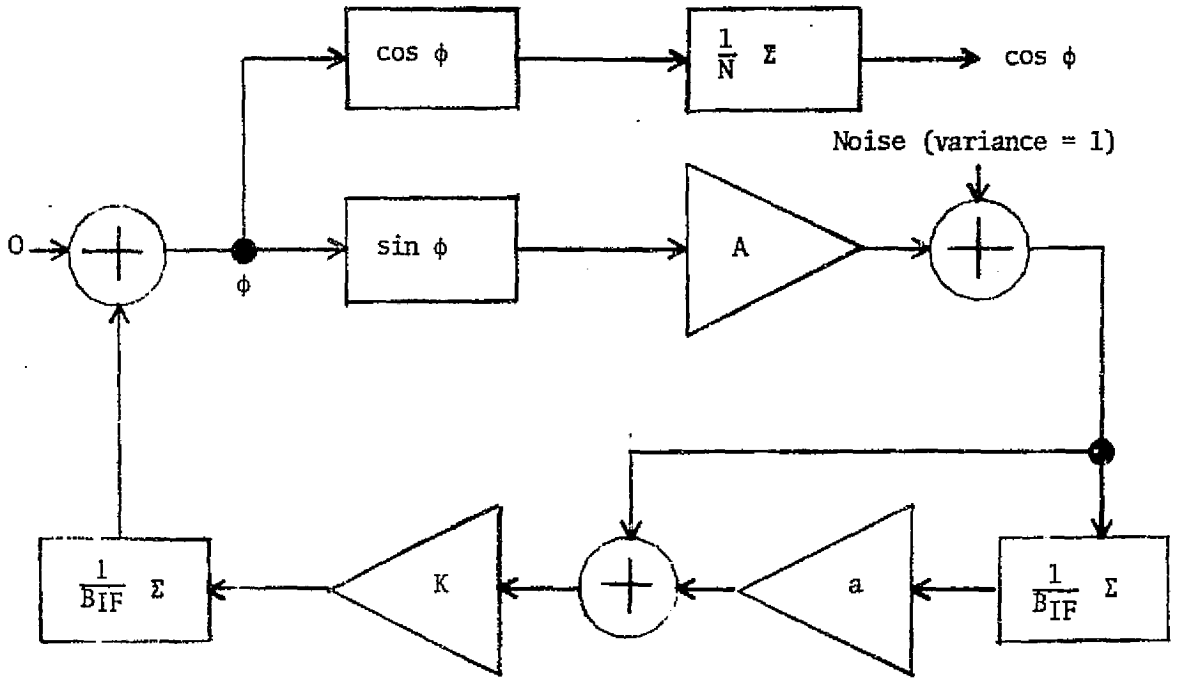

$$a = 8,\ K_L = 246.5,\ B_{IF} = 2{,}000,\ N = \frac{B_{IF}}{RATE}$$

$$\text{Data Signal to Noise Ratio} = \frac{P_D}{N_o} = \frac{E_s}{N_o} \times RATE$$

$$\text{Carrier Signal to Noise Ratio} = \frac{P_c}{N_o} = \frac{\cos^2 (MI)}{\sin^2 (MI)}$$

$$N_L = \frac{P_c}{N_o} \frac{1}{B_{IF}}$$

$$a_L^2 = \frac{.7854\ N_L + .4768\ N_L^2}{1 + 1.024\ N_L + .4768\ N_L^2}$$

$$A = \left(\frac{2a_L^2}{1-a_L^2}\right)^{1/2}$$

$$K = K_L \left(\frac{1-a_L^2}{2}\right)^{1/2}$$

$$\text{Bandwidth} = B_L = (AK+a)/4$$

$$\text{Loop Signal to Noise Ratio} = \frac{P_D}{N_o} \frac{1}{B_L}$$

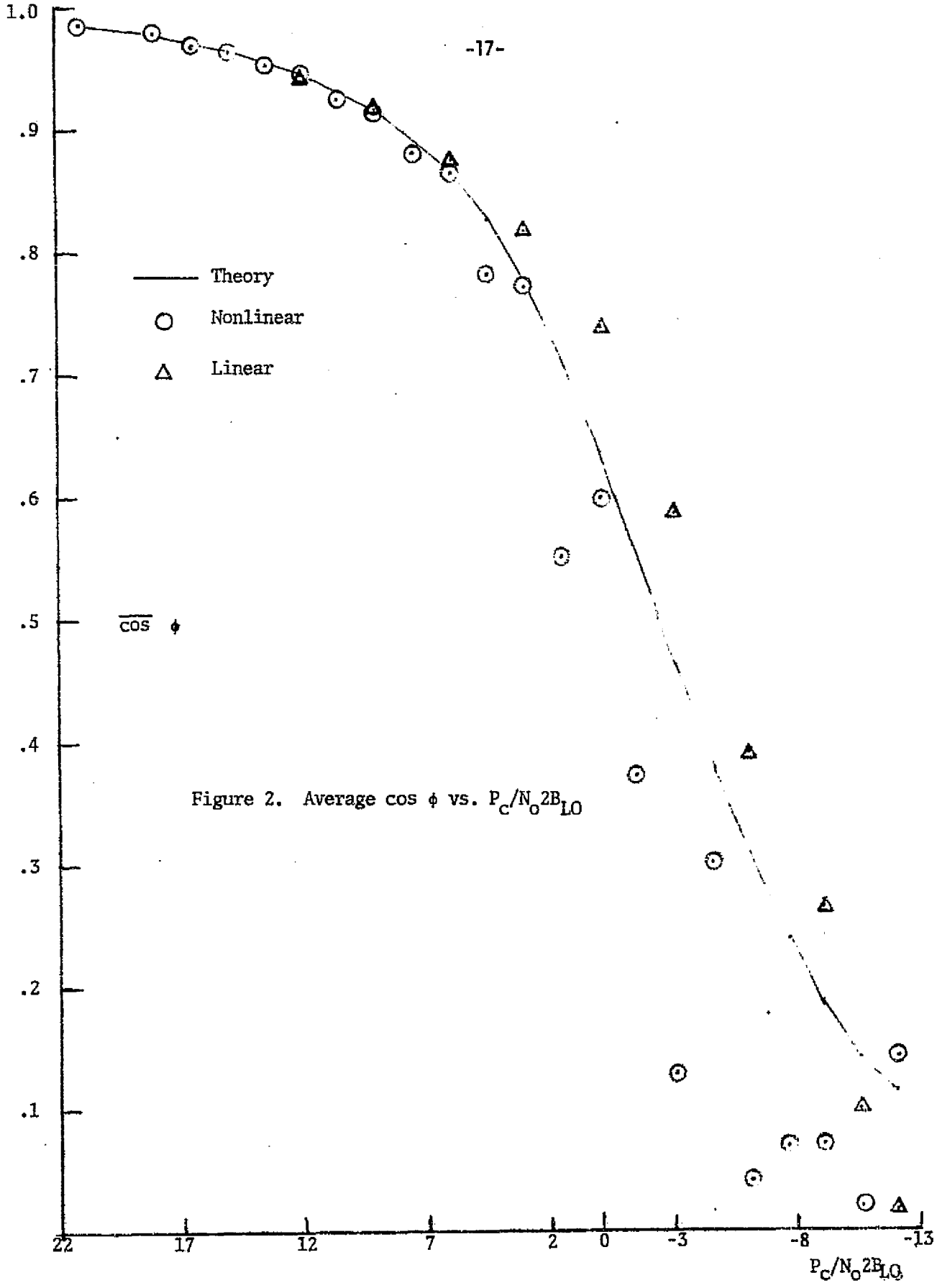

Figure 2. Average cos ϕ vs. P_C/N_o2B_{LO}

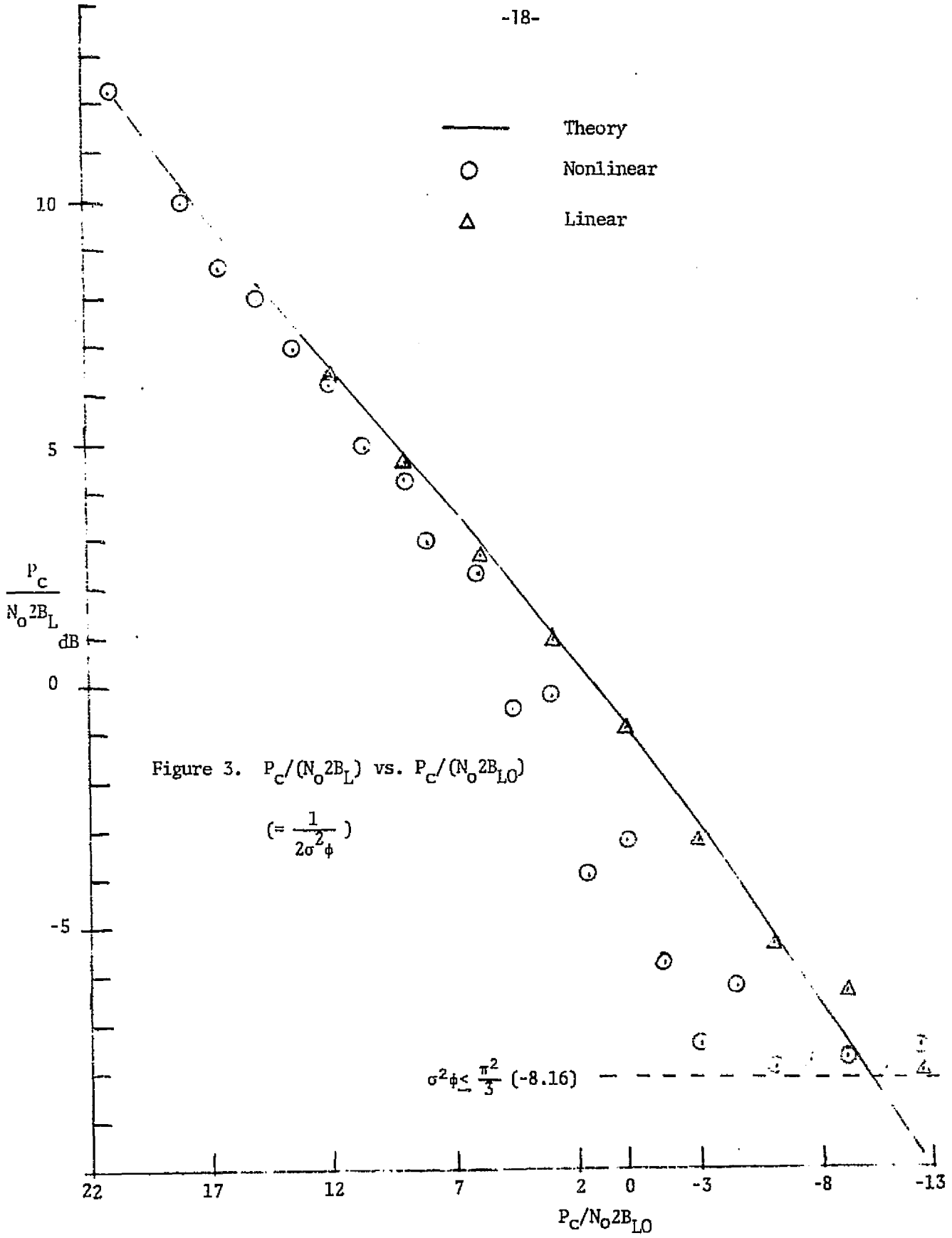

Figure 3. $P_c/(N_o 2B_L)$ vs. $P_c/(N_o 2B_{LO})$

$(= \frac{1}{2\sigma^2\phi})$

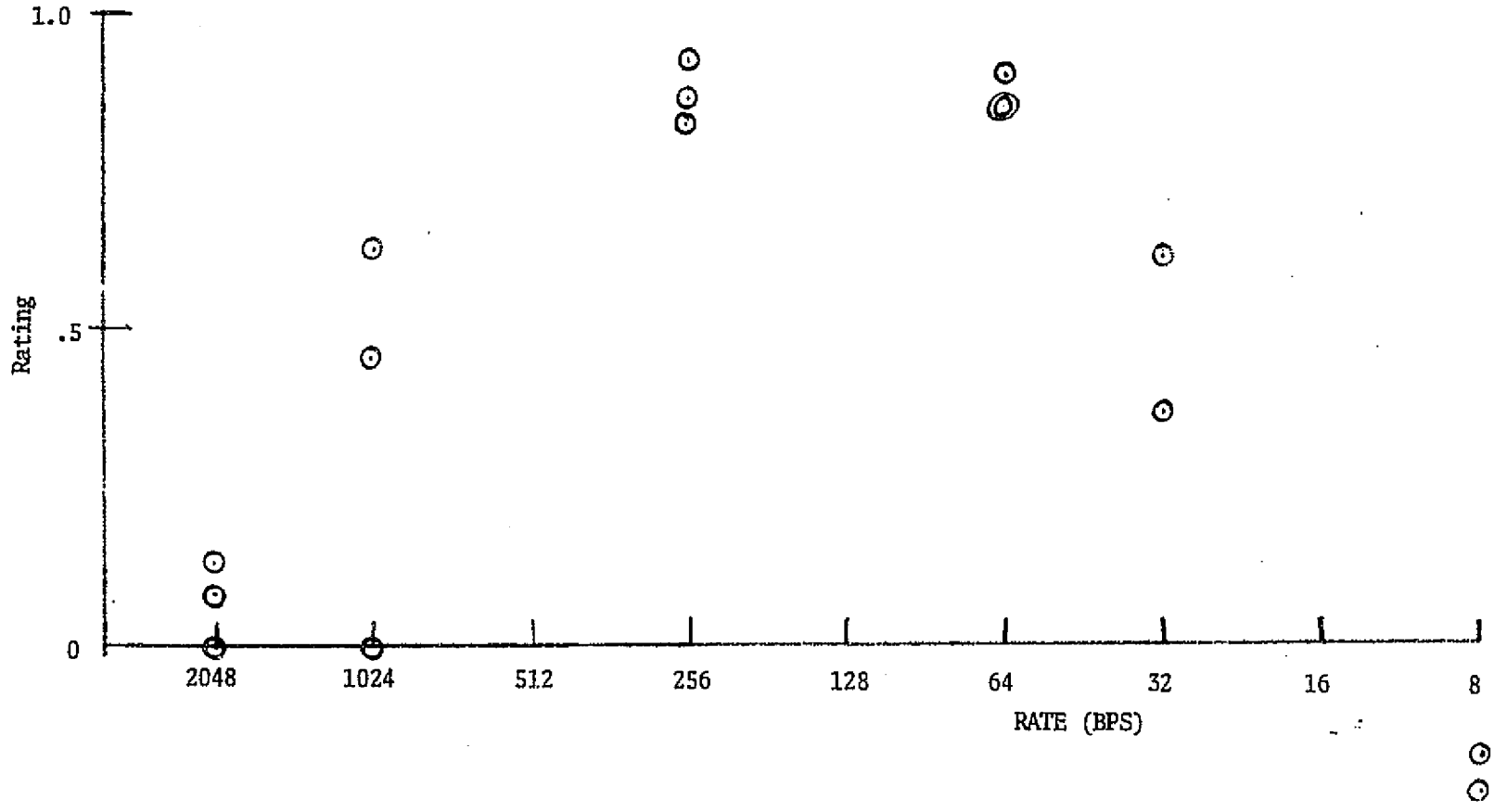

Figure 4. Carrier Simulation Ratings vs. Rate

Figure 5. Subcarrier Loop Simulation

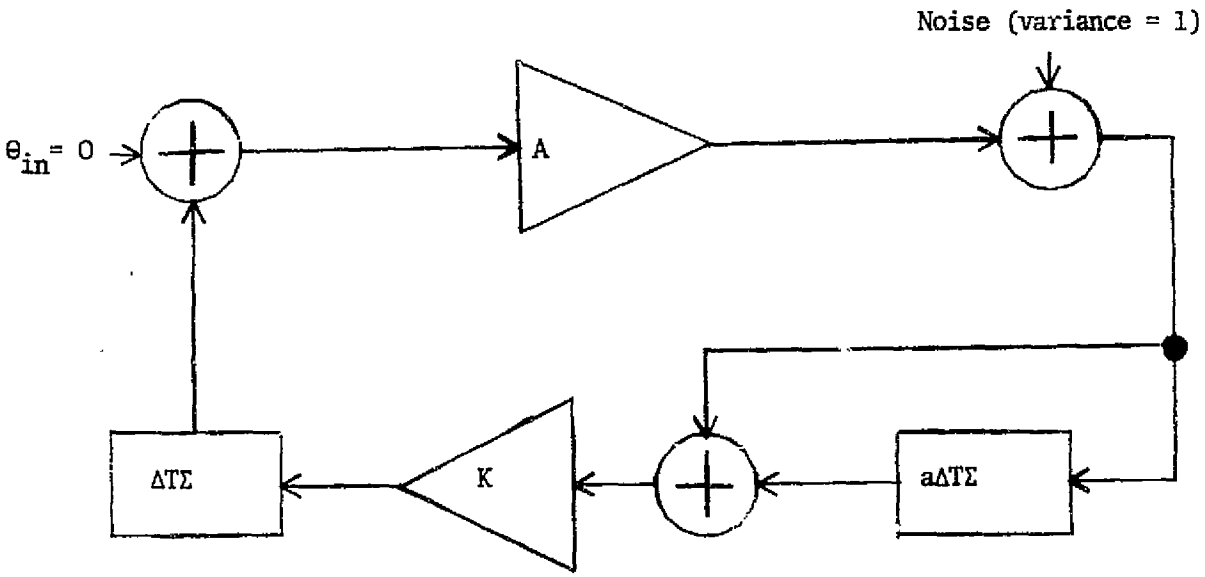

$$\Delta T = (\text{Subcarrier Rate})^{-1}$$

Rate <600	a = .02	$K_L = 3.38$
Rate ≥600	a = .25	$K_L = 16.9$

$$A = \frac{2}{\pi}\frac{a_p}{\sigma}, \quad K = a_{SL} K_L \sigma$$

$$a_p = .769\left[\frac{.877 + .2\,(2E_s/N_o)^{1.2}}{1.0 + .2\,(2E_s/N_o)^{1.2}}\right] \text{erf}\left(\frac{4E_s}{3N_o}\right)^{1/2}$$

$$SF = (a_p)^2 \frac{E_s}{N_o}\frac{\text{Rate}}{500}$$

$$\Gamma = \frac{1 + .345\,(SF) + 50\,(SF)^5}{.862 + .690\,(SF) + 50\,(SF)^5}$$

$$a_{SL} = \text{erf}\left(\frac{SF}{2\pi}\right)^{1/2}$$

$$\sigma = \left(\Gamma/\frac{E_s}{N_o}\,(\text{RATE})\,\Delta T\right)^{1/2}$$

$$\text{Bandwidth} = B_L = (AK + a)/4$$

$$\text{Loop Signal-to-Noise Ratio} = \frac{E_s}{N_o}\,\frac{\text{Rate}}{2B_L}\,\frac{a_p^2\, a_{SL}^2}{\Gamma}$$

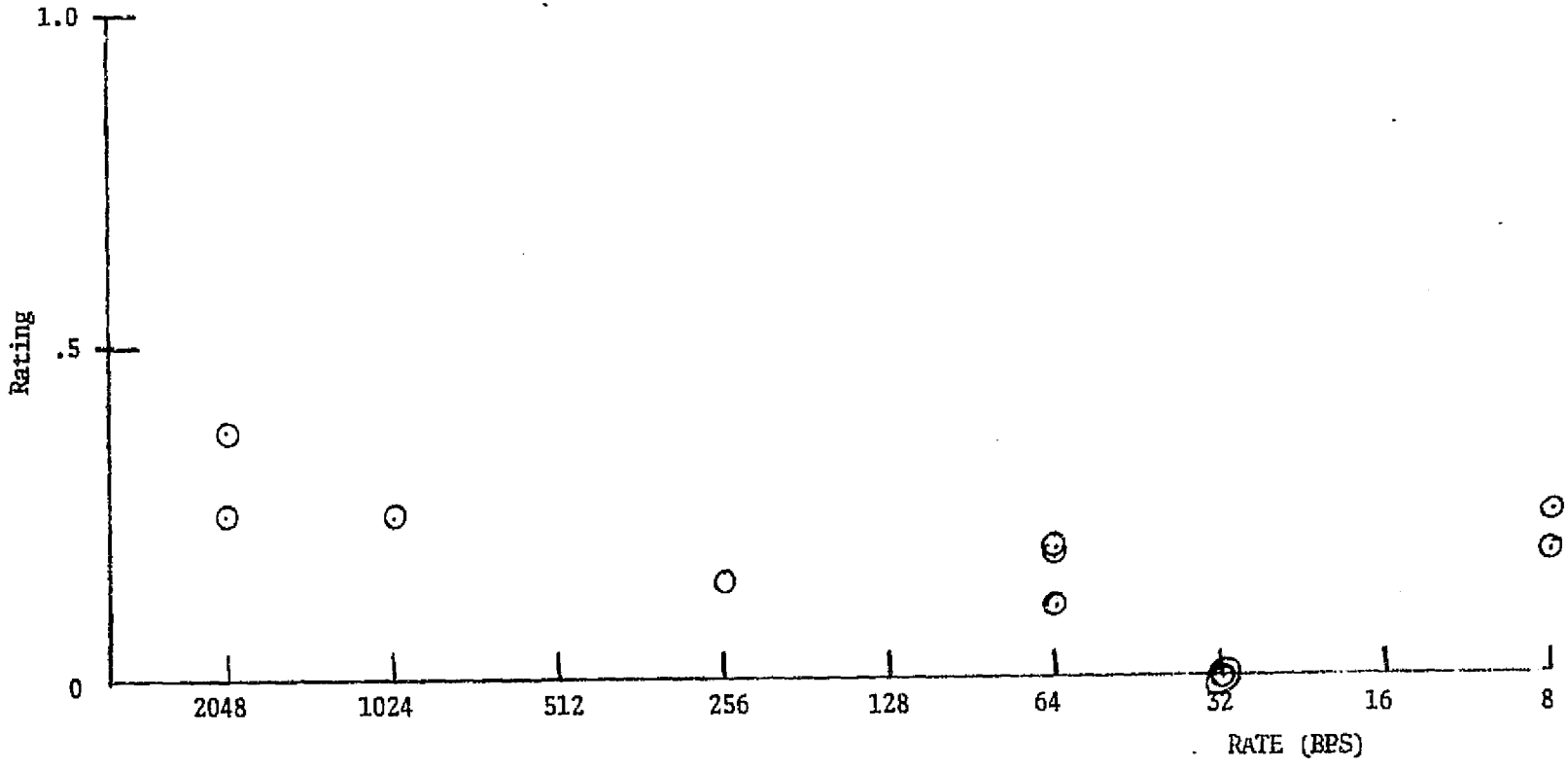

Figure 6. Subcarrier Simulation Ratings vs. Rate

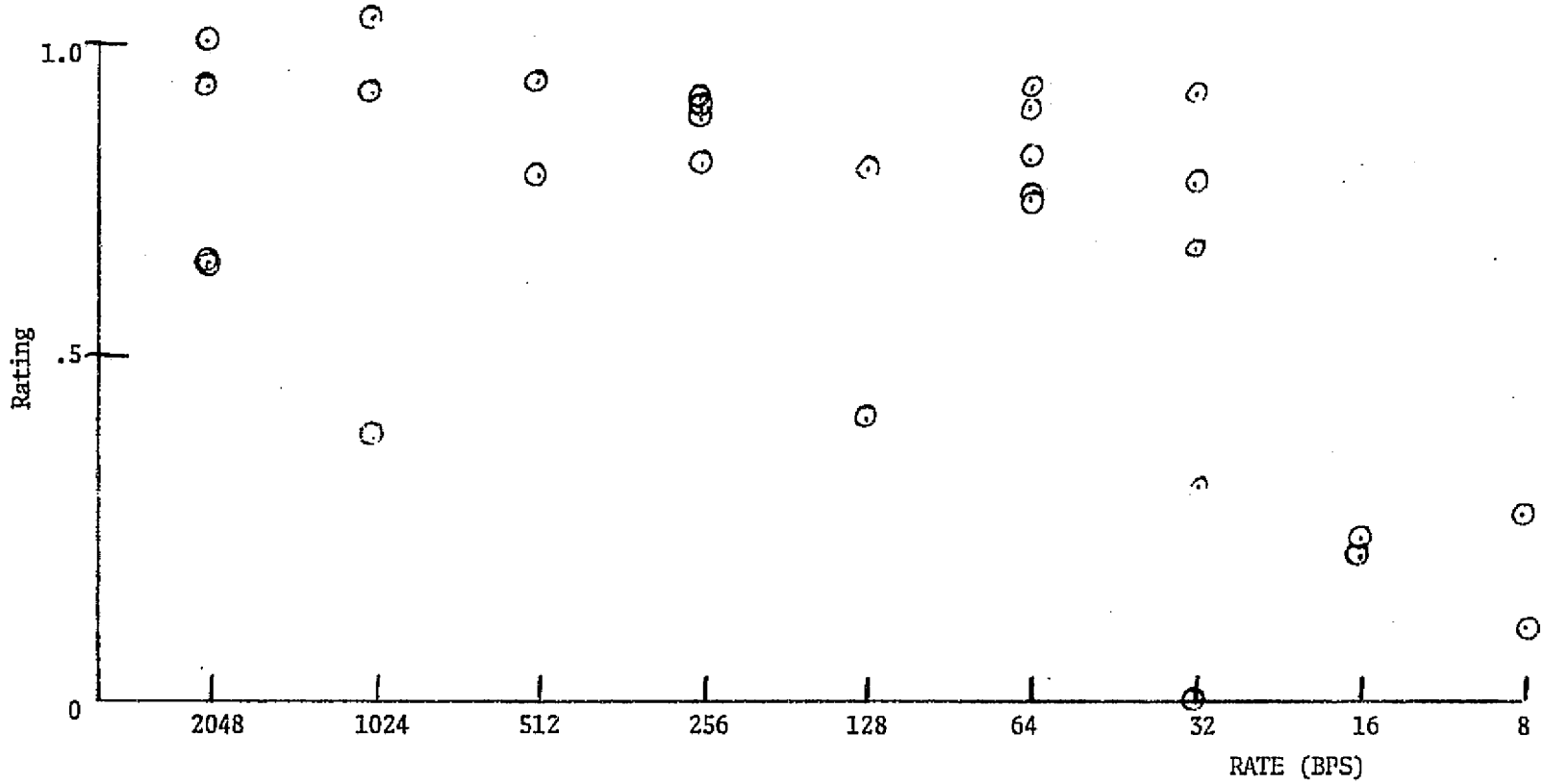

Figure 7. Carrier and Subcarrier Simulation Ratings vs. Rate

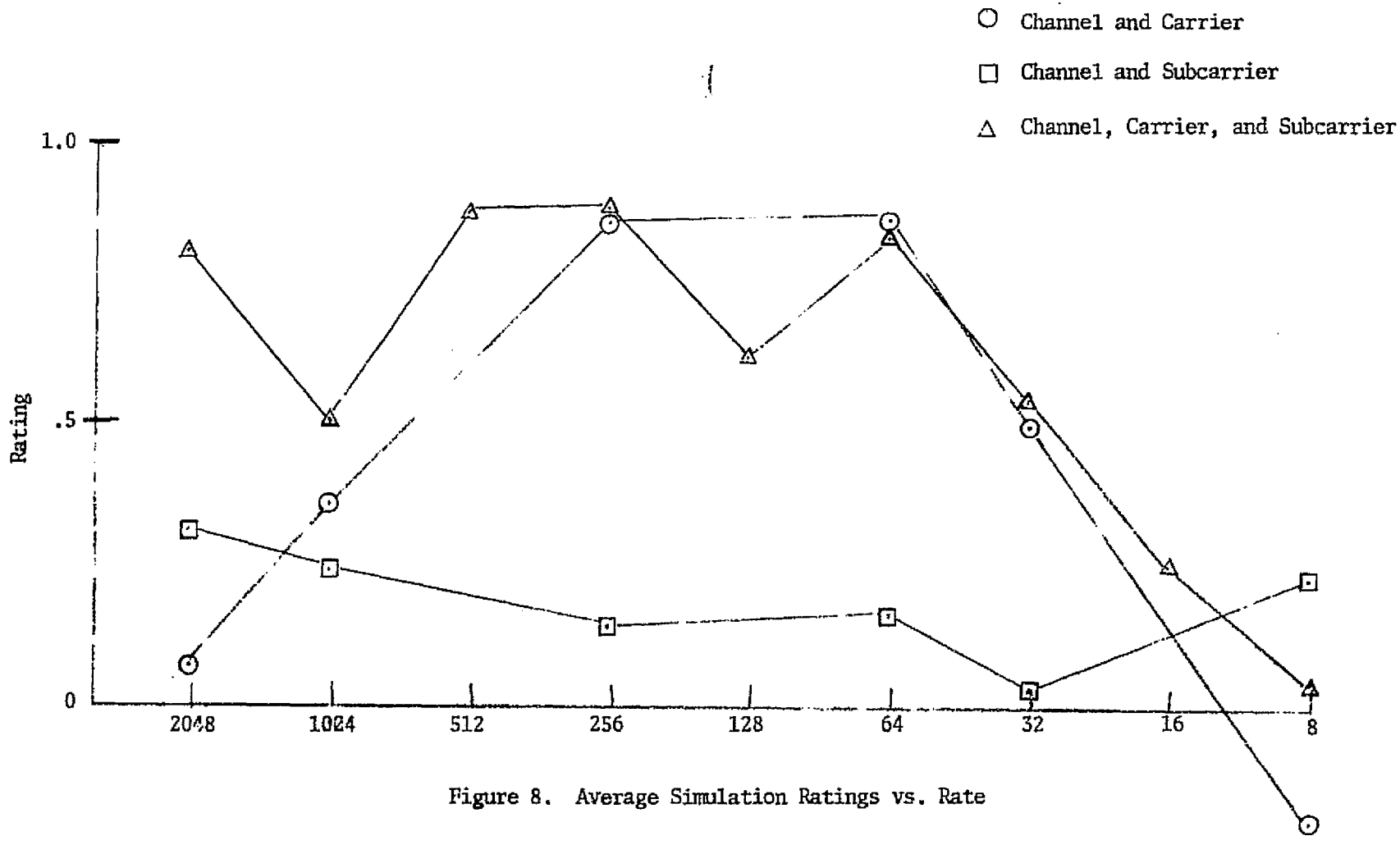

Figure 8. Average Simulation Ratings vs. Rate

Figure 9. P_{DEL} for High Rates

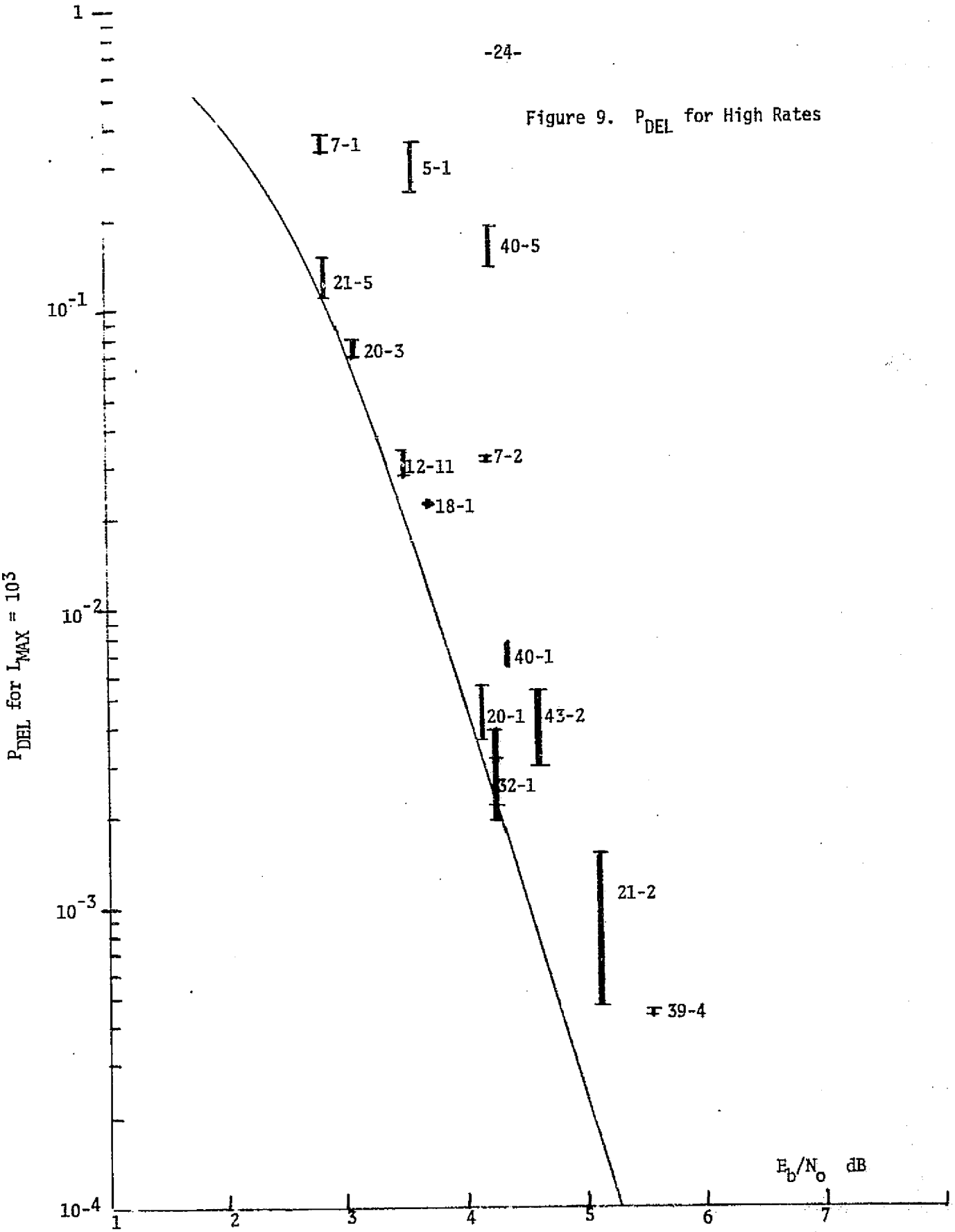

Figure 10. P_{DEL} for Low Rates

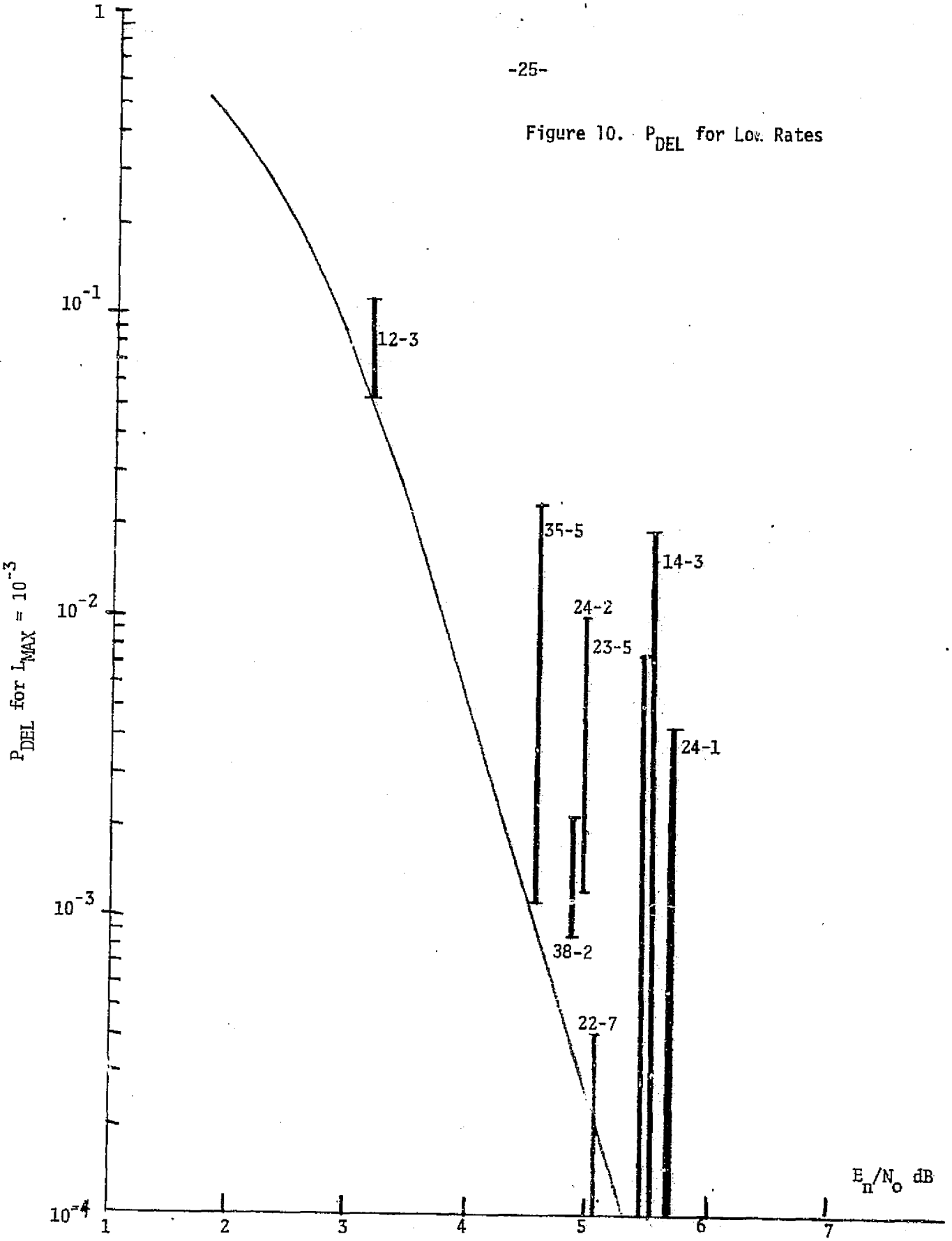

APPENDIX A

This appendix contains experimental data (EXP XX-X), gaussian channel only simulations (SIM XX-X/1), and gaussian channel with carrier phase lock loop simulations (SIM XX-X and SIM XX-X/2), for the following runs in order of decreasing rate.

SEQUENTIAL DECODING COMPUTATION DISTRIBUTION

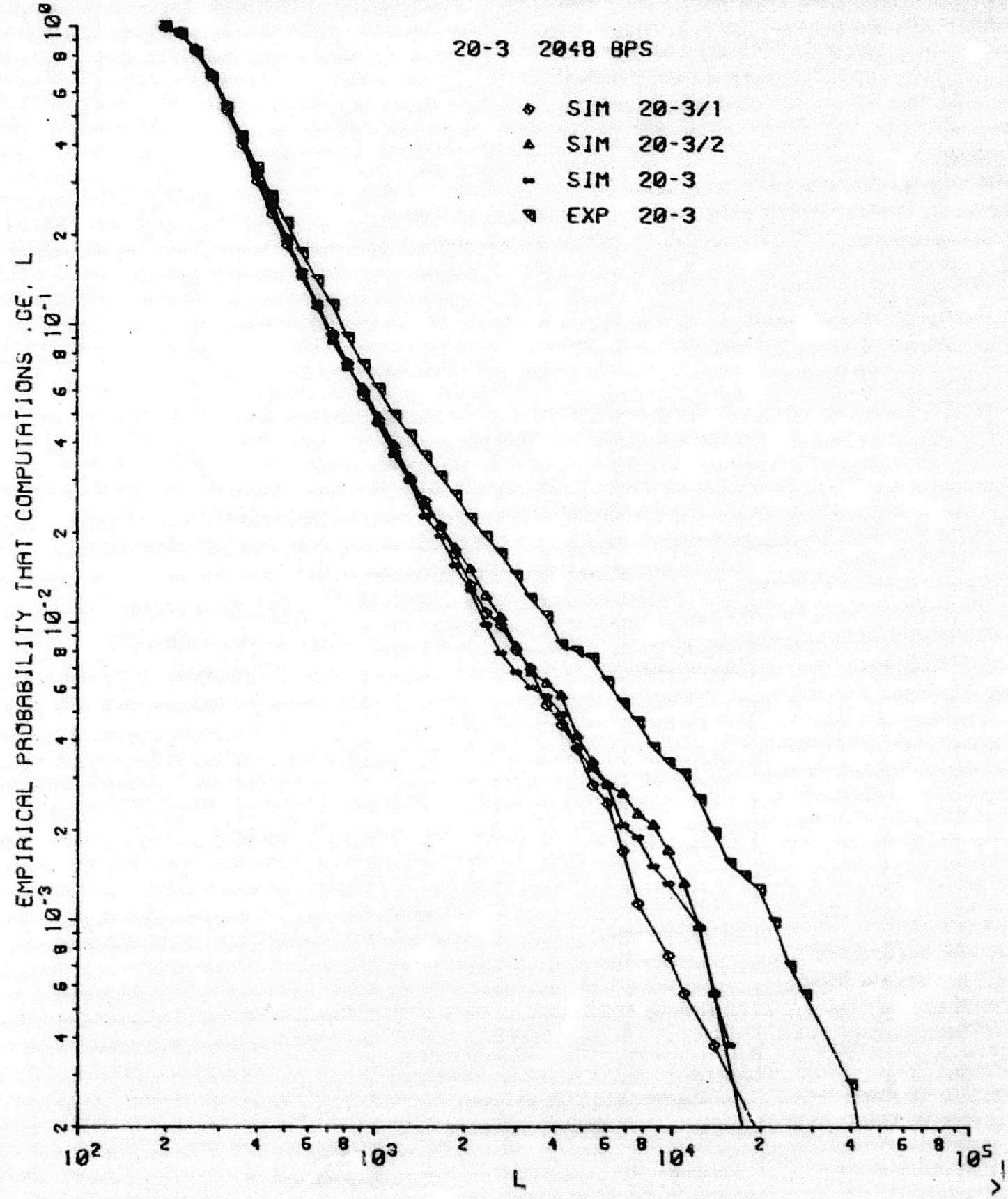

SEQUENTIAL DECODING COMPUTATION DISTRIBUTION

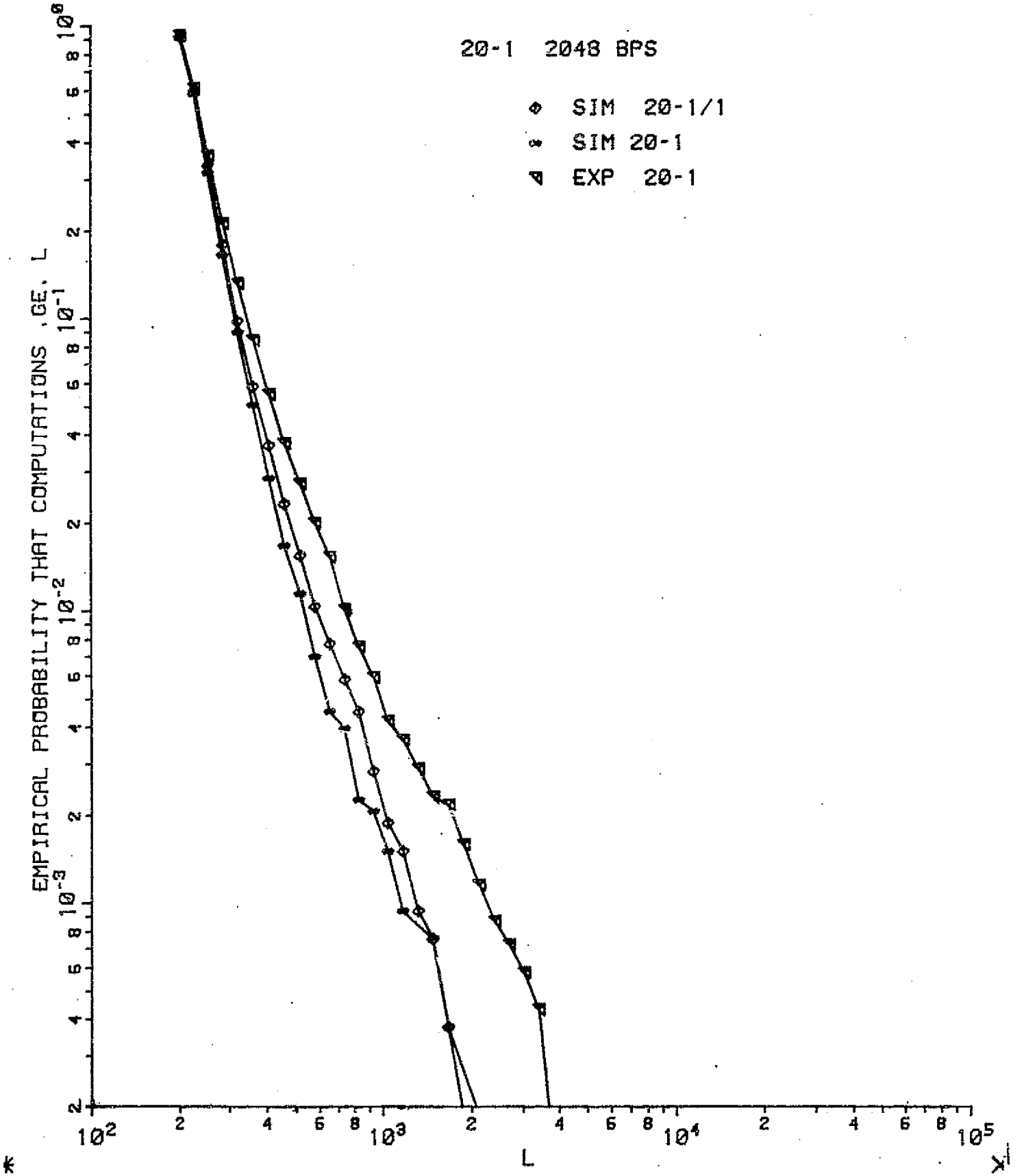

SEQUENTIAL DECODING COMPUTATION DISTRIBUTION

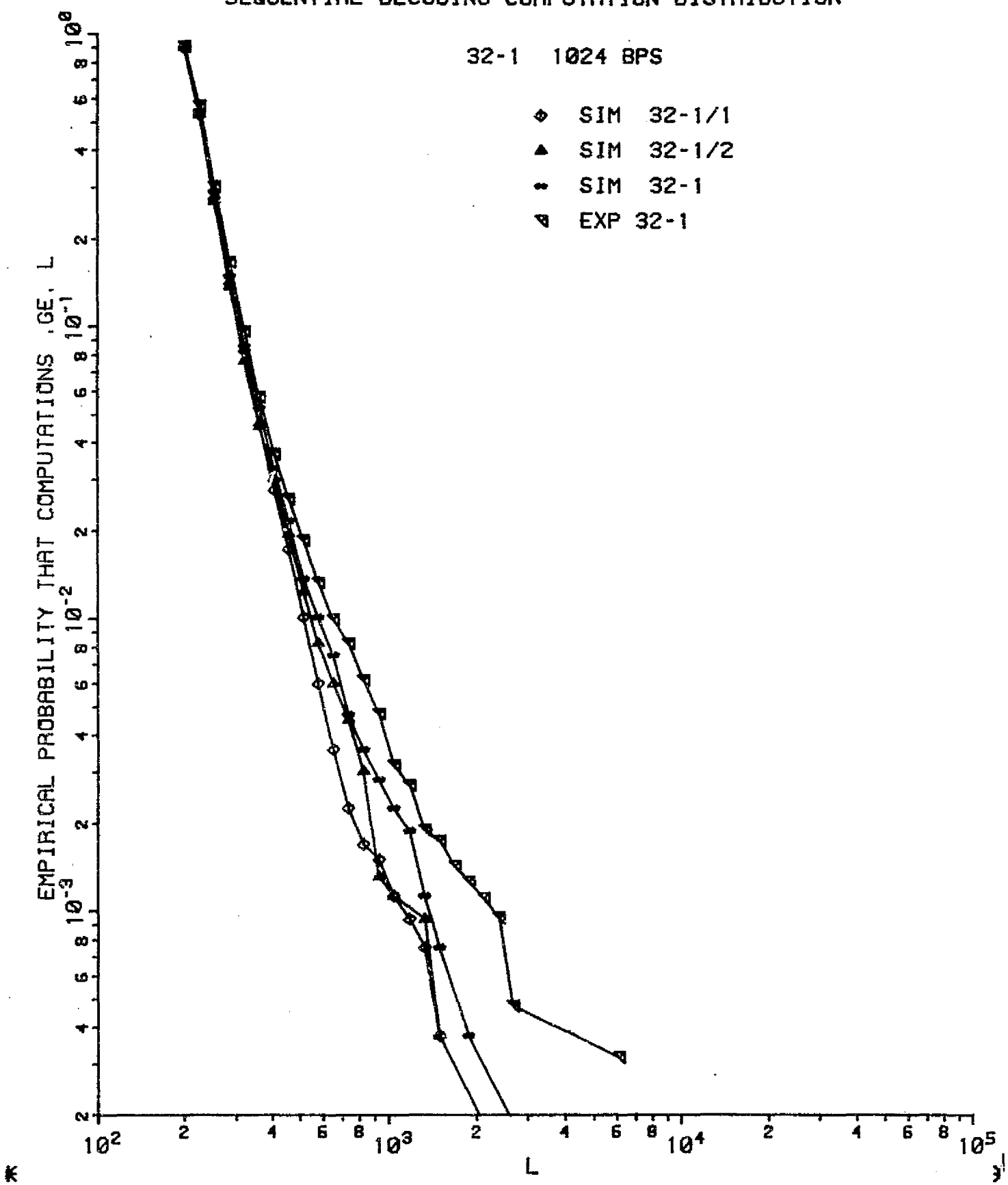

SEQUENTIAL DECODING COMPUTATION DISTRIBUTION

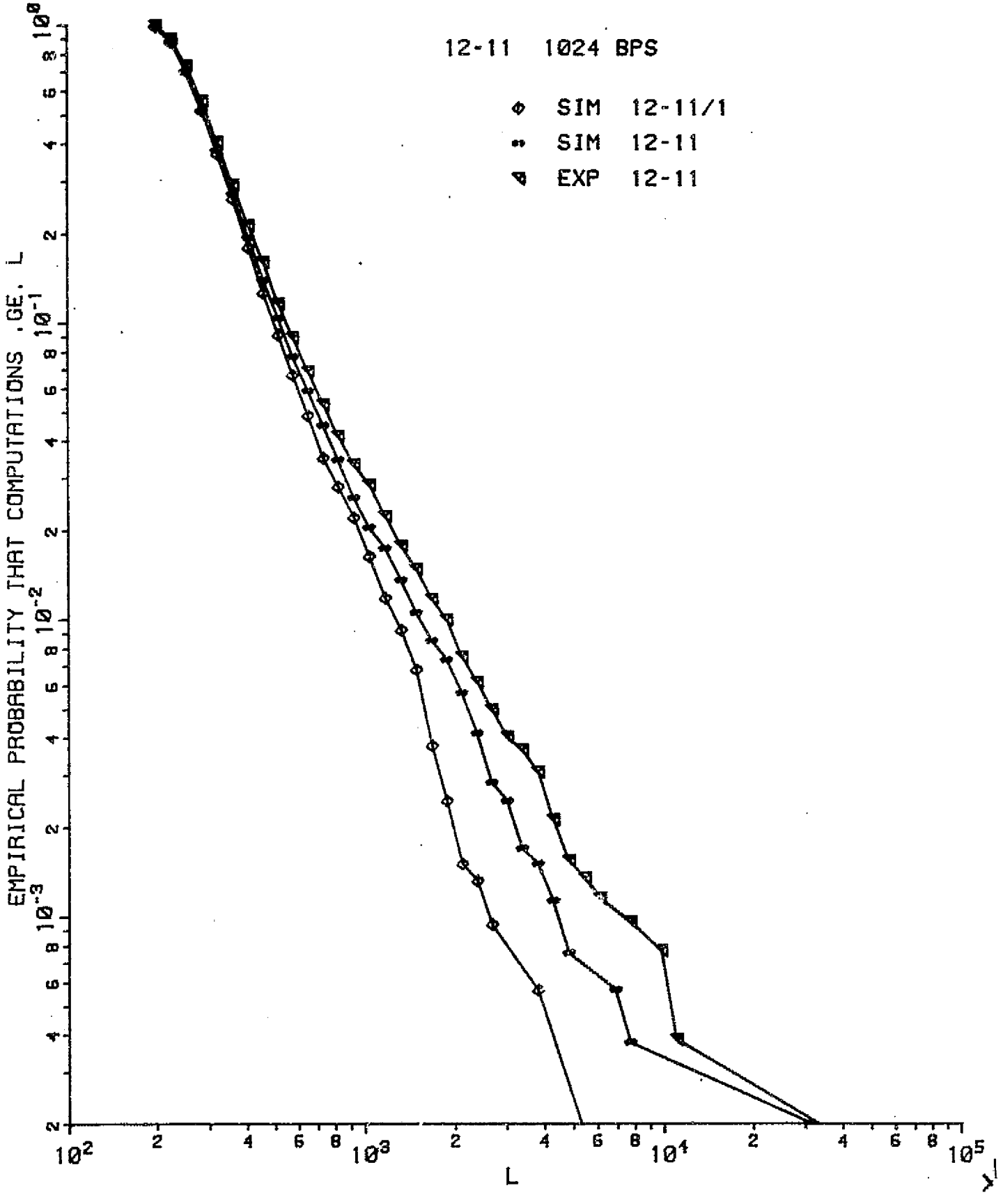

SEQUENTIAL DECODING COMPUTATION DISTRIBUTION

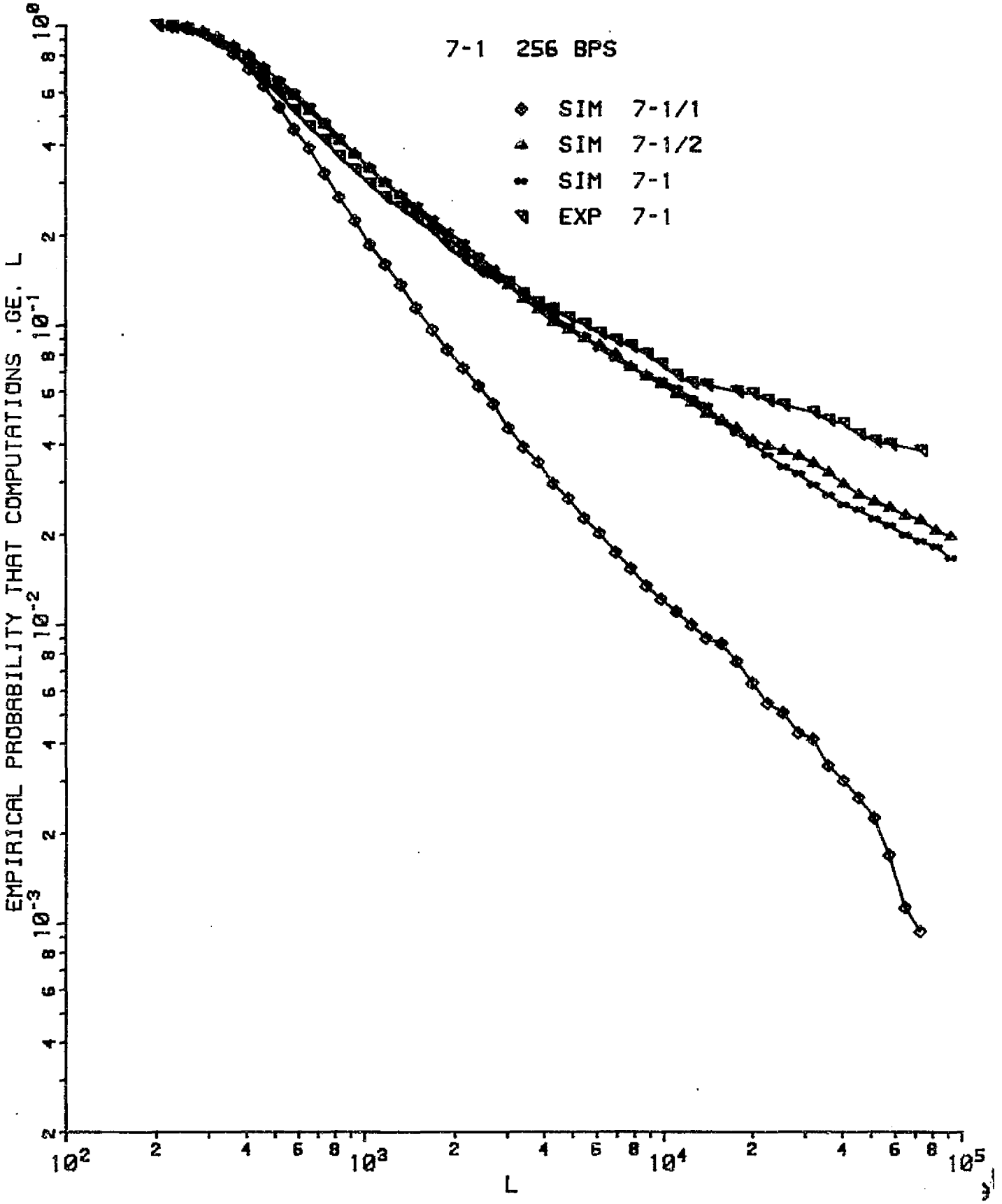

SEQUENTIAL DECODING COMPUTATION DISTRIBUTION

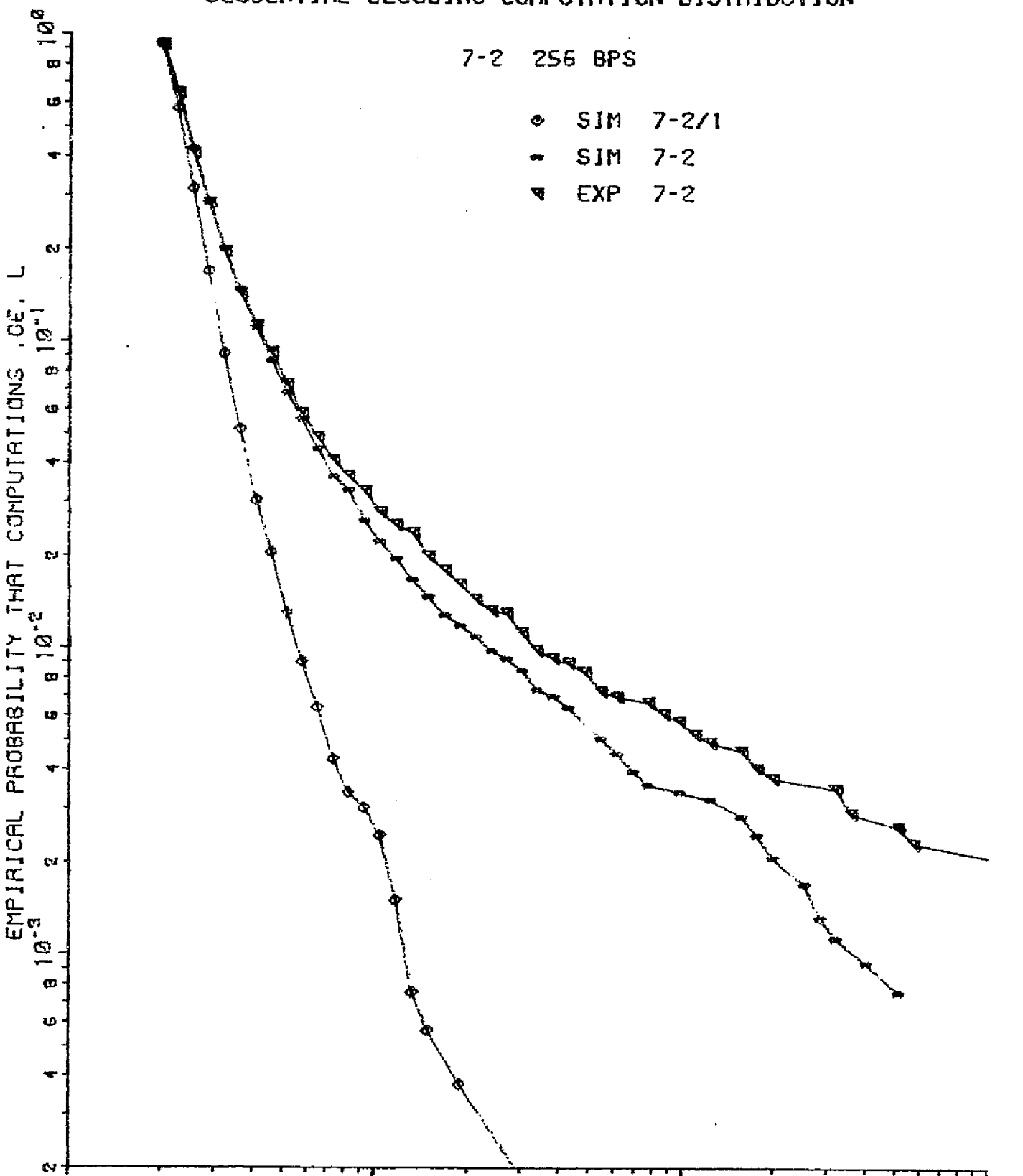

SEQUENTIAL DECODING COMPUTATION DISTRIBUTION

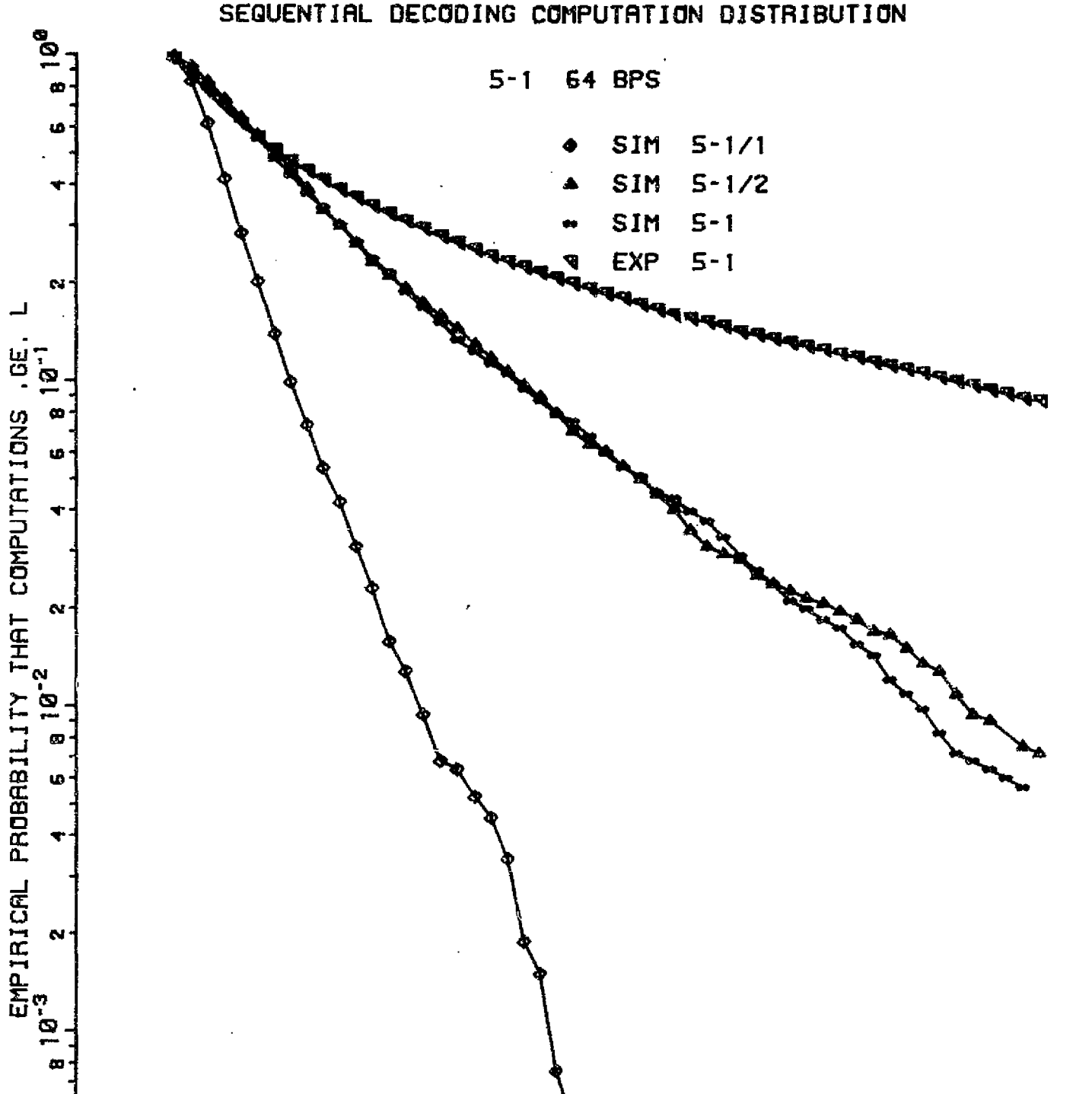

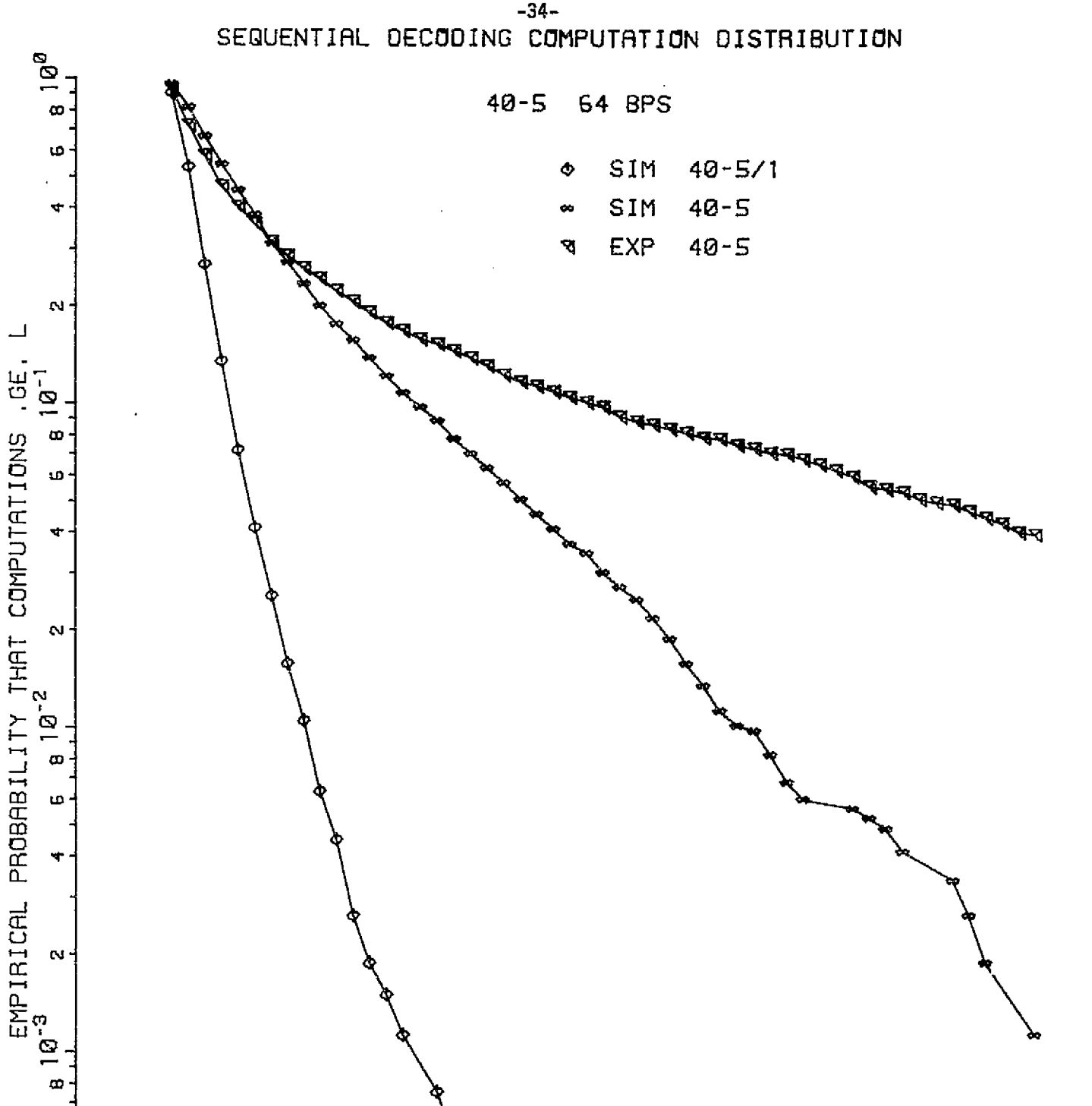
SEQUENTIAL DECODING COMPUTATION DISTRIBUTION
40-5 64 BPS
SIM 40-5/1
SIM 40-5
EXP 40-5
EMPIRICAL PROBABILITY THAT COMPUTATIONS .GE. L
L

SEQUENTIAL DECODING COMPUTATION DISTRIBUTION

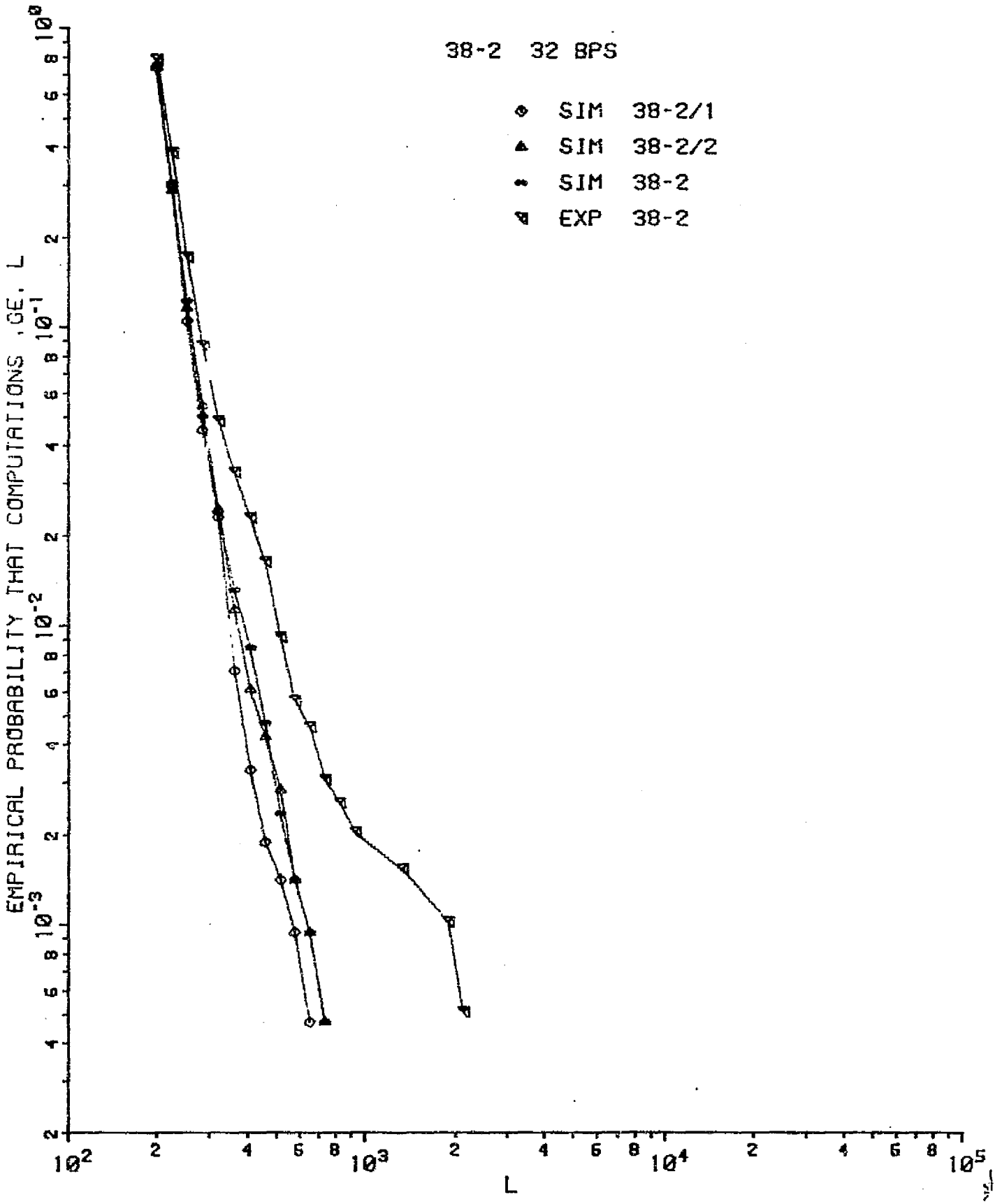

SEQUENTIAL DECODING COMPUTATION DISTRIBUTION

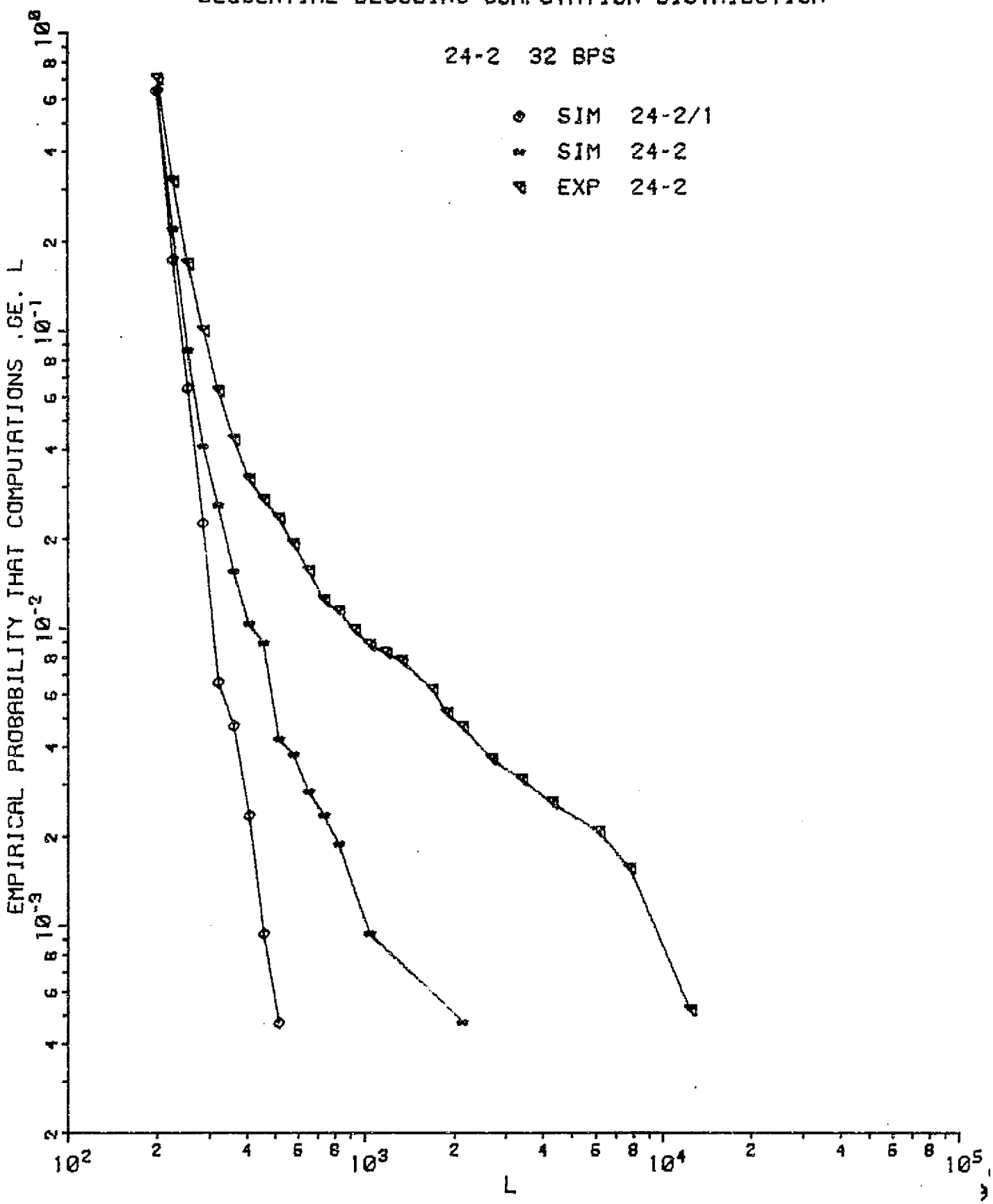

SEQUENTIAL DECODING COMPUTATION DISTRIBUTION

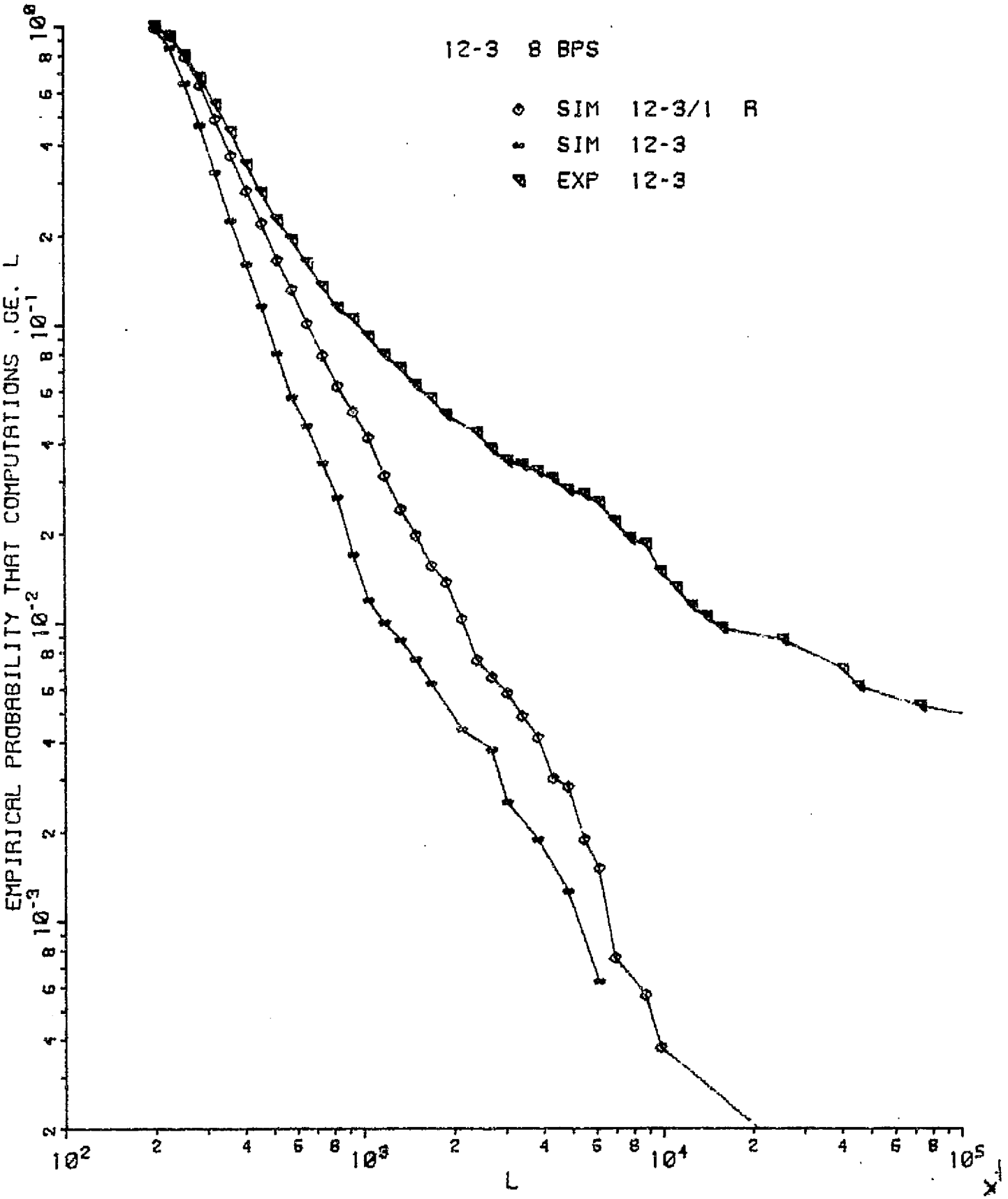

SEQUENTIAL DECODING COMPUTATION DISTRIBUTION

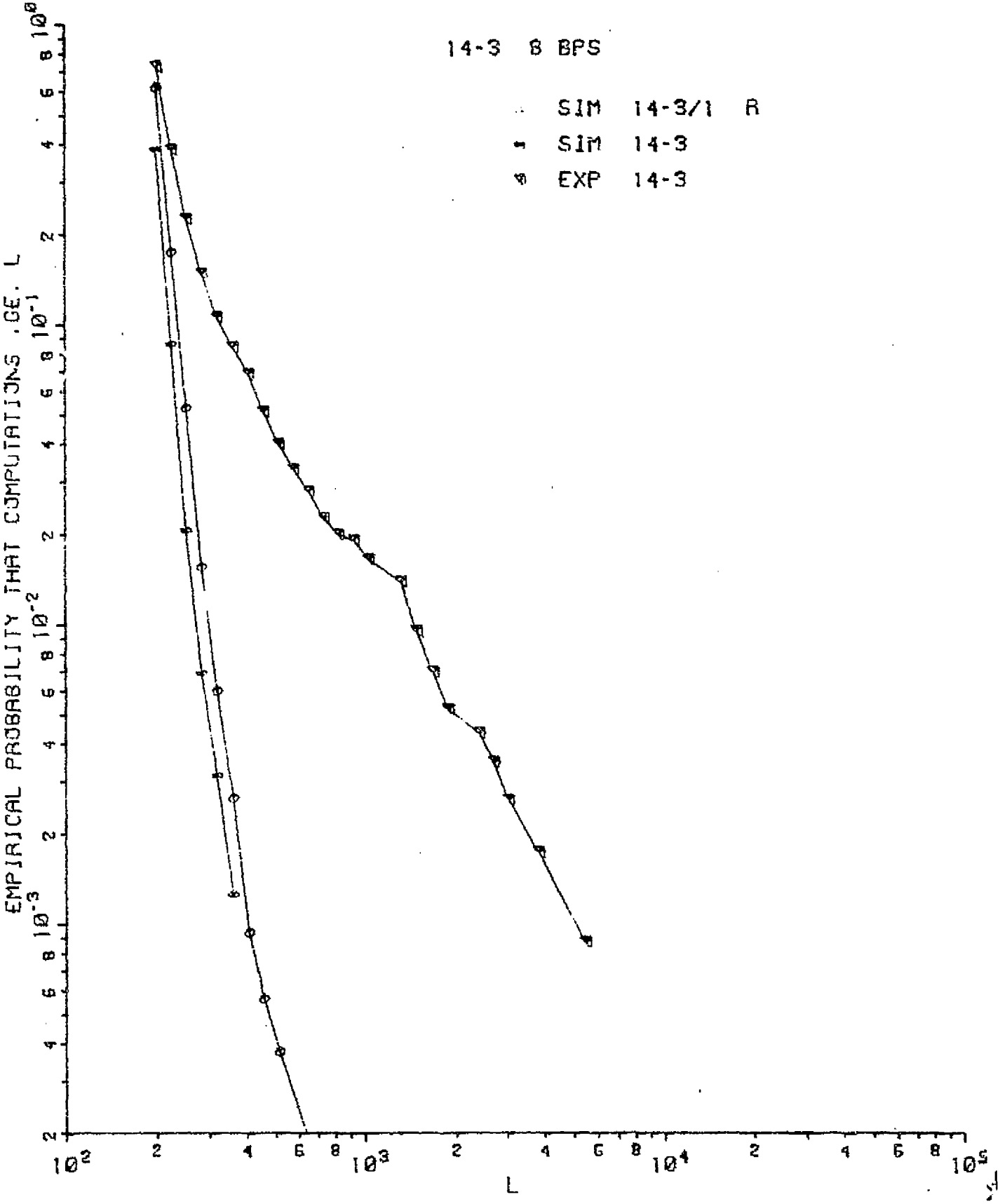

APPENDIX B

This appendix contains experimental data (EXP XX-X), gaussian channel only simulations (SIM XX-X/1), and gaussian channel with subcarrier loop simulations (SIM XX-X/3 and SIM XX-X/6), for the following runs in order of decreasing rate.

SEQUENTIAL DECODING COMPUTATION DISTRIBUTION

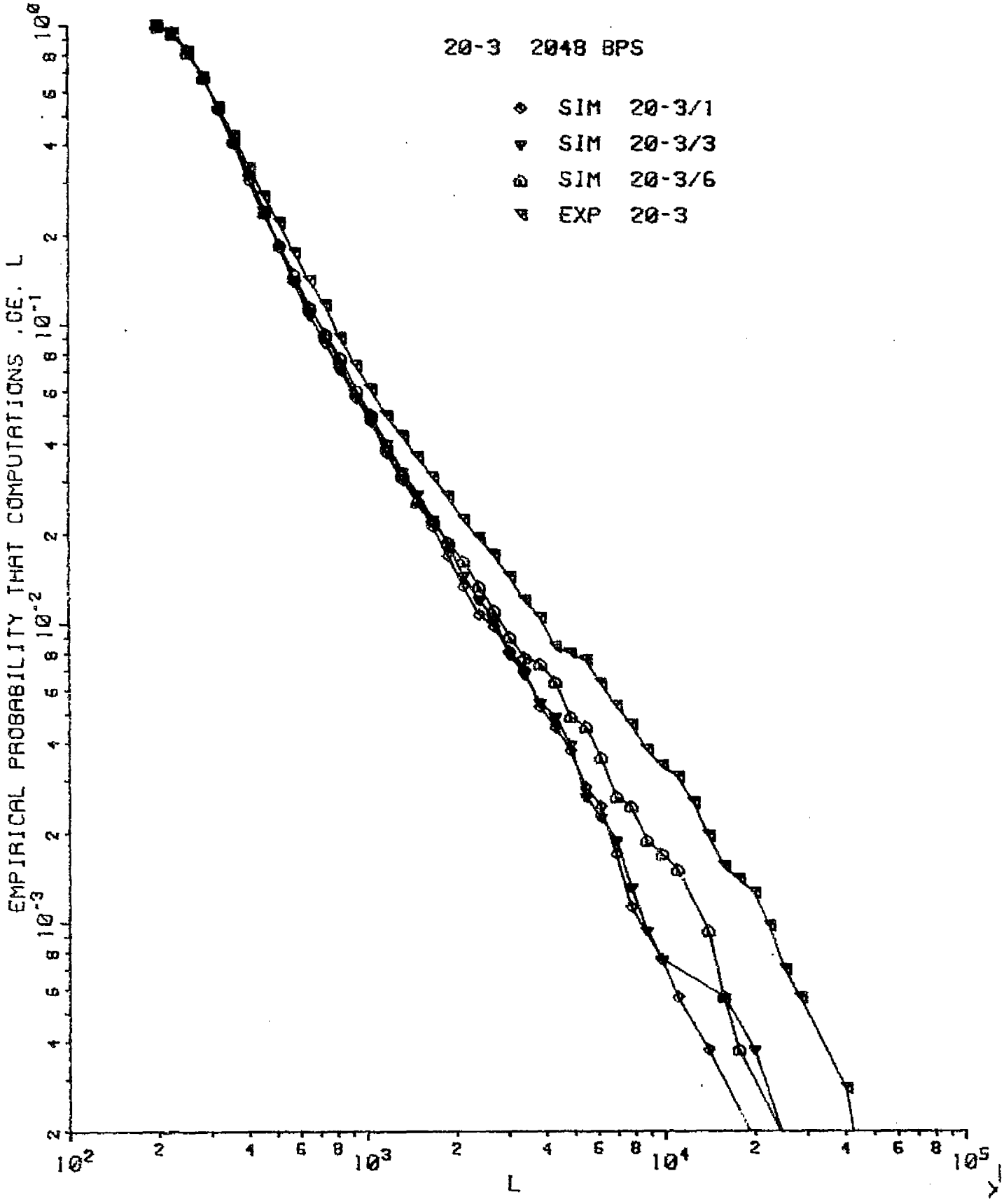

SEQUENTIAL DECODING COMPUTATION DISTRIBUTION

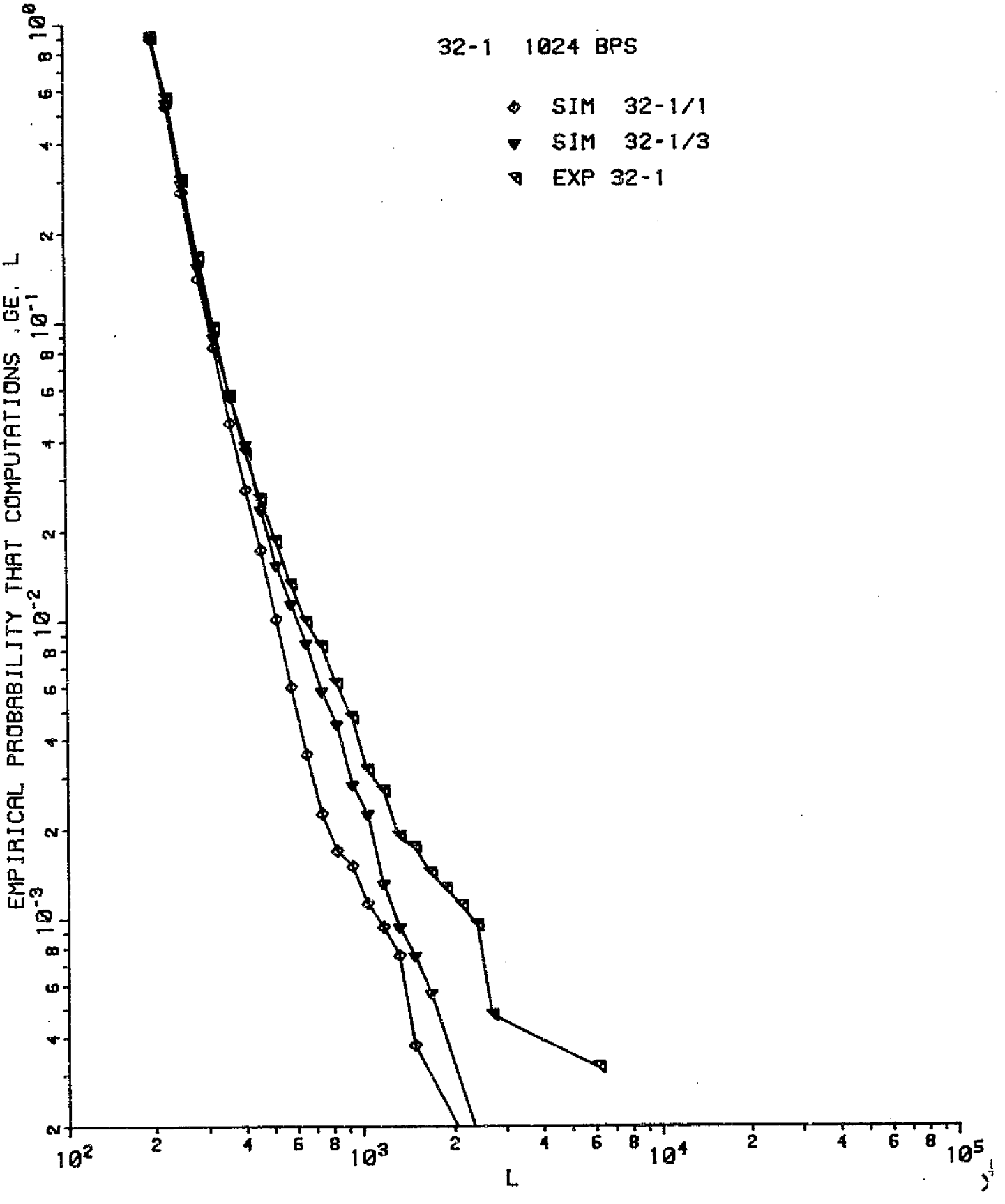

SEQUENTIAL DECODING COMPUTATION DISTRIBUTION

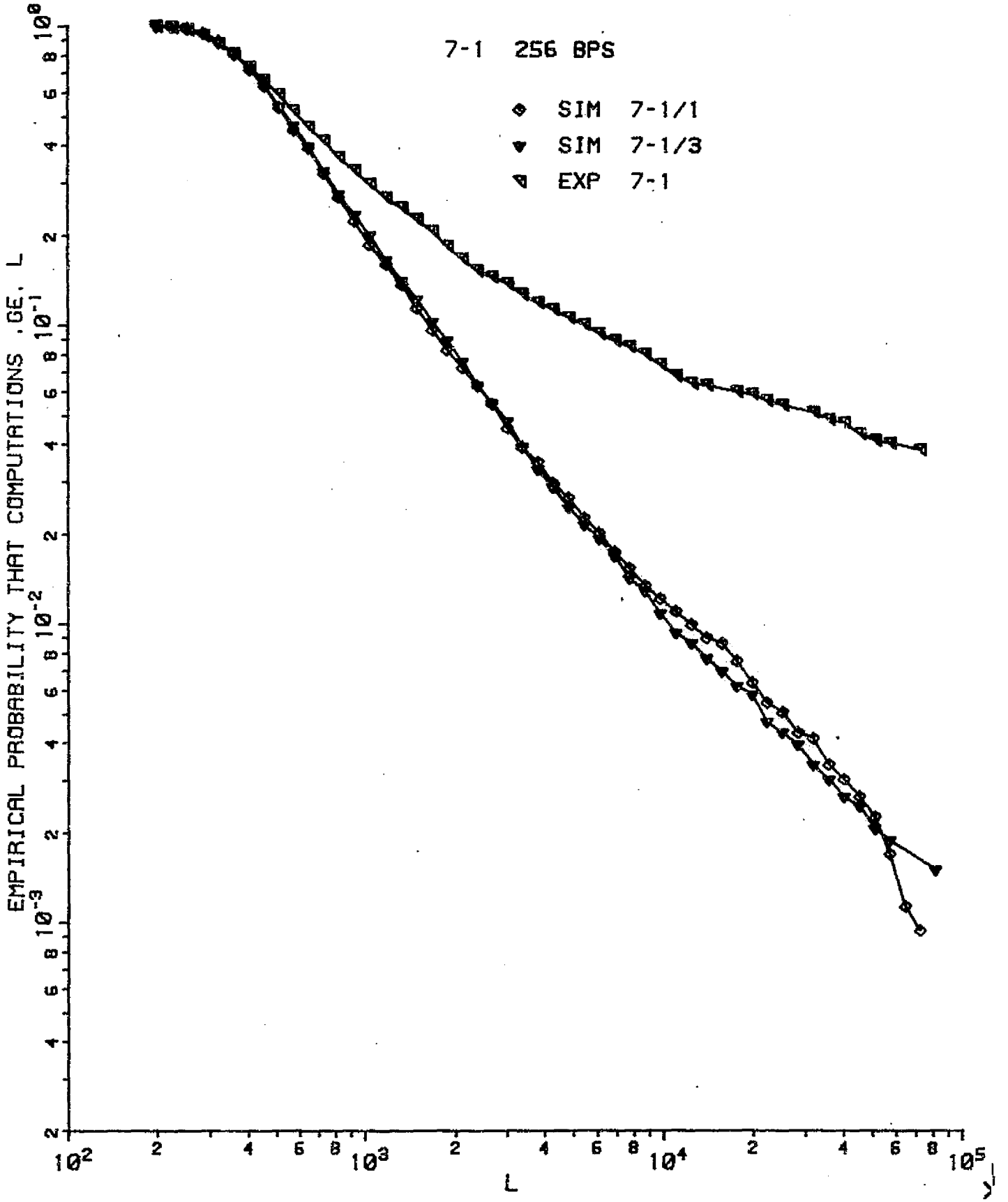

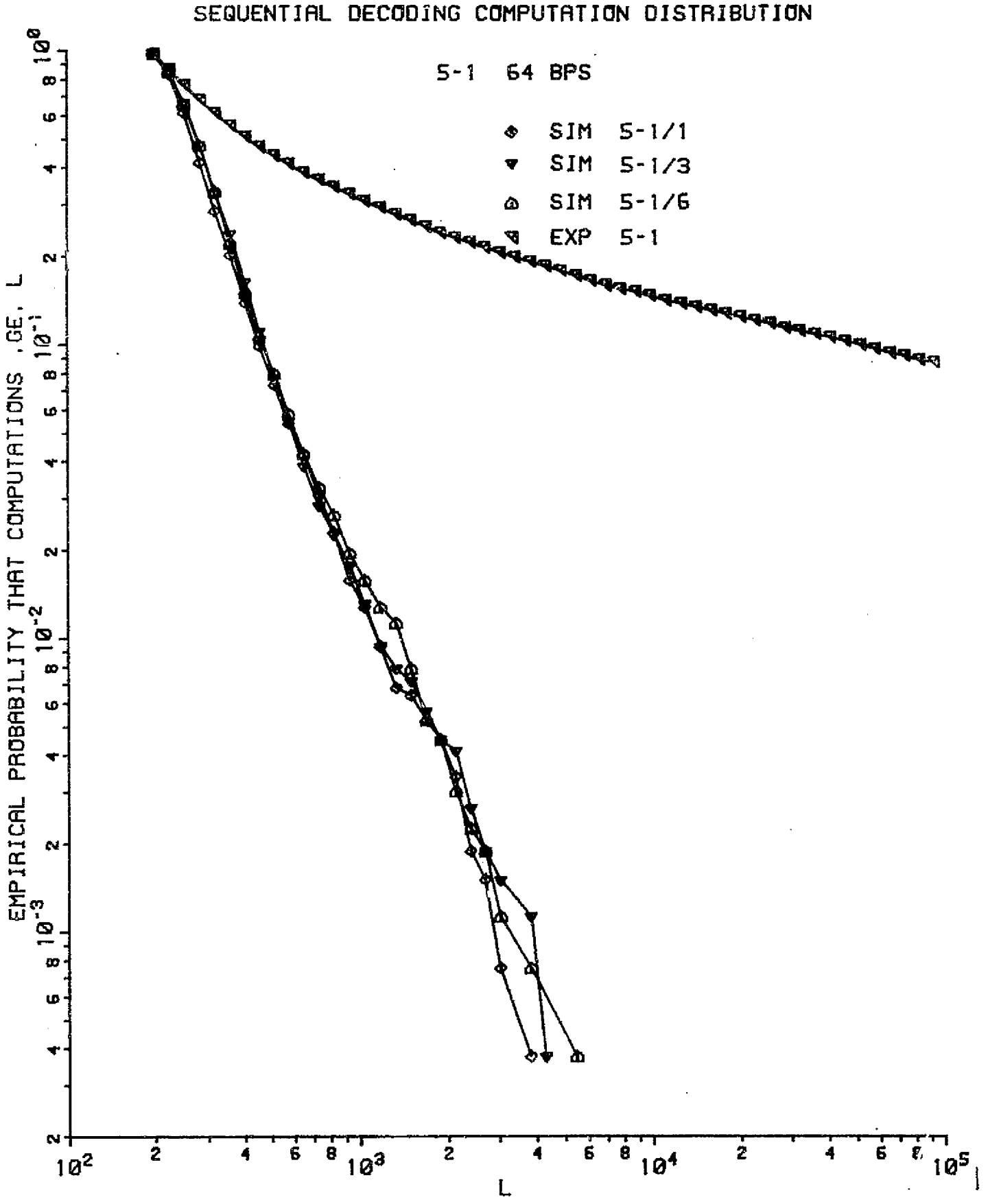
SEQUENTIAL DECODING COMPUTATION DISTRIBUTION
5-1 64 BPS
SIM 5-1/1
SIM 5-1/3
SIM 5-1/6
EXP 5-1
EMPIRICAL PROBABILITY THAT COMPUTATIONS ,GE, L
L

SEQUENTIAL DECODING COMPUTATION DISTRIBUTION

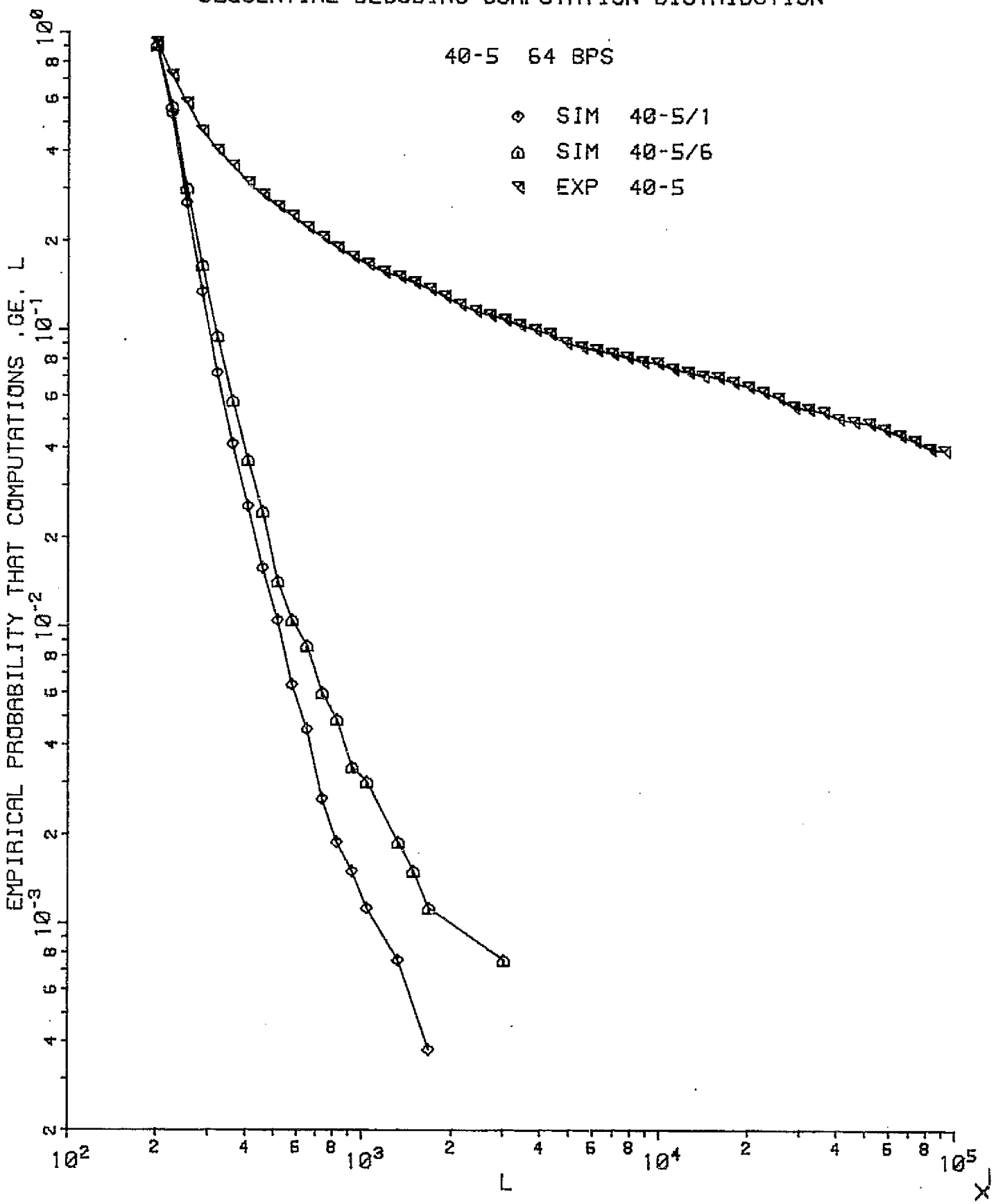

SEQUENTIAL DECODING COMPUTATION DISTRIBUTION

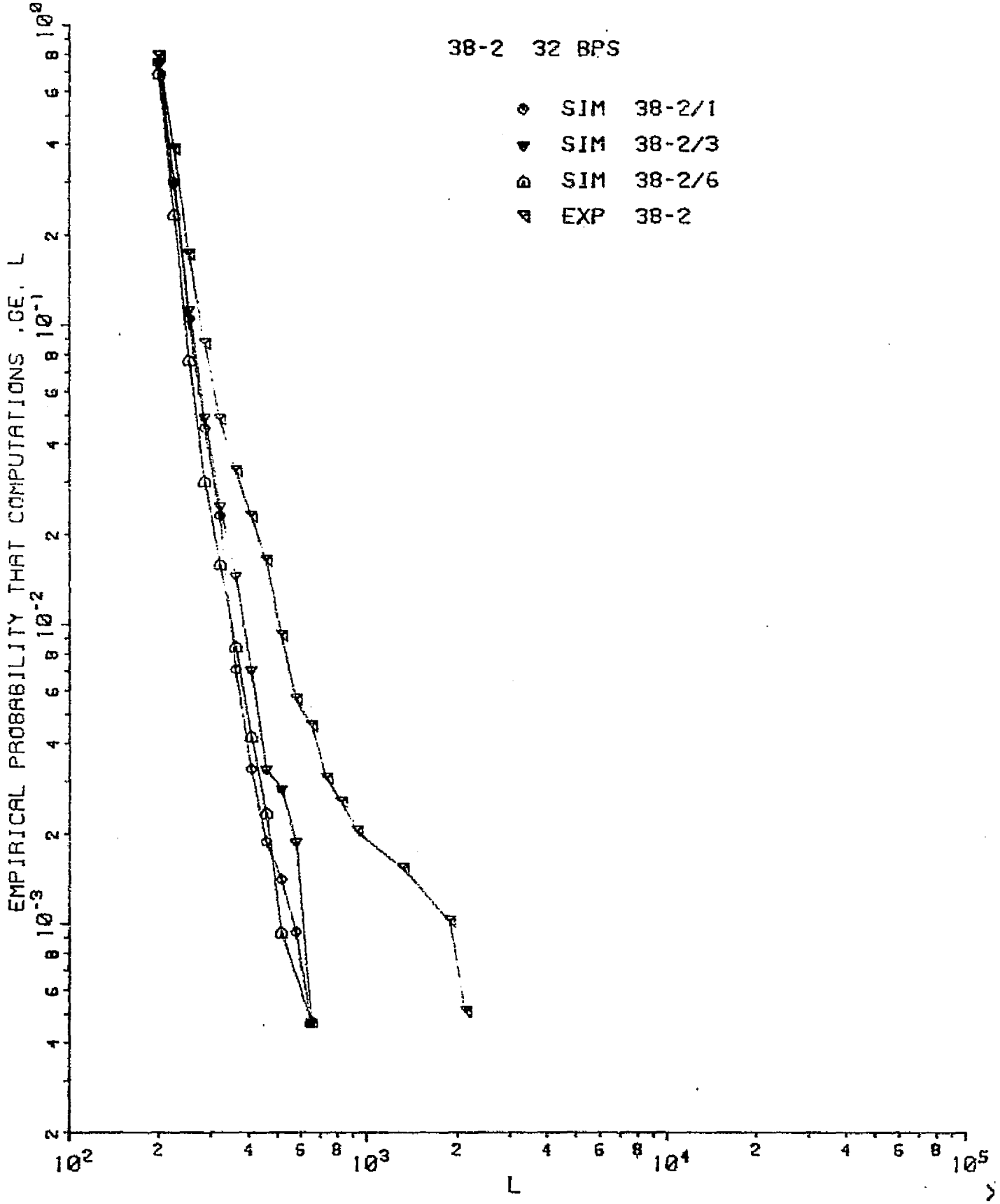

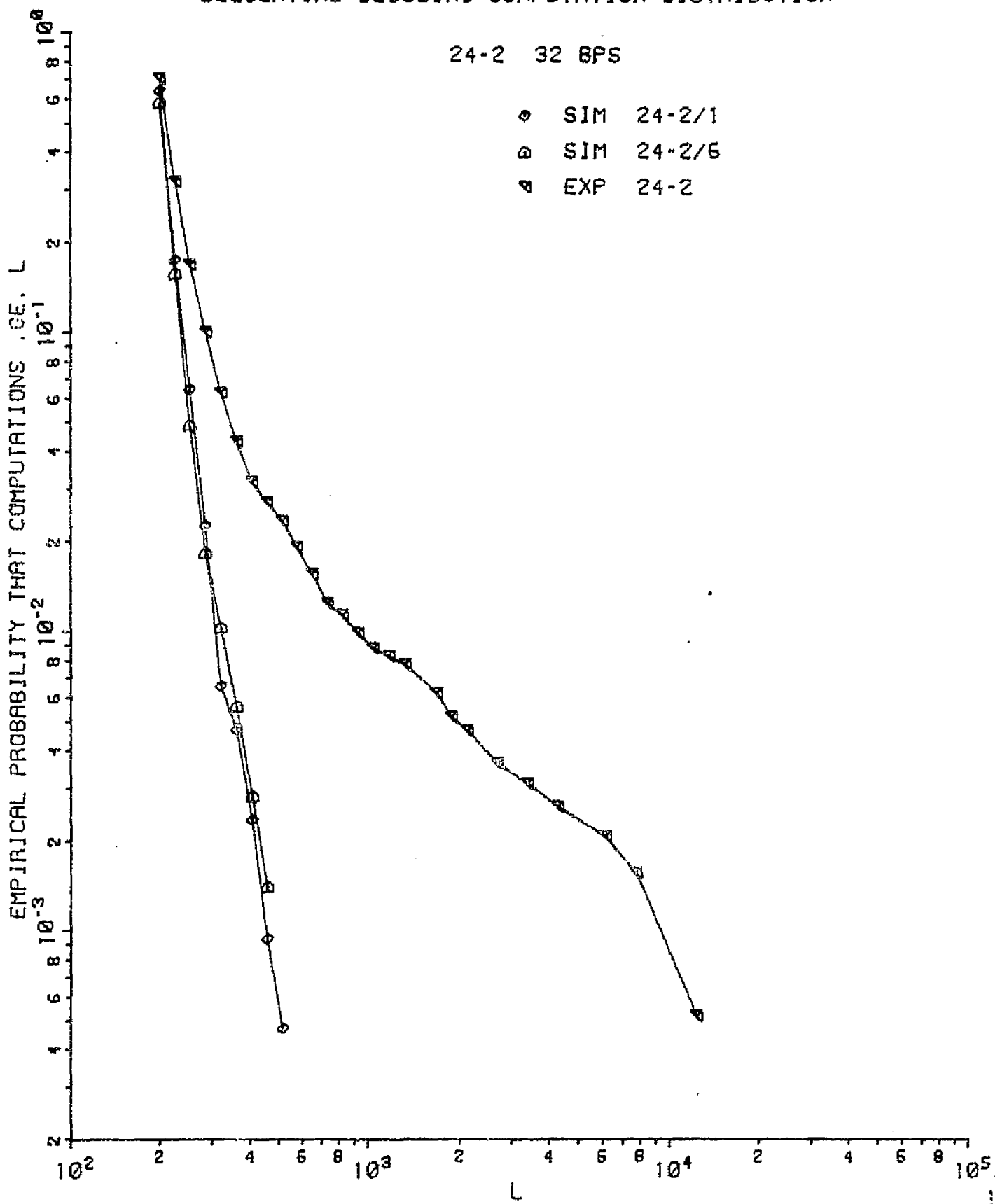
SEQUENTIAL DECODING COMPUTATION DISTRIBUTION
24-2 32 BPS
SIM 24-2/1
SIM 24-2/6
EXP 24-2
EMPIRICAL PROBABILITY THAT COMPUTATIONS .GE. L
L

SEQUENTIAL DECODING COMPUTATION DISTRIBUTION

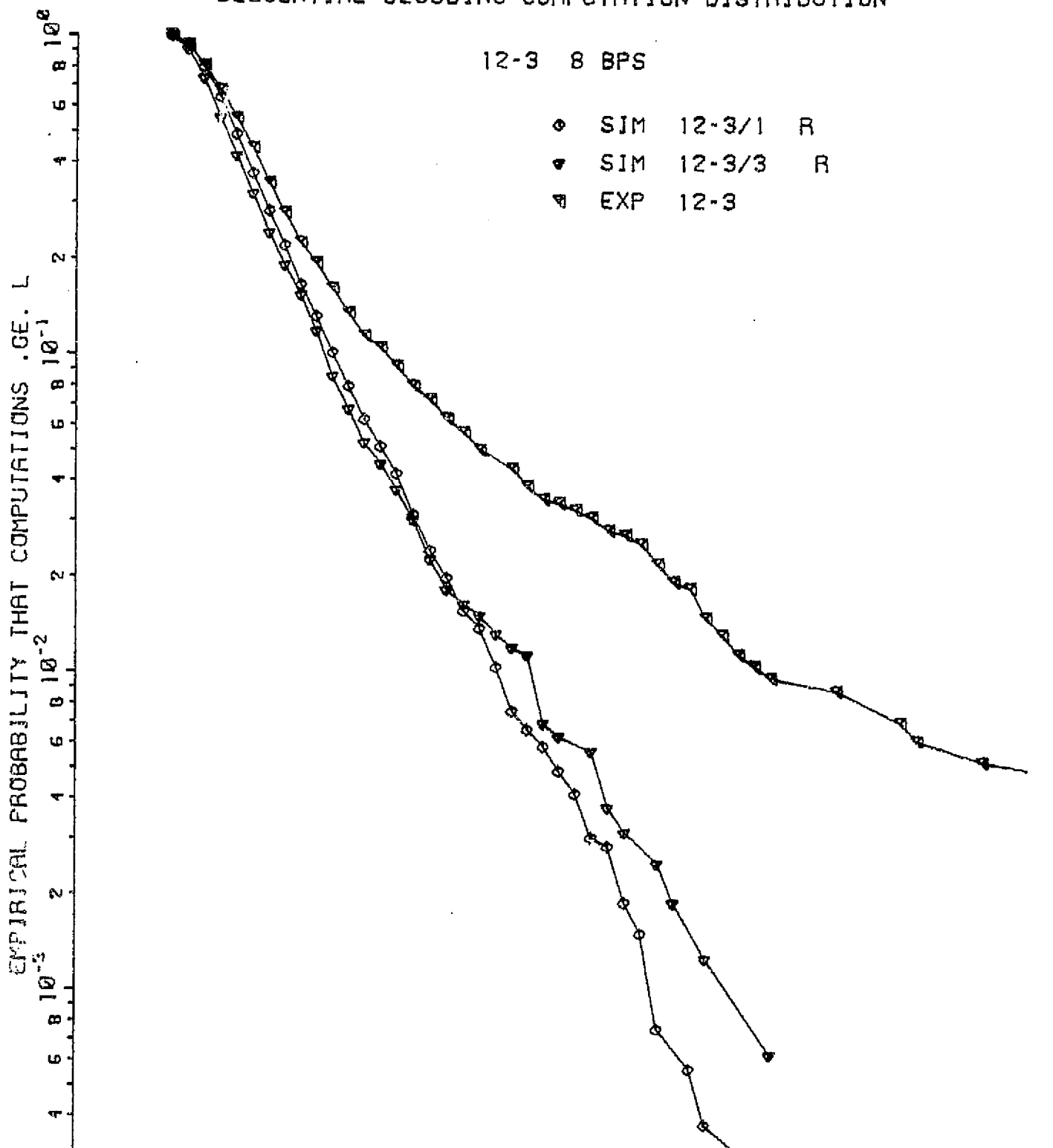

SEQUENTIAL DECODING COMPUTATION DISTRIBUTION

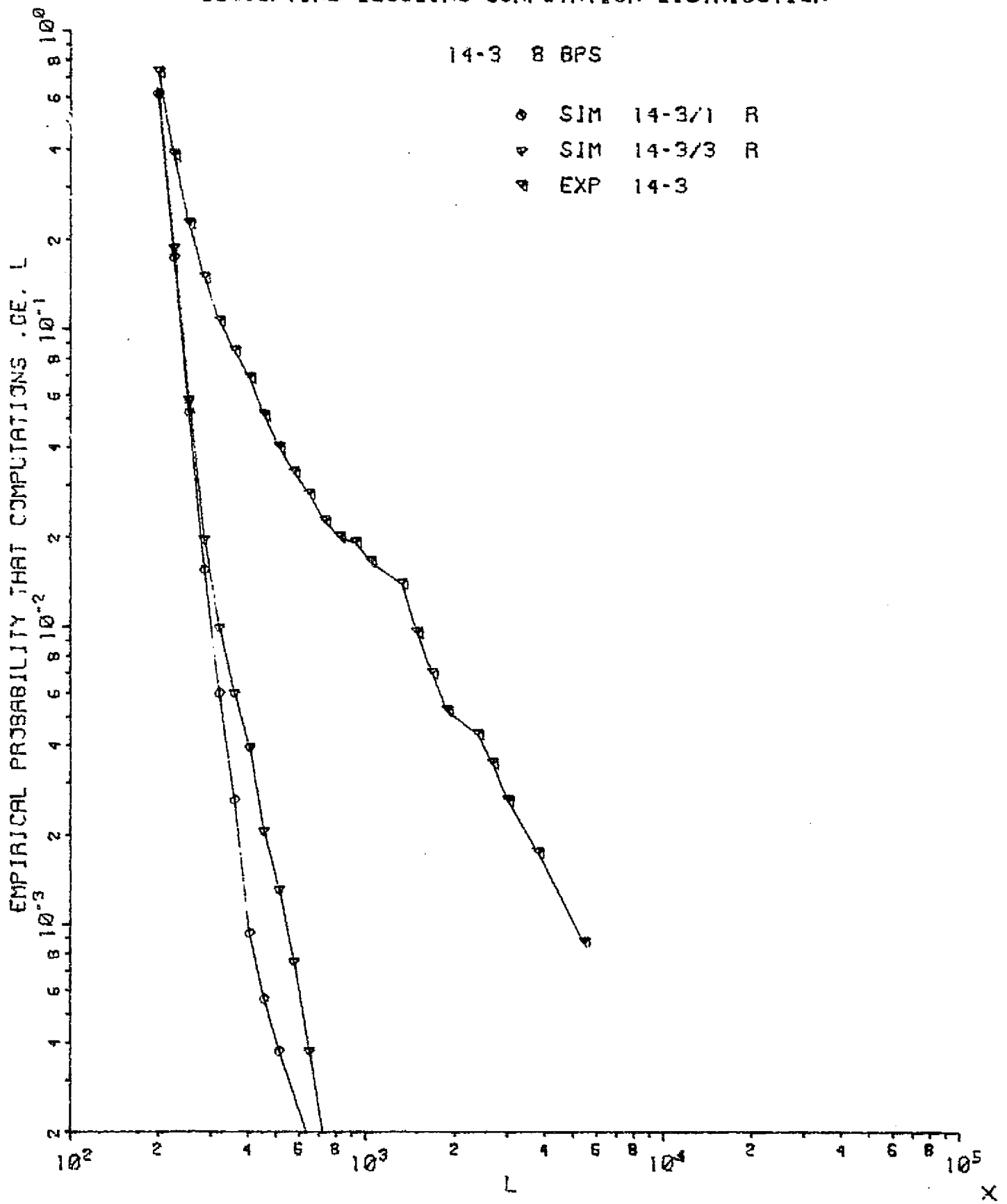

APPENDIX C

This appendix contains experimental data (EXP XX-X), gaussian channel only simulations (SIM XX-X/1), and gaussian channel with both carrier phase lock loop and subcarrier (SDA) phase lock loop (SIM XX-X/4, SIM XX-X/5, SIM XX-X/7), for the following runs in order of decreasing rate.

SEQUENTIAL DECODING COMPUTATION DISTRIBUTION

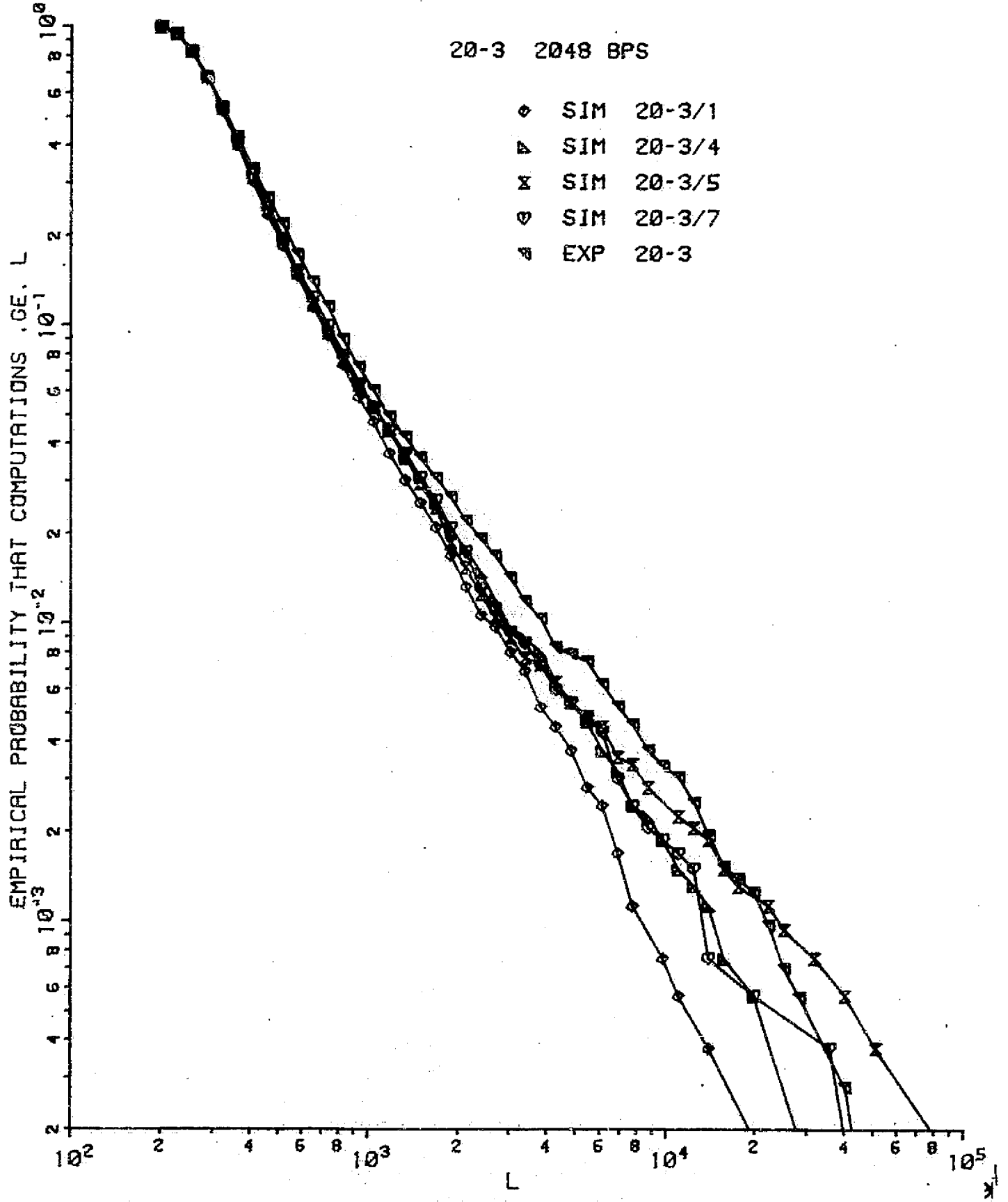

SEQUENTIAL DECODING COMPUTATION DISTRIBUTION

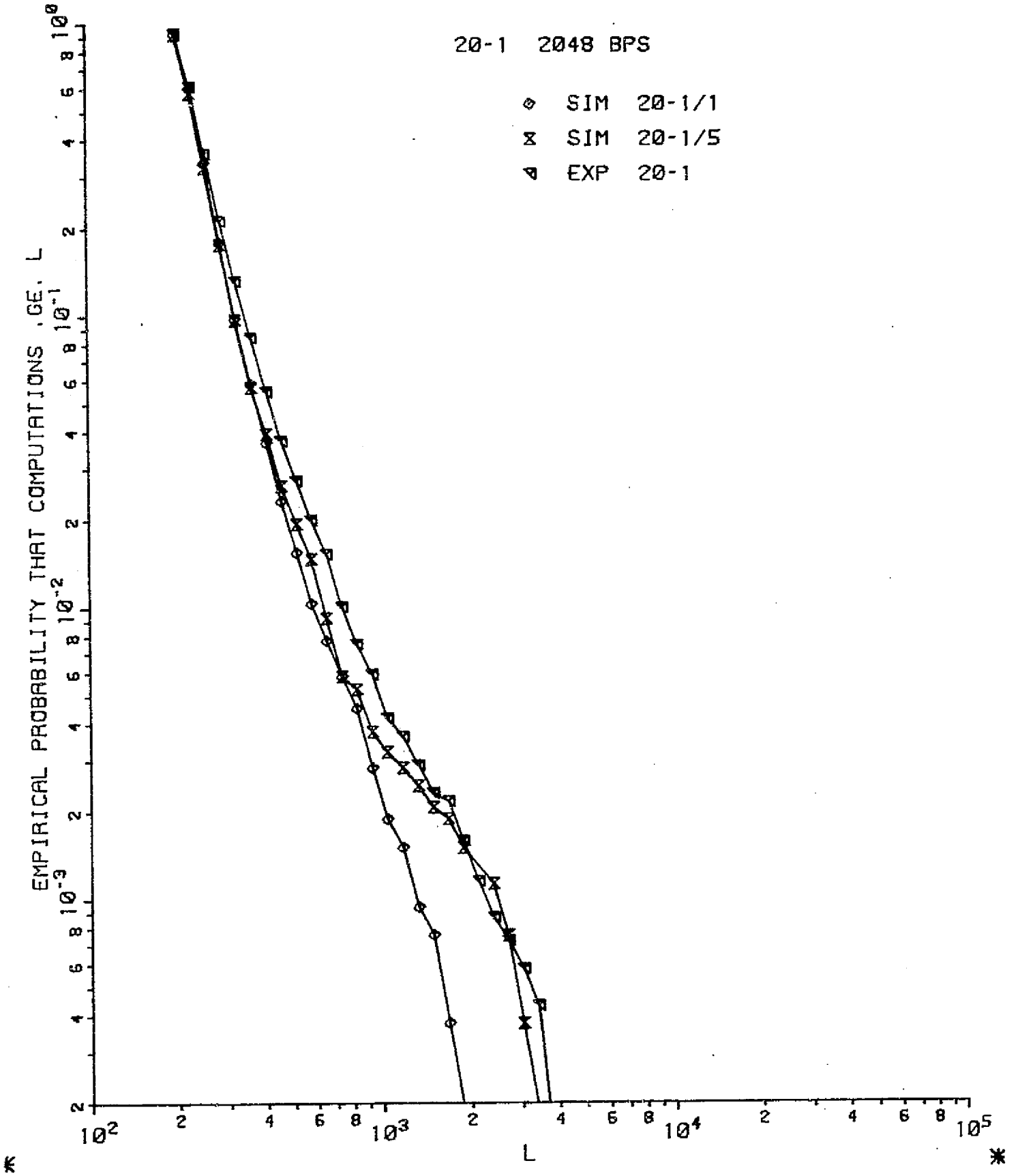

SEQUENTIAL DECODING COMPUTATION DISTRIBUTION

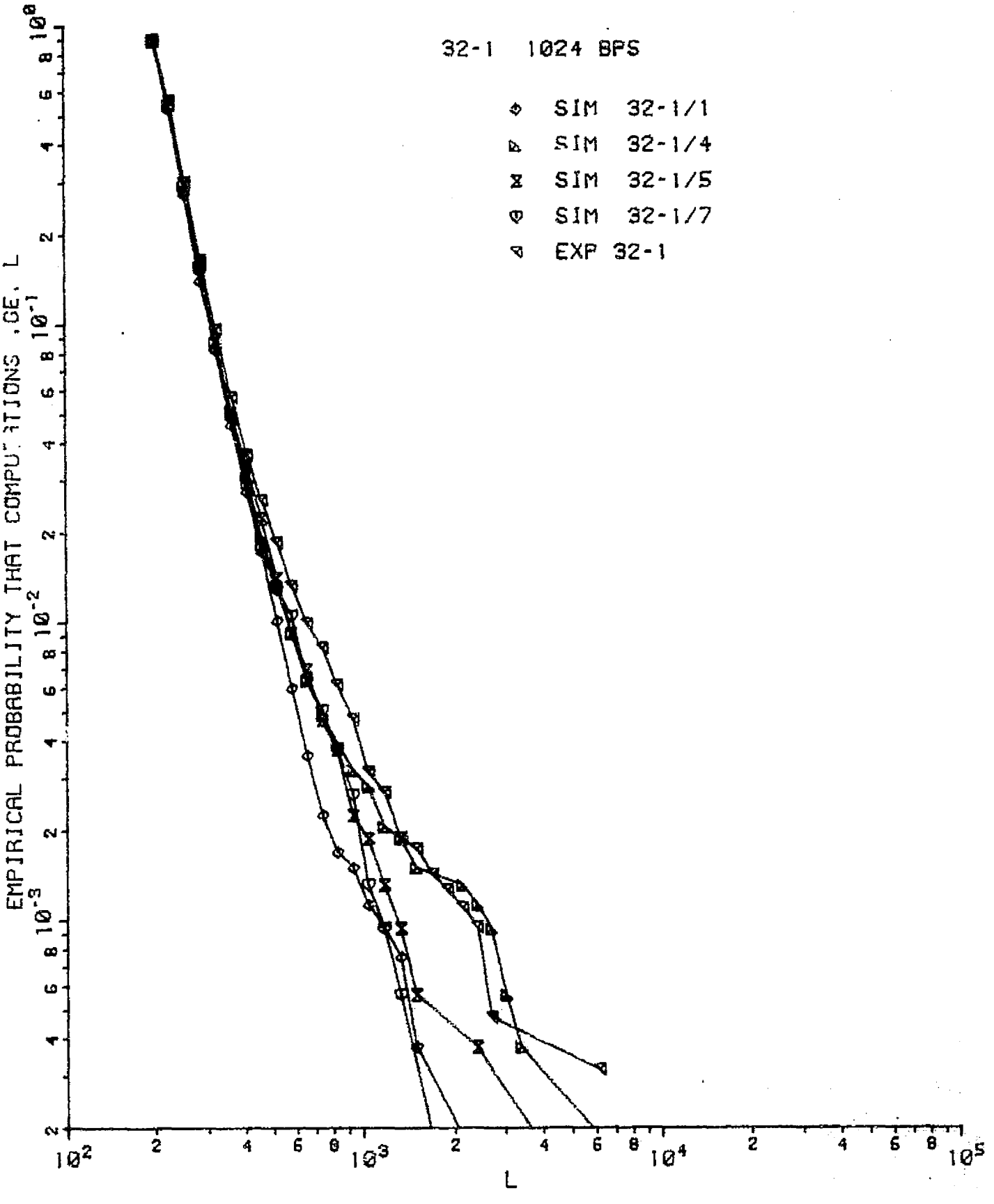

*

SEQUENTIAL DECODING COMPUTATION DISTRIBUTION

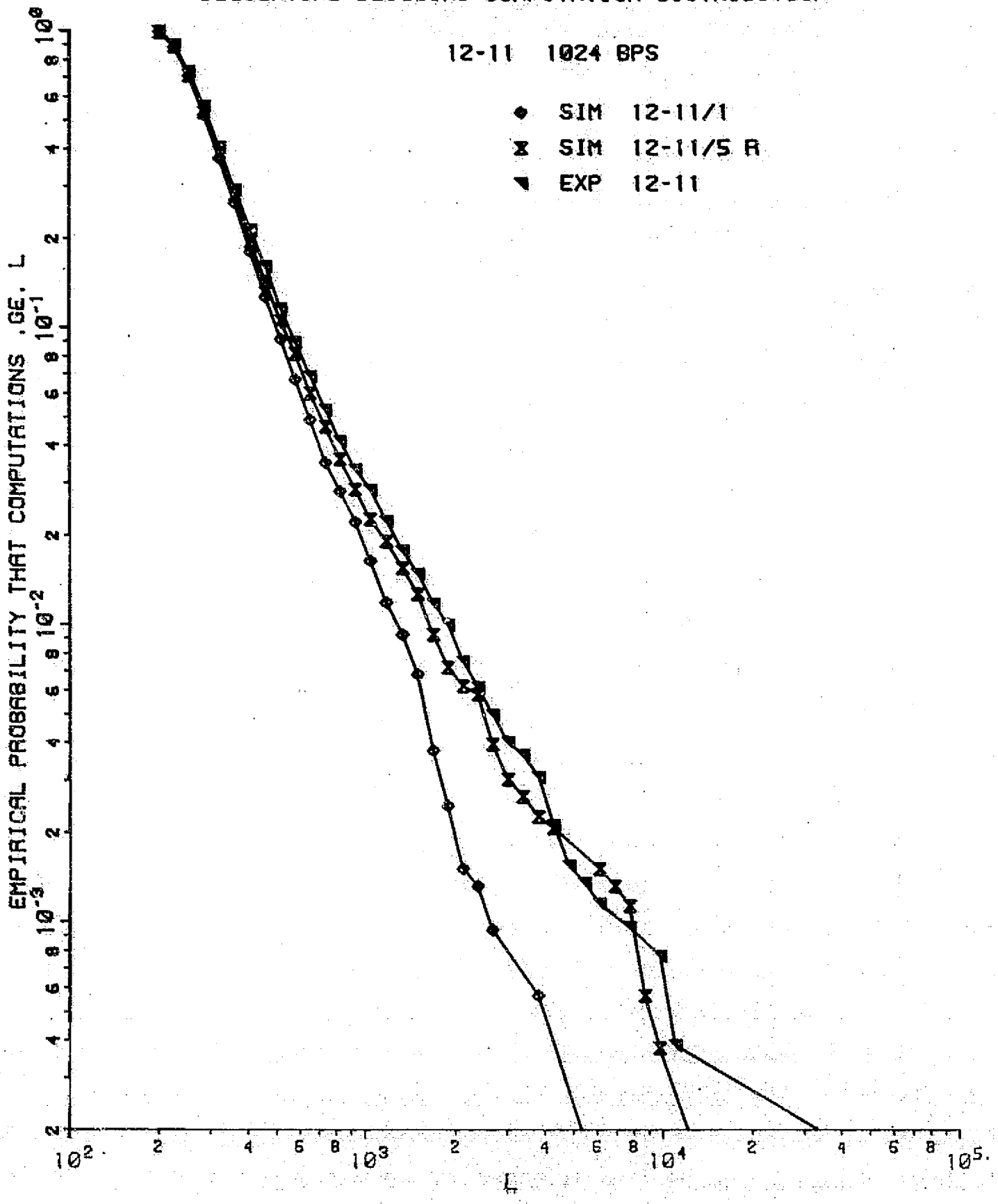

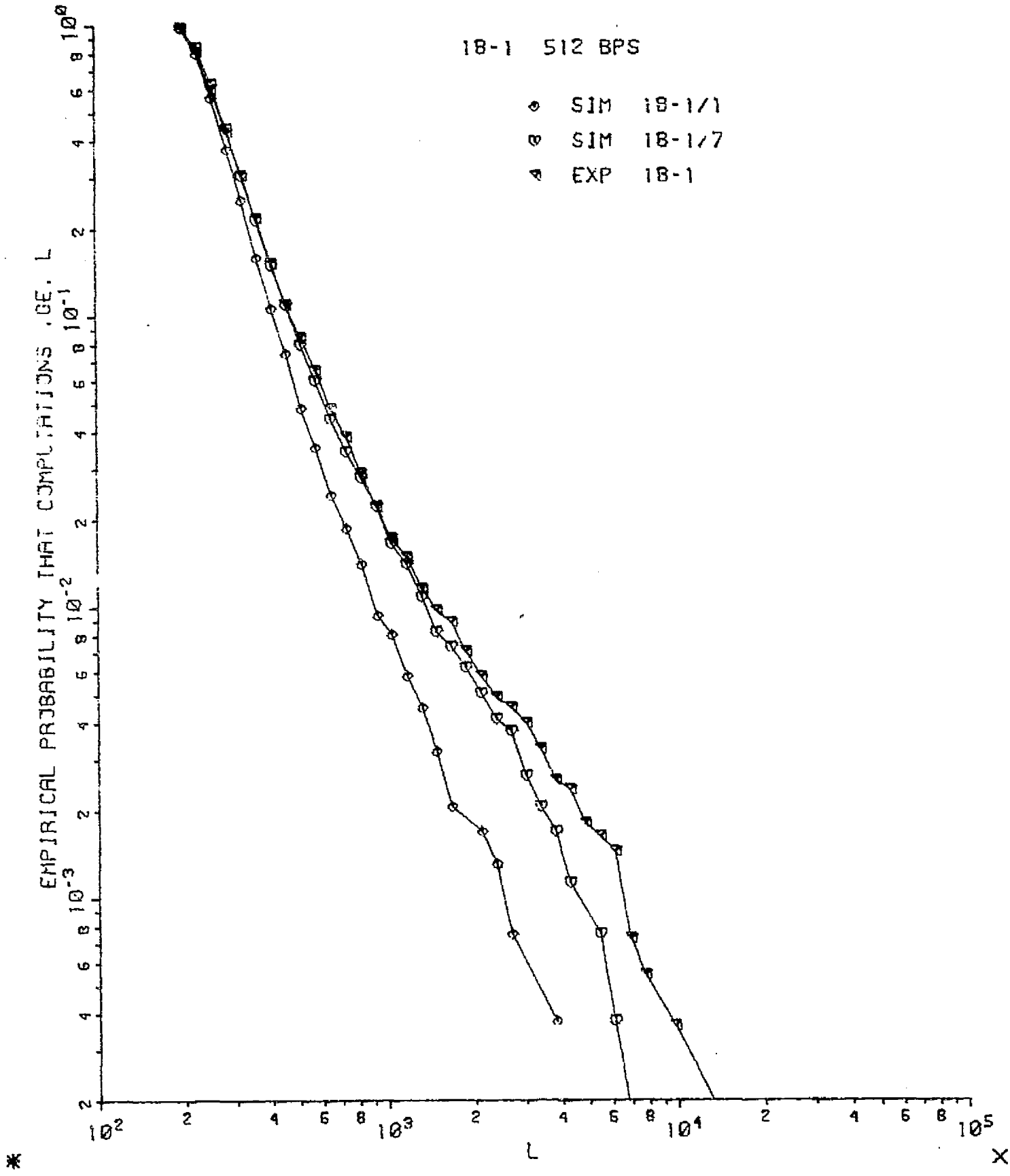
SEQUENTIAL DECODING COMPUTATION DISTRIBUTION
18-1 512 BPS
SIM 18-1/1
SIM 18-1/7
EXP 18-1
EMPIRICAL PROBABILITY THAT COMPUTATIONS .GE. L
L

SEQUENTIAL DECODING COMPUTATION DISTRIBUTION

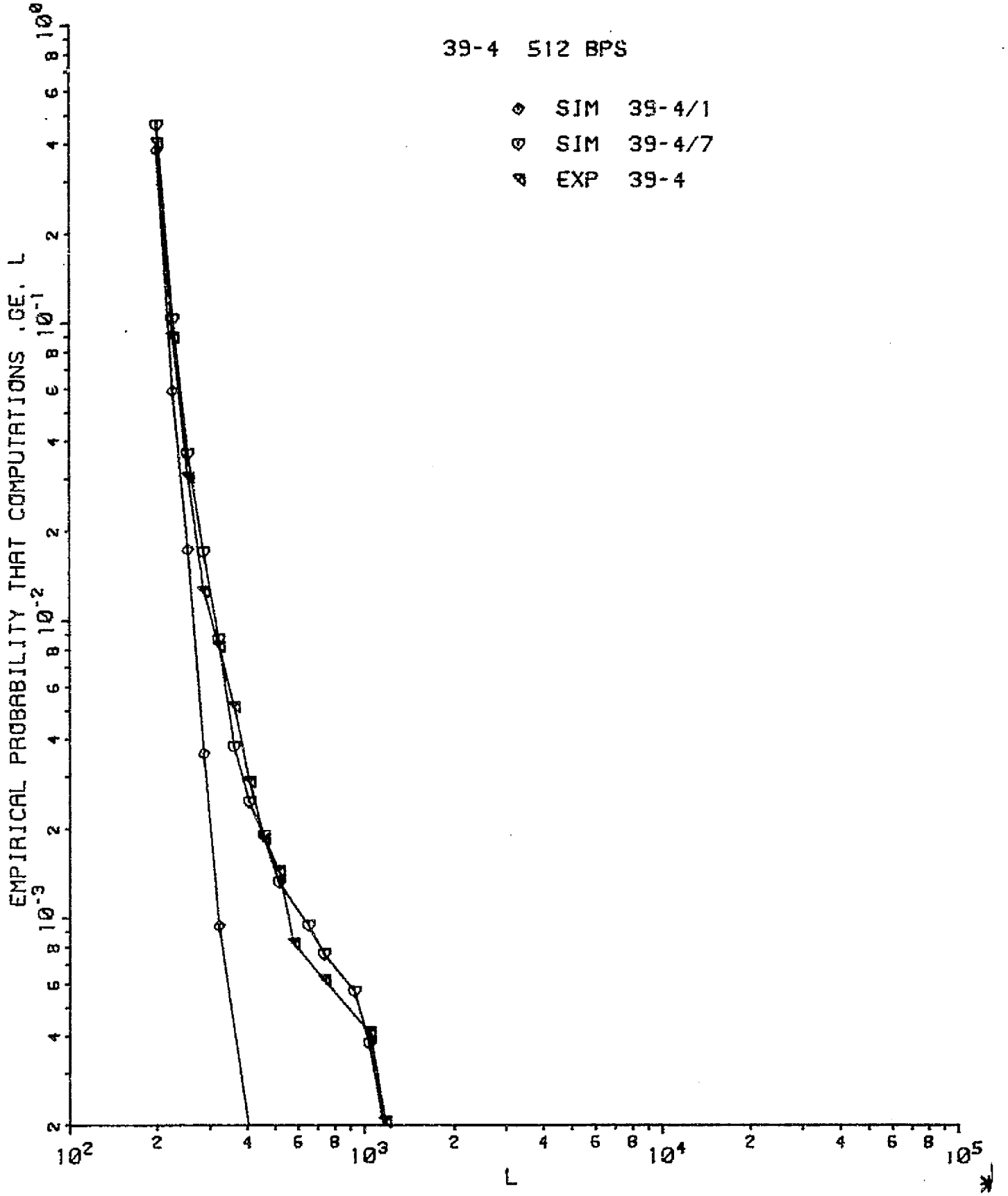

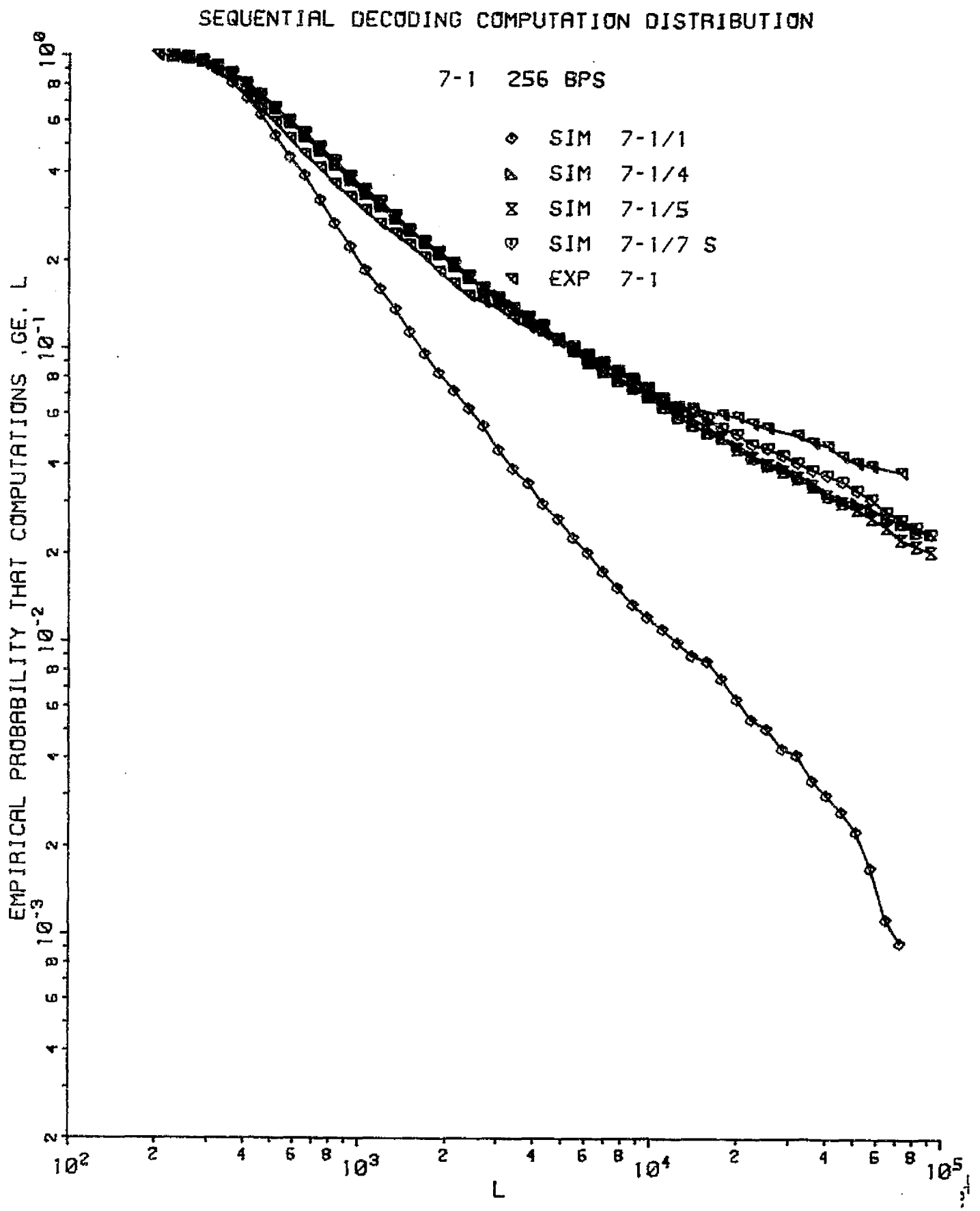
SEQUENTIAL DECODING COMPUTATION DISTRIBUTION
7-1 256 BPS
SIM 7-1/1
SIM 7-1/4
SIM 7-1/5
SIM 7-1/7 S
EXP 7-1
EMPIRICAL PROBABILITY THAT COMPUTATIONS .GE. L
L
10^0
10^{-1}
10^{-2}
10^{-3}
10^2
10^3
10^4
10^5

SEQUENTIAL DECODING COMPUTATION DISTRIBUTION

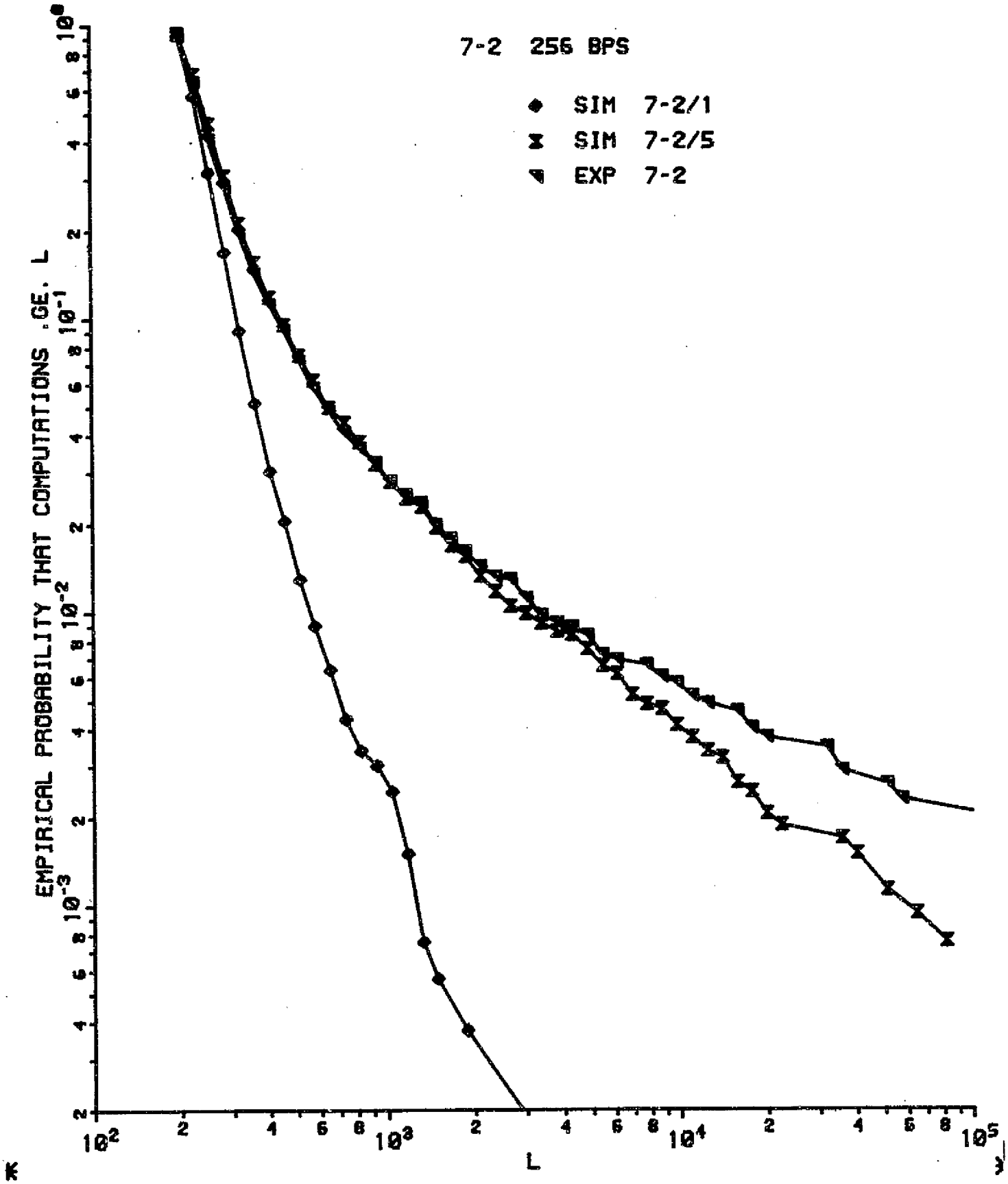

SEQUENTIAL DECODING COMPUTATION DISTRIBUTION

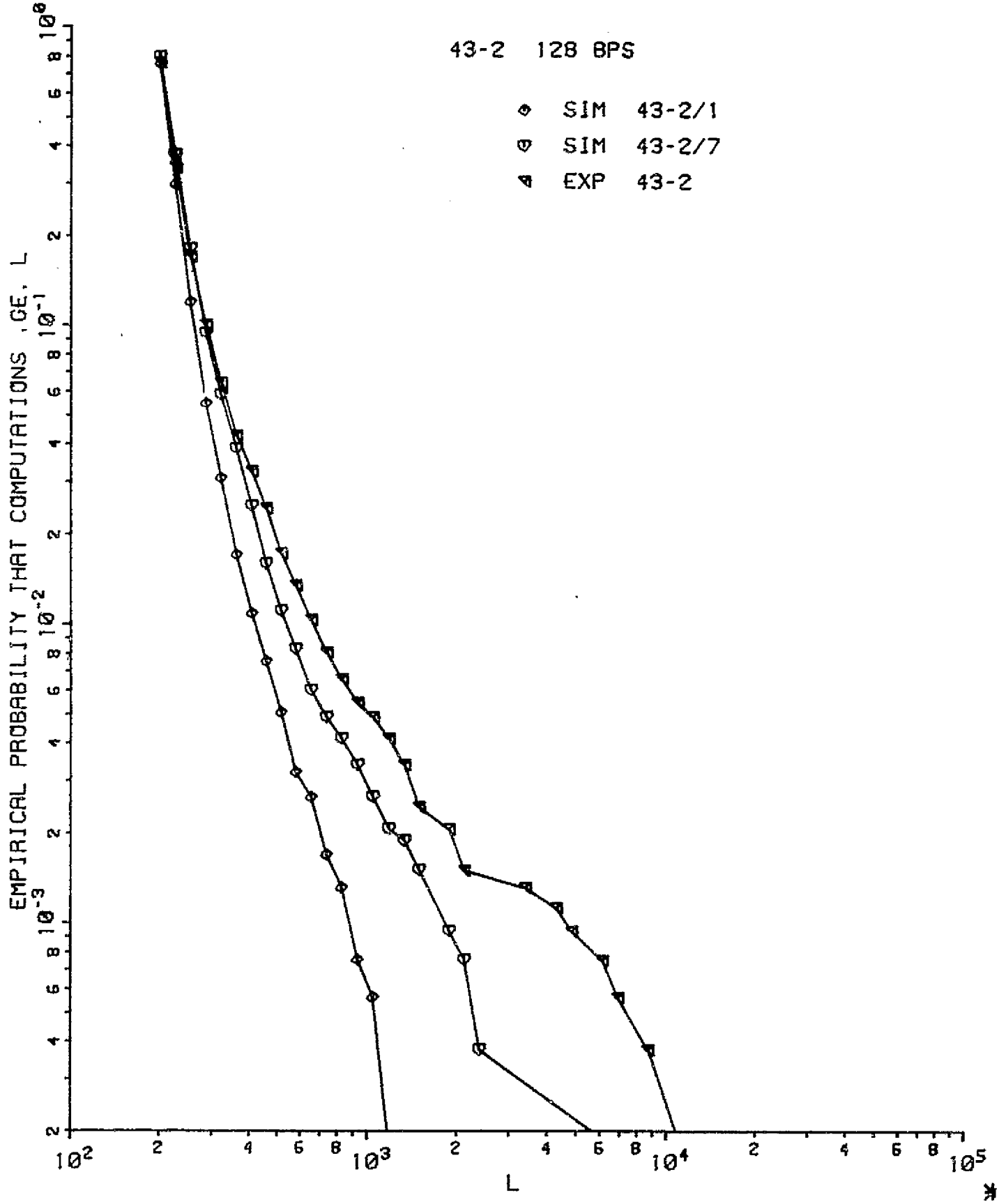

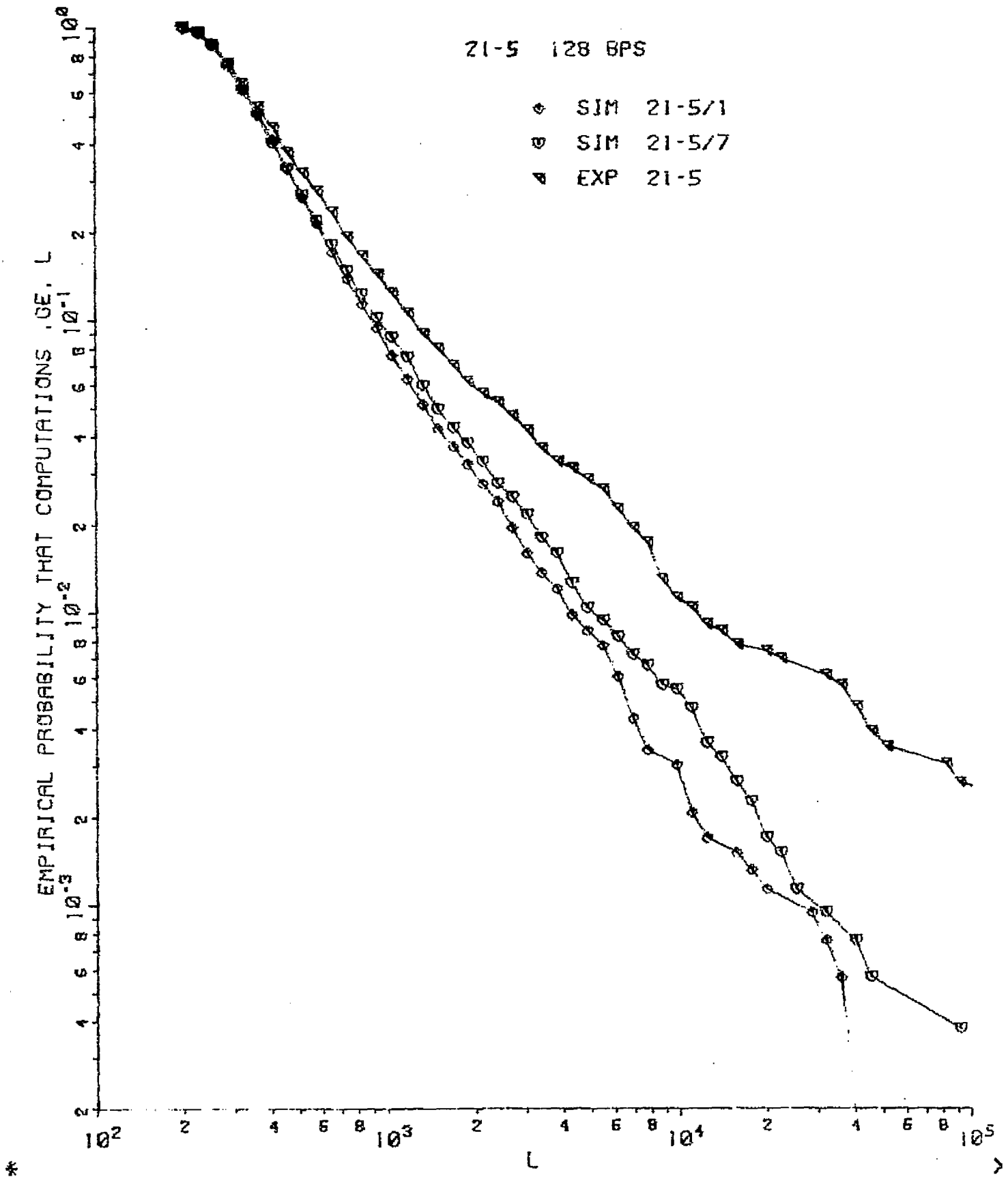
SEQUENTIAL DECODING COMPUTATION DISTRIBUTION
21-5 128 BPS
SIM 21-5/1
SIM 21-5/7
EXP 21-5
EMPIRICAL PROBABILITY THAT COMPUTATIONS .GE. L
L

SEQUENTIAL DECODING COMPUTATION DISTRIBUTION

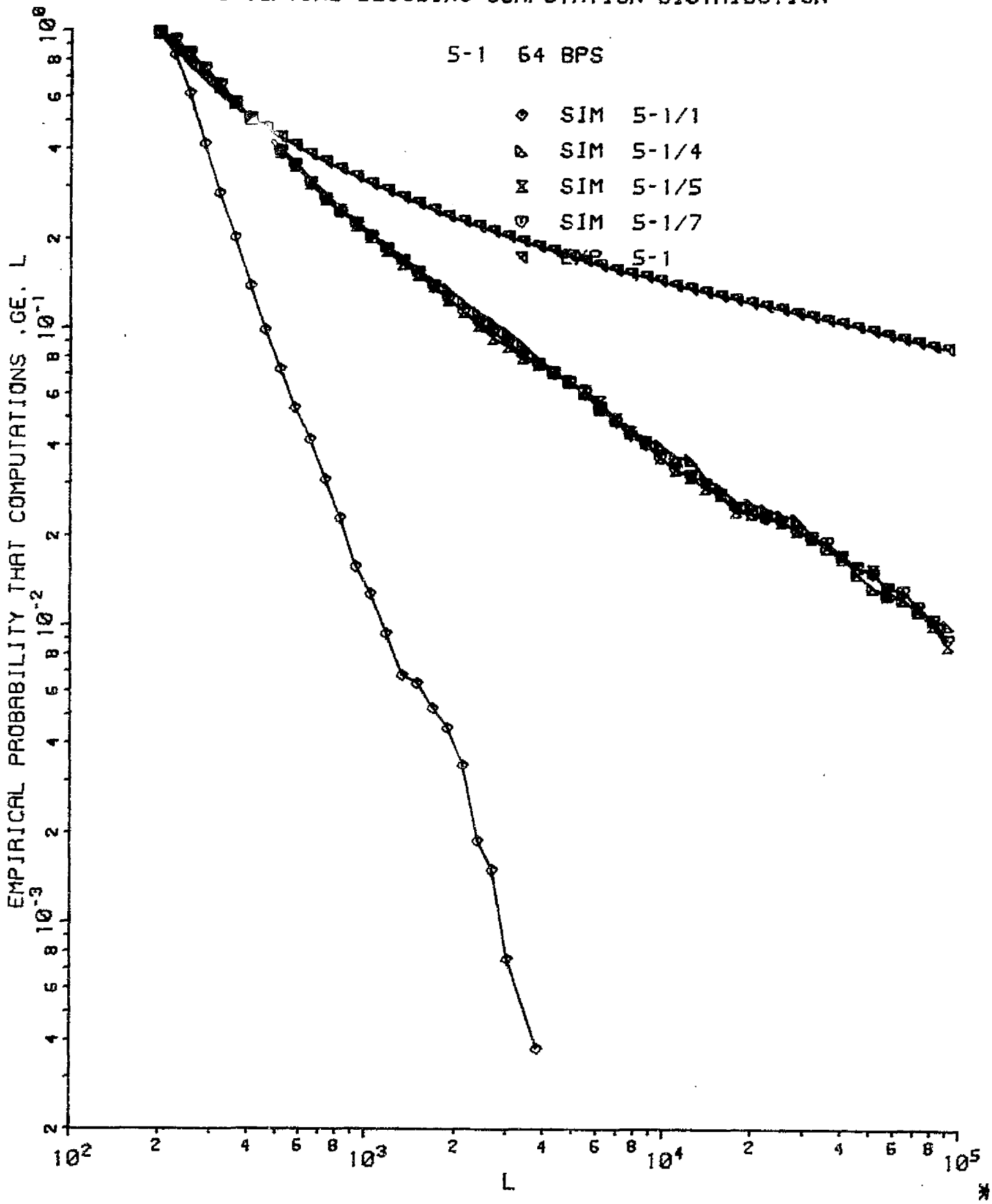

SEQUENTIAL DECODING COMPUTATION DISTRIBUTION

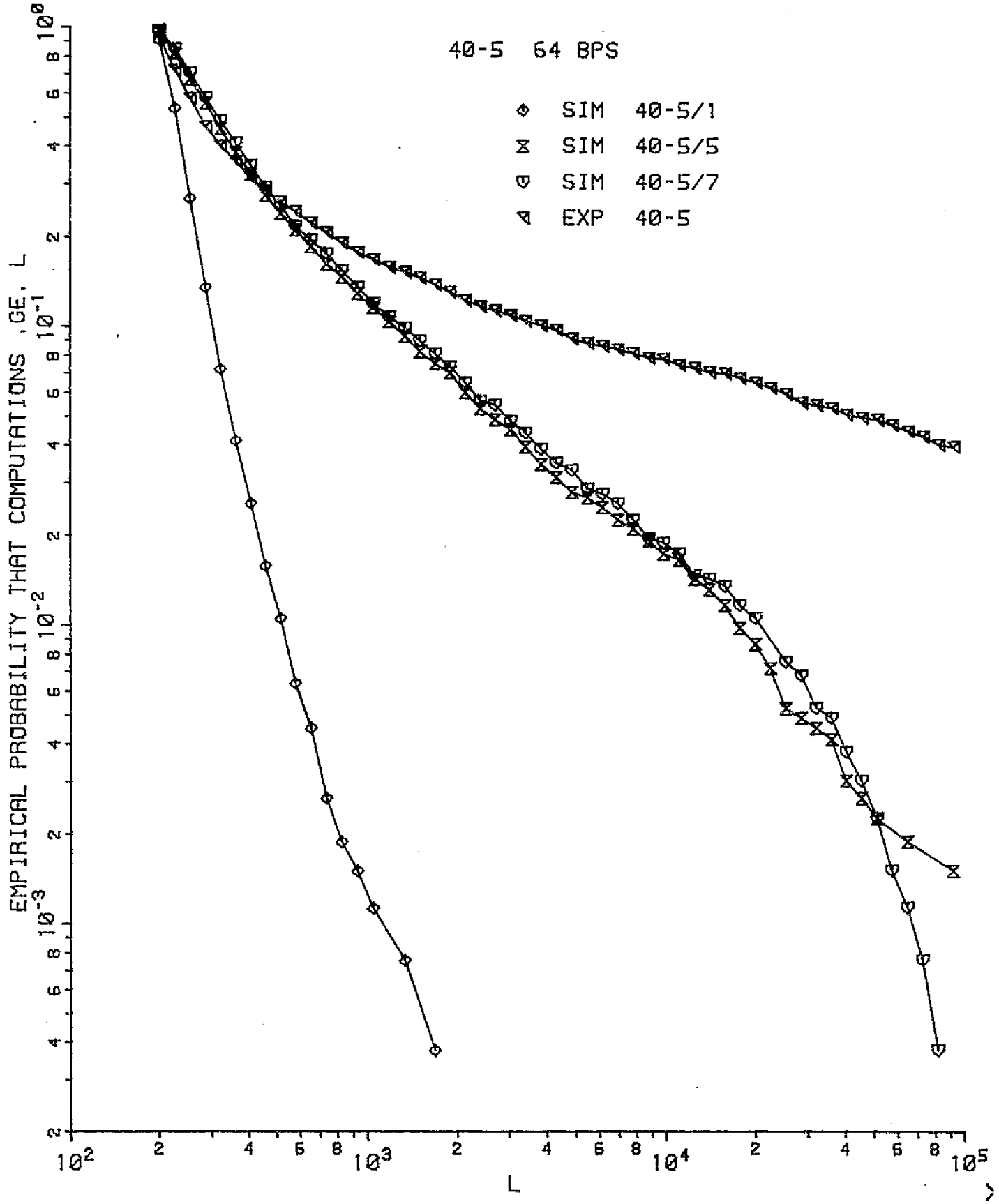

SEQUENTIAL DECODING COMPUTATION DISTRIBUTION

SEQUENTIAL DECODING COMPUTATION DISTRIBUTION

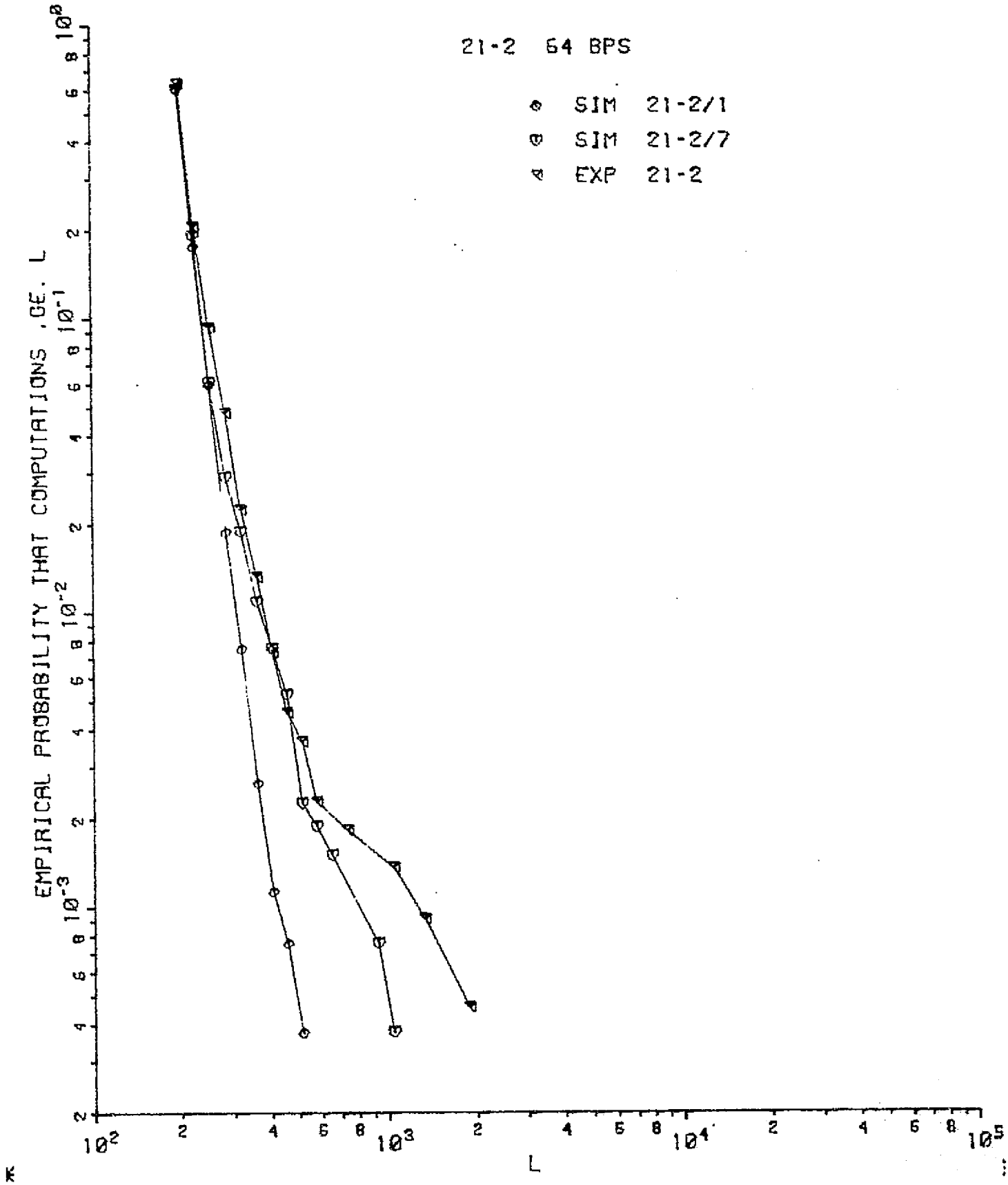

SEQUENTIAL DECODING COMPUTATION DISTRIBUTION

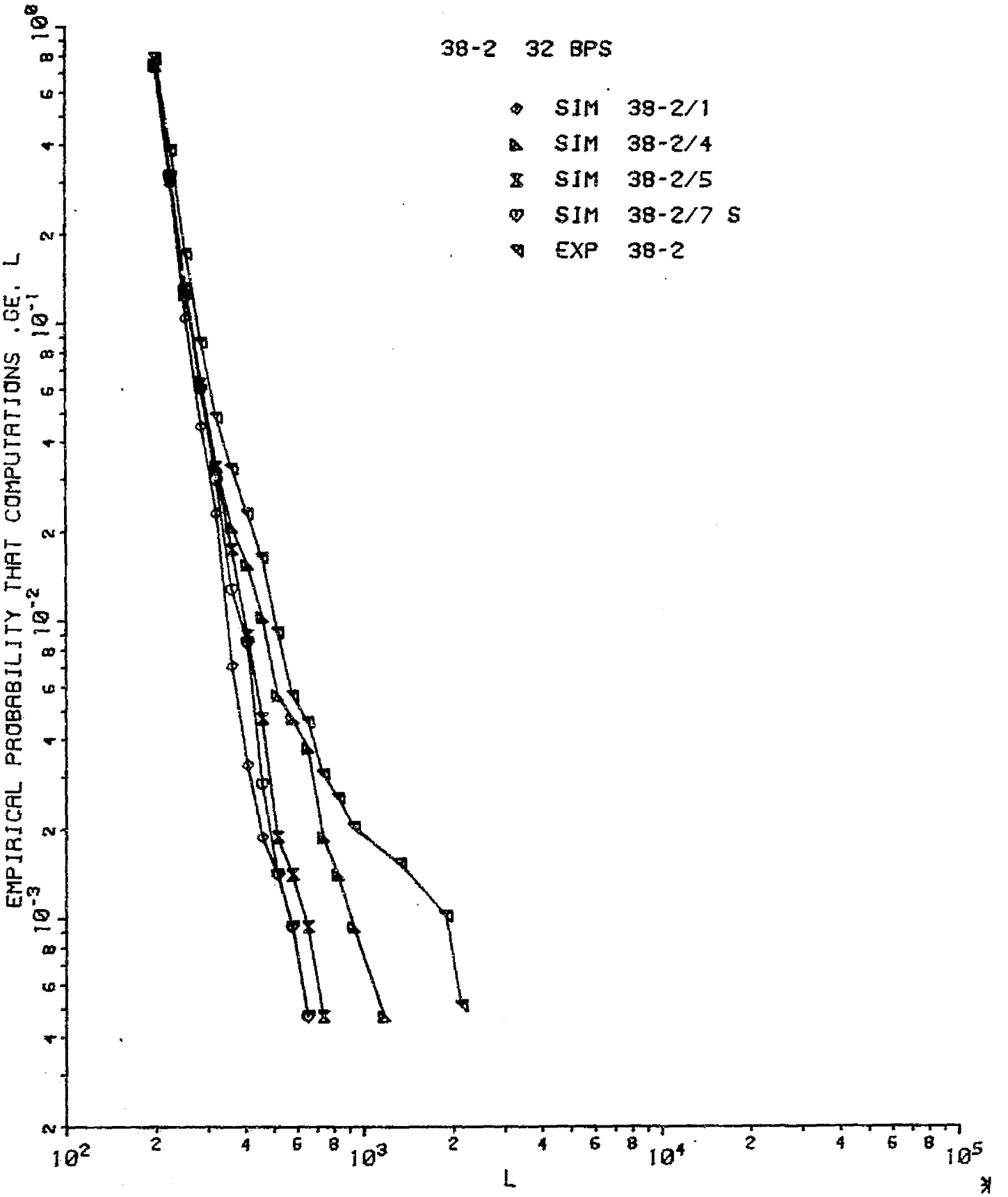

SEQUENTIAL DECODING COMPUTATION DISTRIBUTION

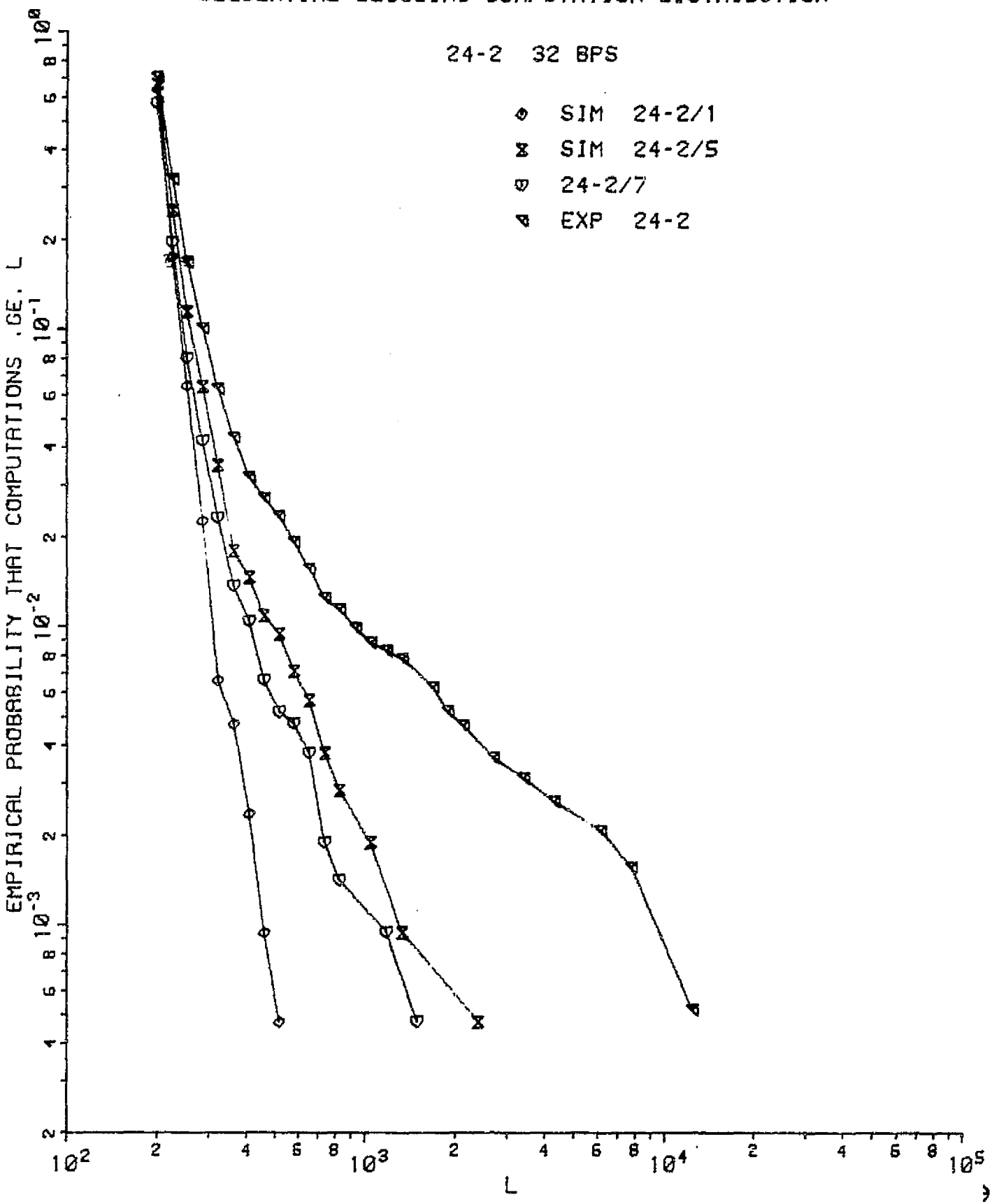

SEQUENTIAL DECODING COMPUTATION DISTRIBUTION

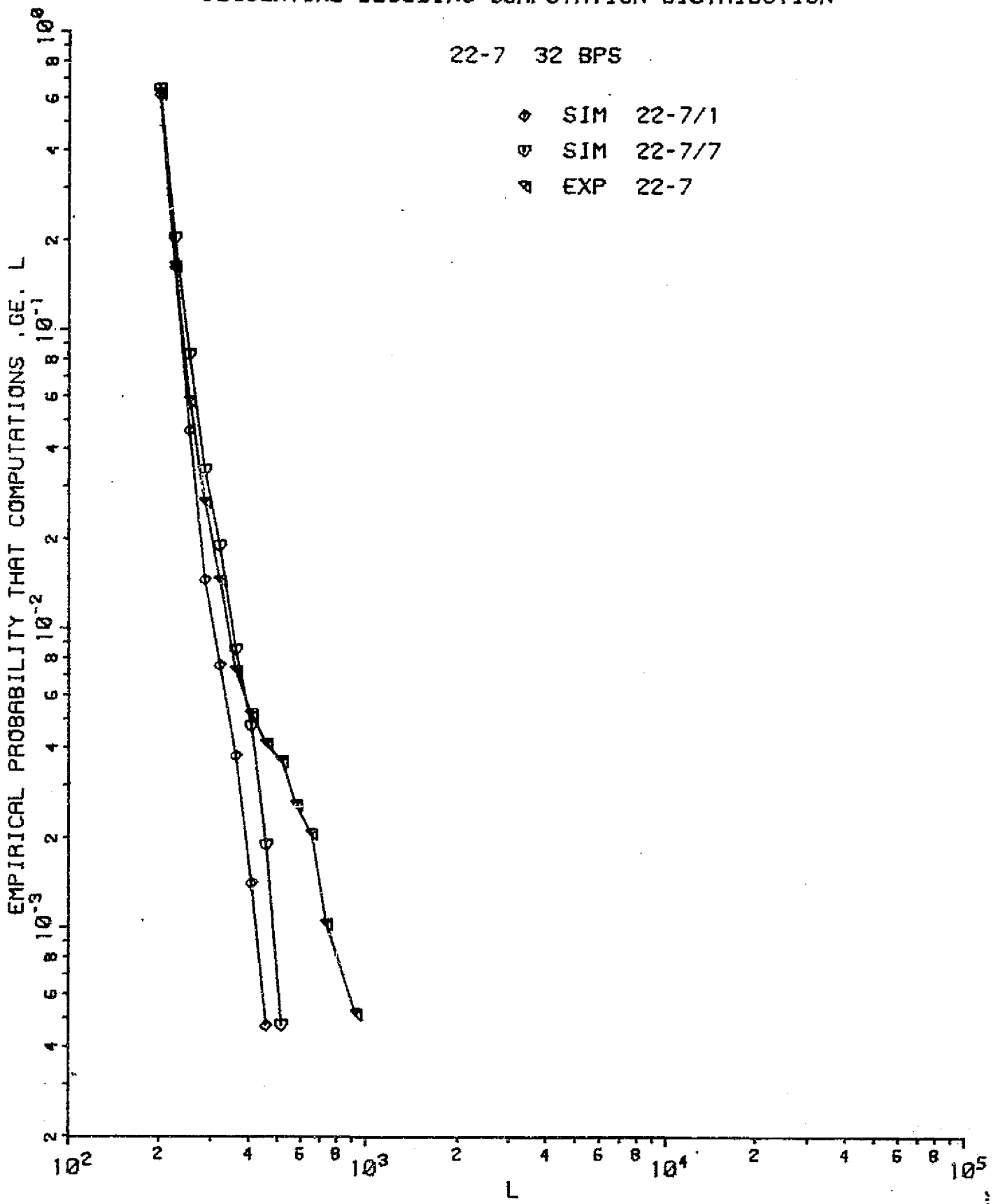

SEQUENTIAL DECODING COMPUTATION DISTRIBUTION

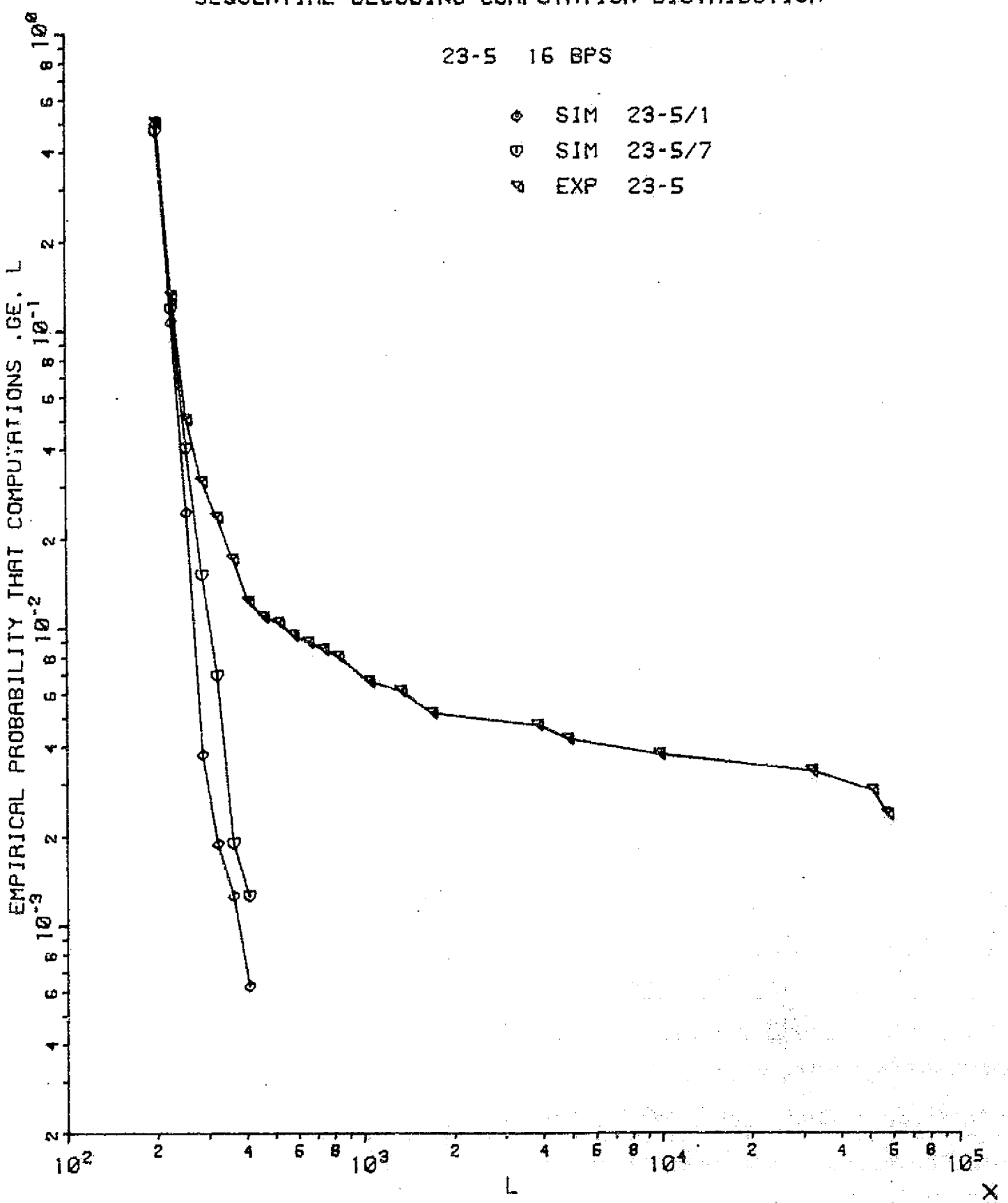

SEQUENTIAL DECODING COMPUTATION DISTRIBUTION

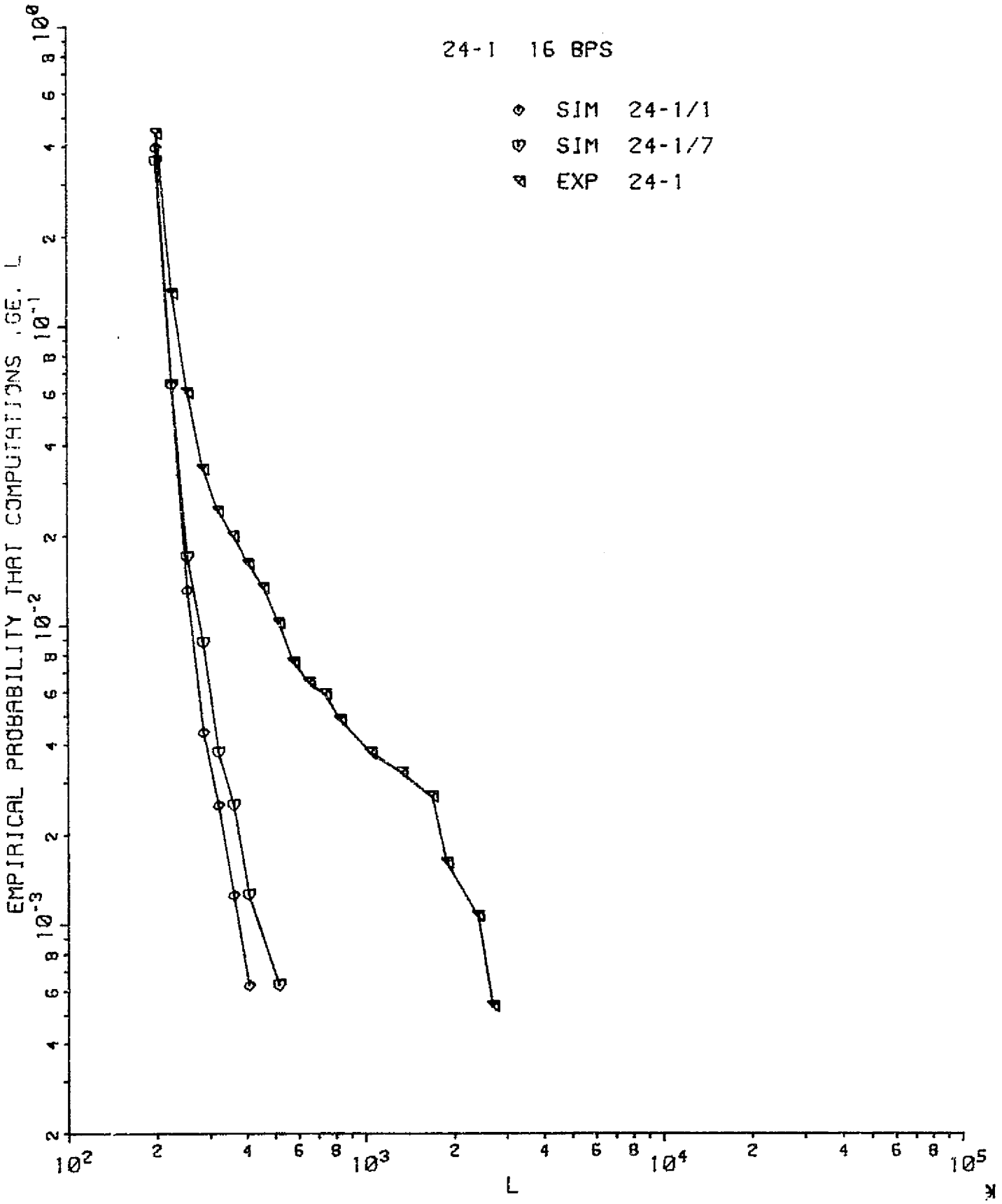

SEQUENTIAL DECODING COMPUTATION DISTRIBUTION

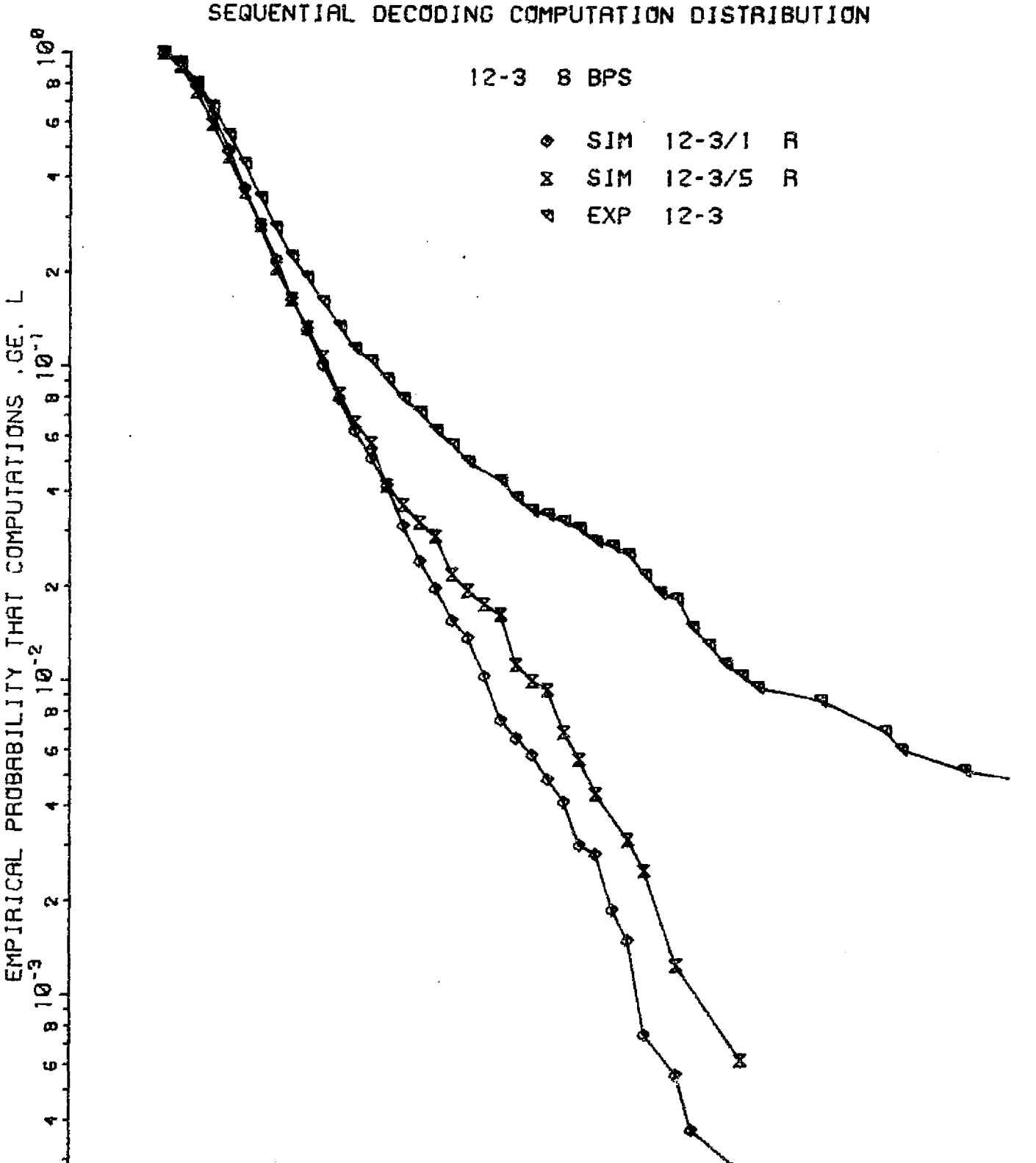

*

SEQUENTIAL DECODING COMPUTATION DISTRIBUTION

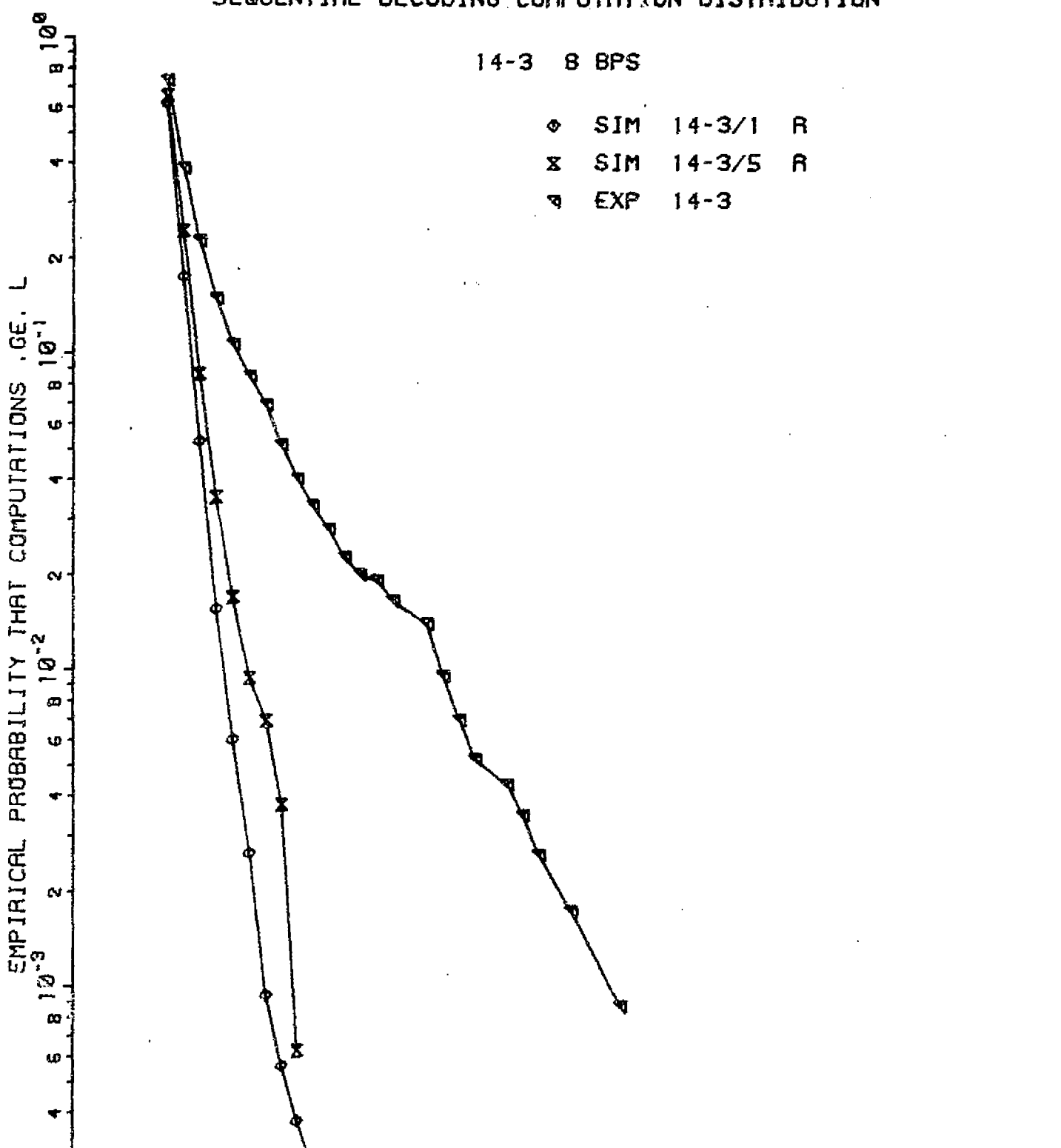

SEQUENTIAL DECODING COMPUTATION DISTRIBUTION

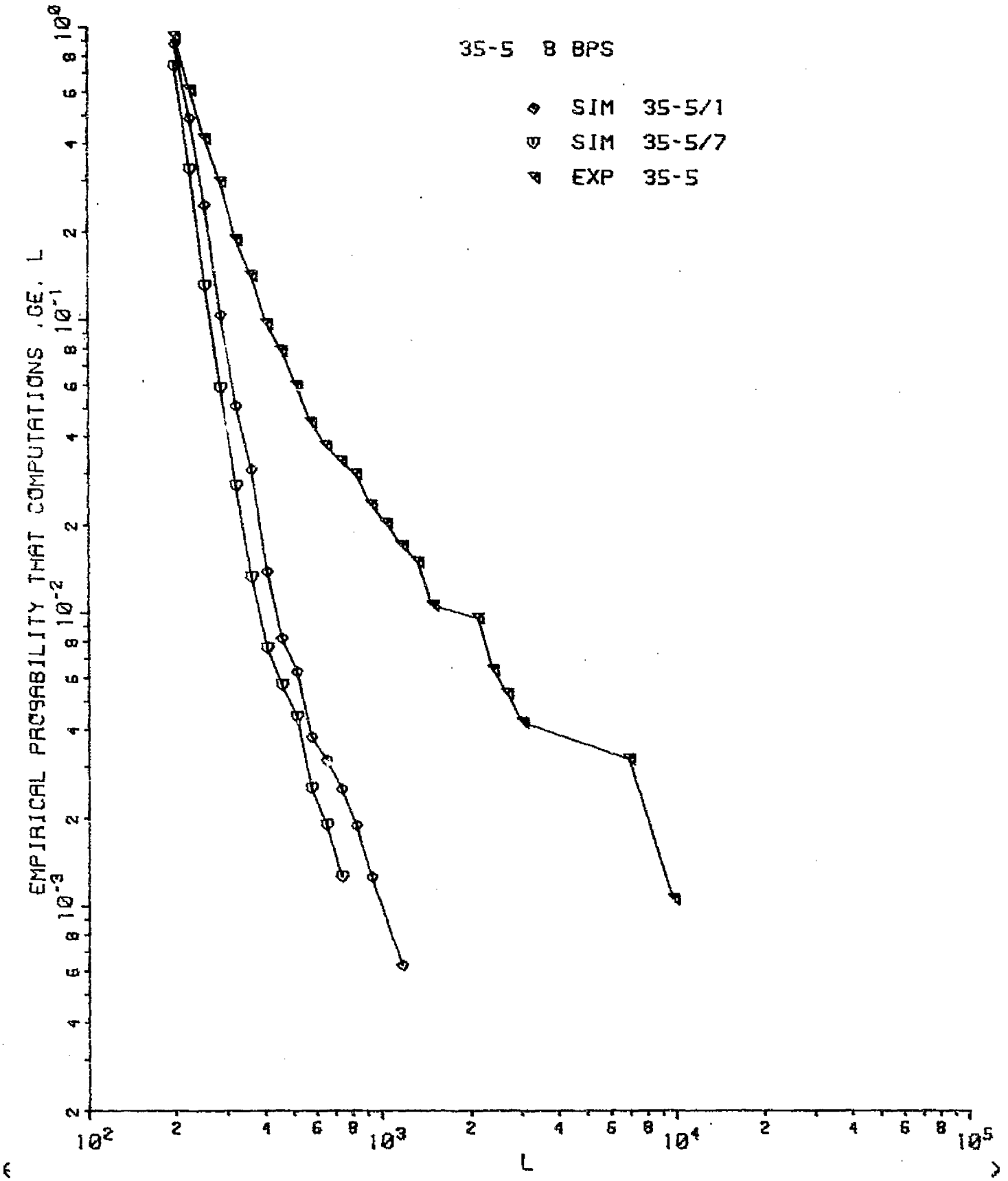

APPENDIX D

This appendix contains special graphs referred to in the test.

SEQUENTIAL DECODING COMPUTATION DISTRIBUTION

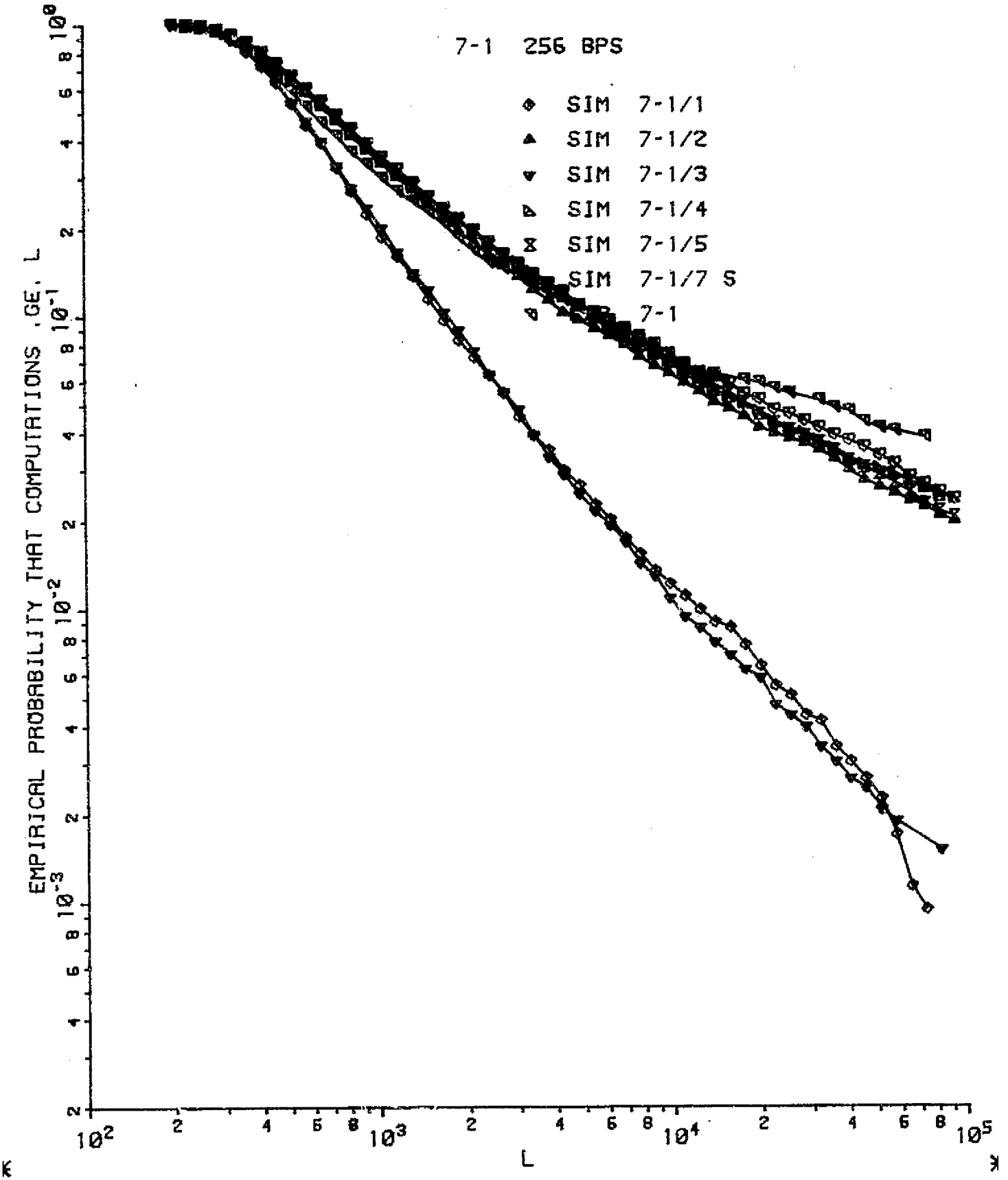

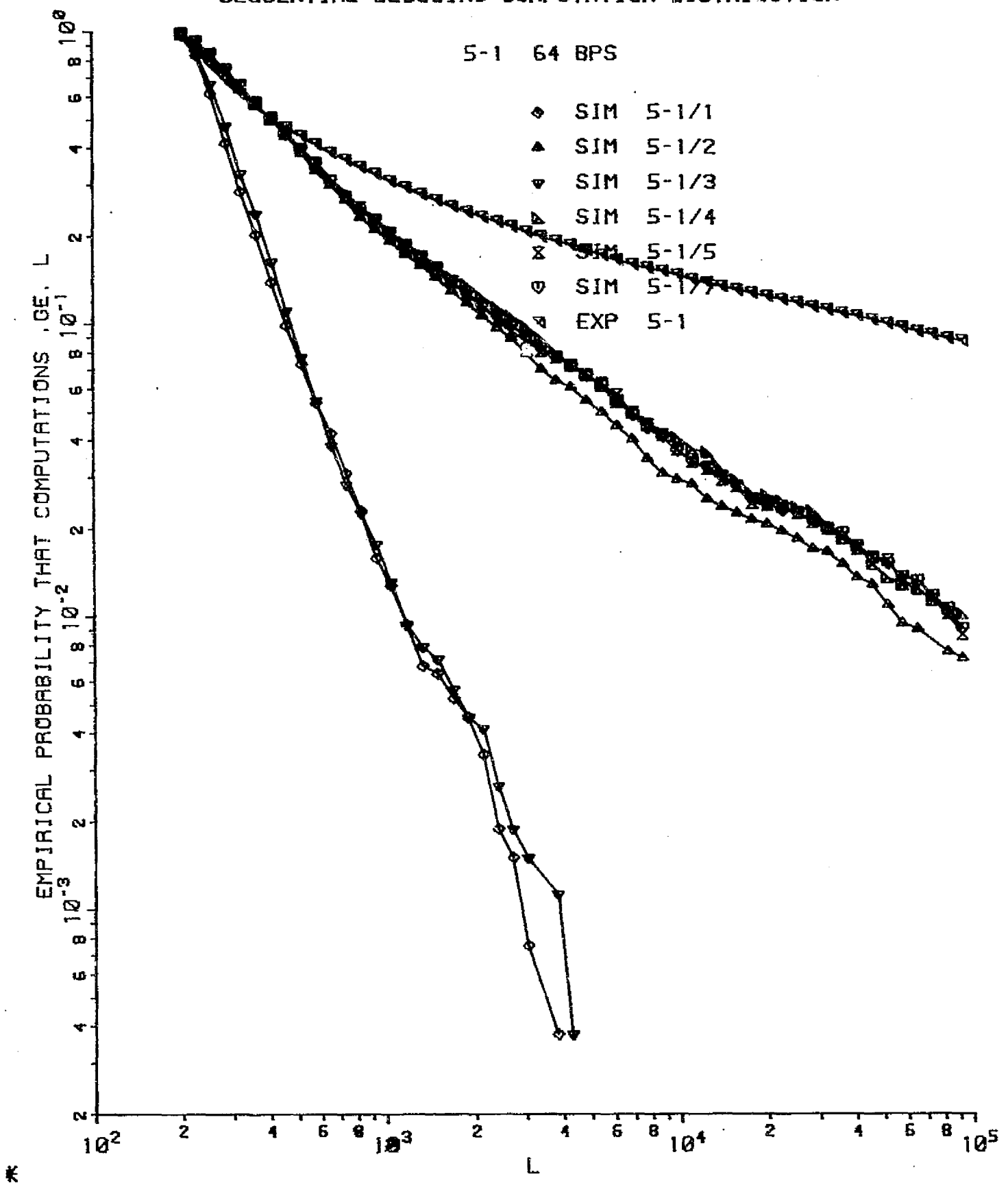
SEQUENTIAL DECODING COMPUTATION DISTRIBUTION
5-1 64 BPS
SIM 5-1/1
SIM 5-1/2
SIM 5-1/3
SIM 5-1/4
SIM 5-1/5
SIM 5-1/7
EXP 5-1
EMPIRICAL PROBABILITY THAT COMPUTATIONS .GE. L
L
10^{0}
10^{-1}
10^{-2}
10^{-3}
10^{2}
10^{3}
10^{4}
10^{5}

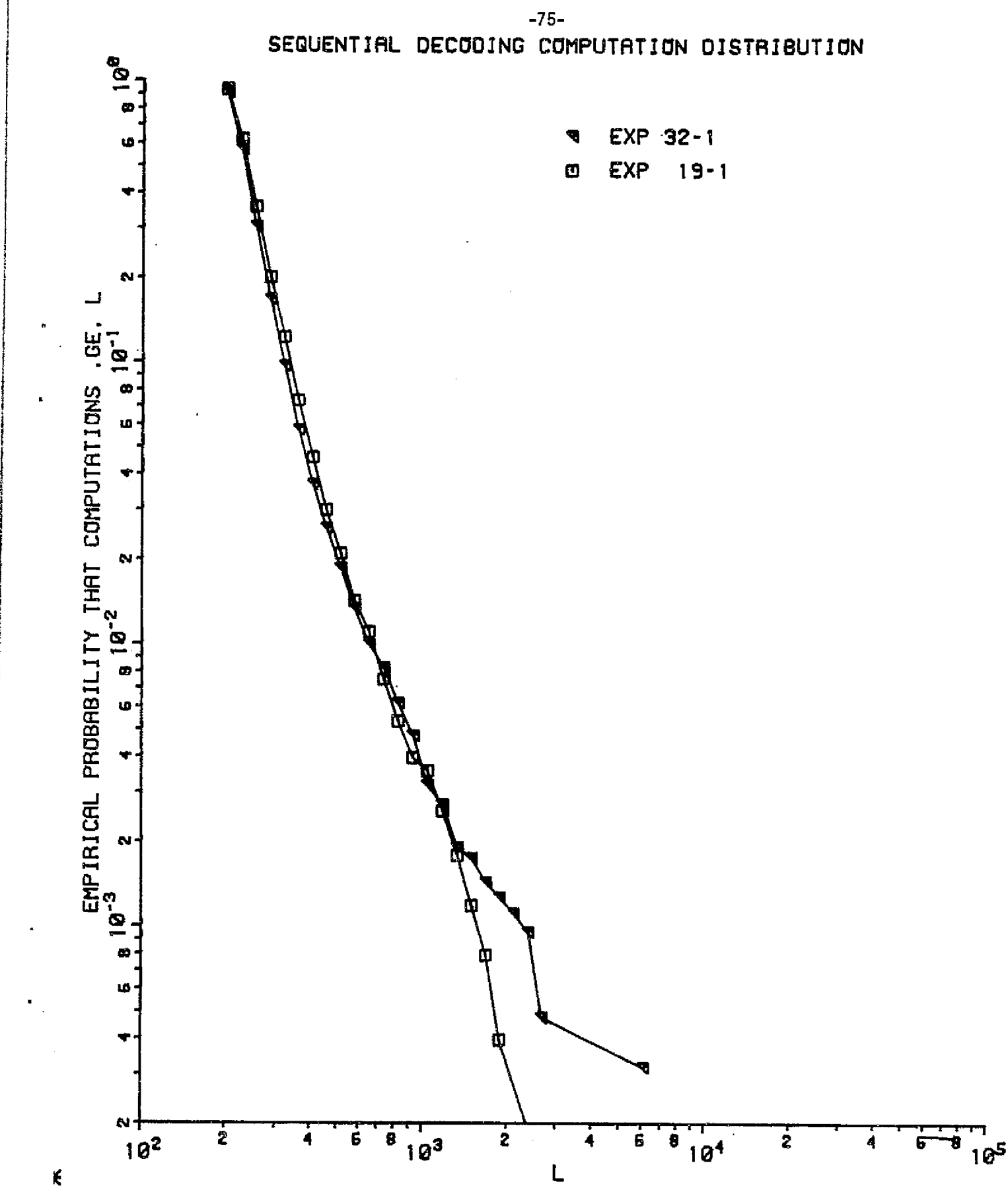
SEQUENTIAL DECODING COMPUTATION DISTRIBUTION
EXP 32-1
EXP 19-1
EMPIRICAL PROBABILITY THAT COMPUTATIONS .GE. L
L

SEQUENTIAL DECODING COMPUTATION DISTRIBUTION

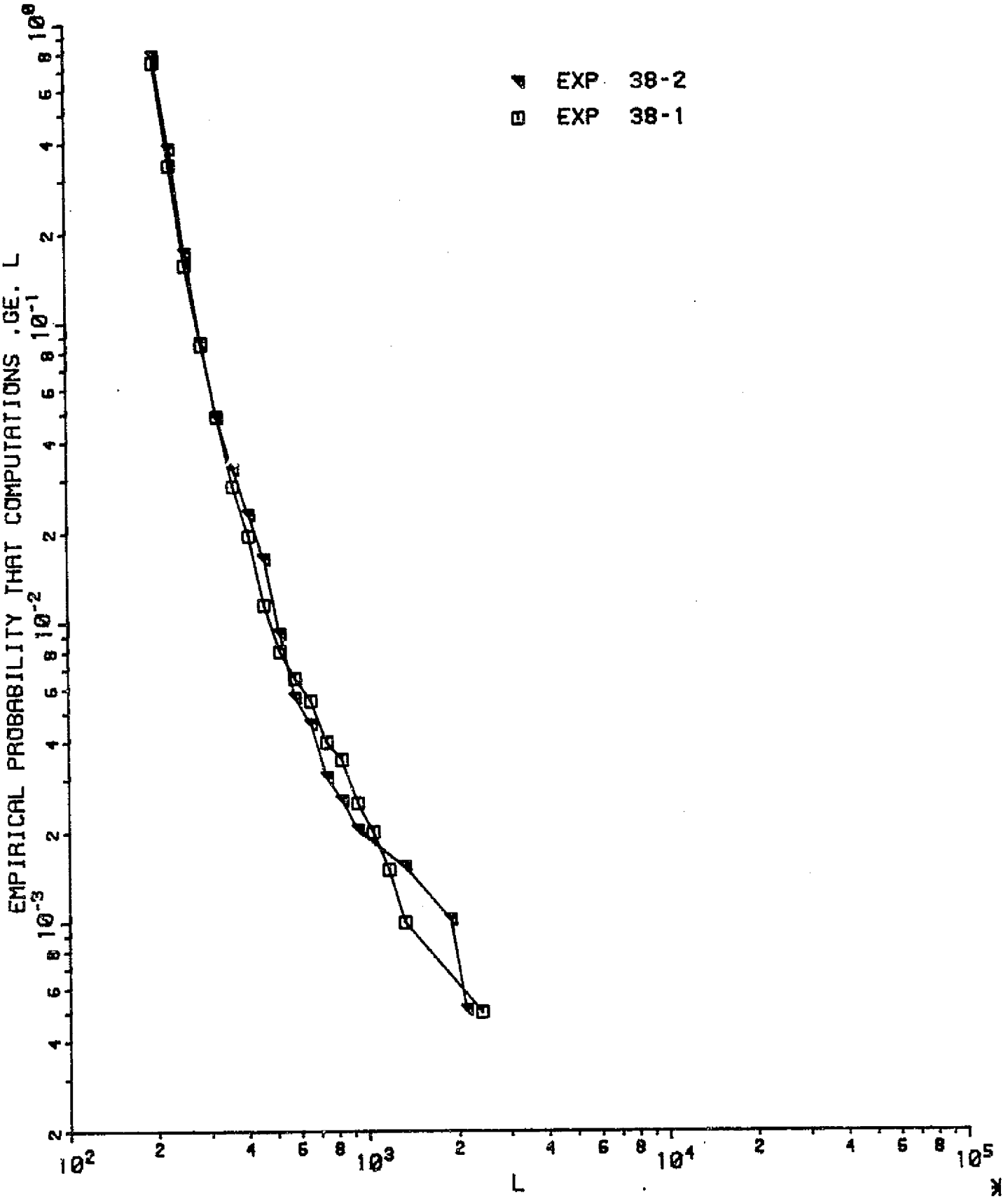

SEQUENTIAL DECODING COMPUTATION DISTRIBUTION

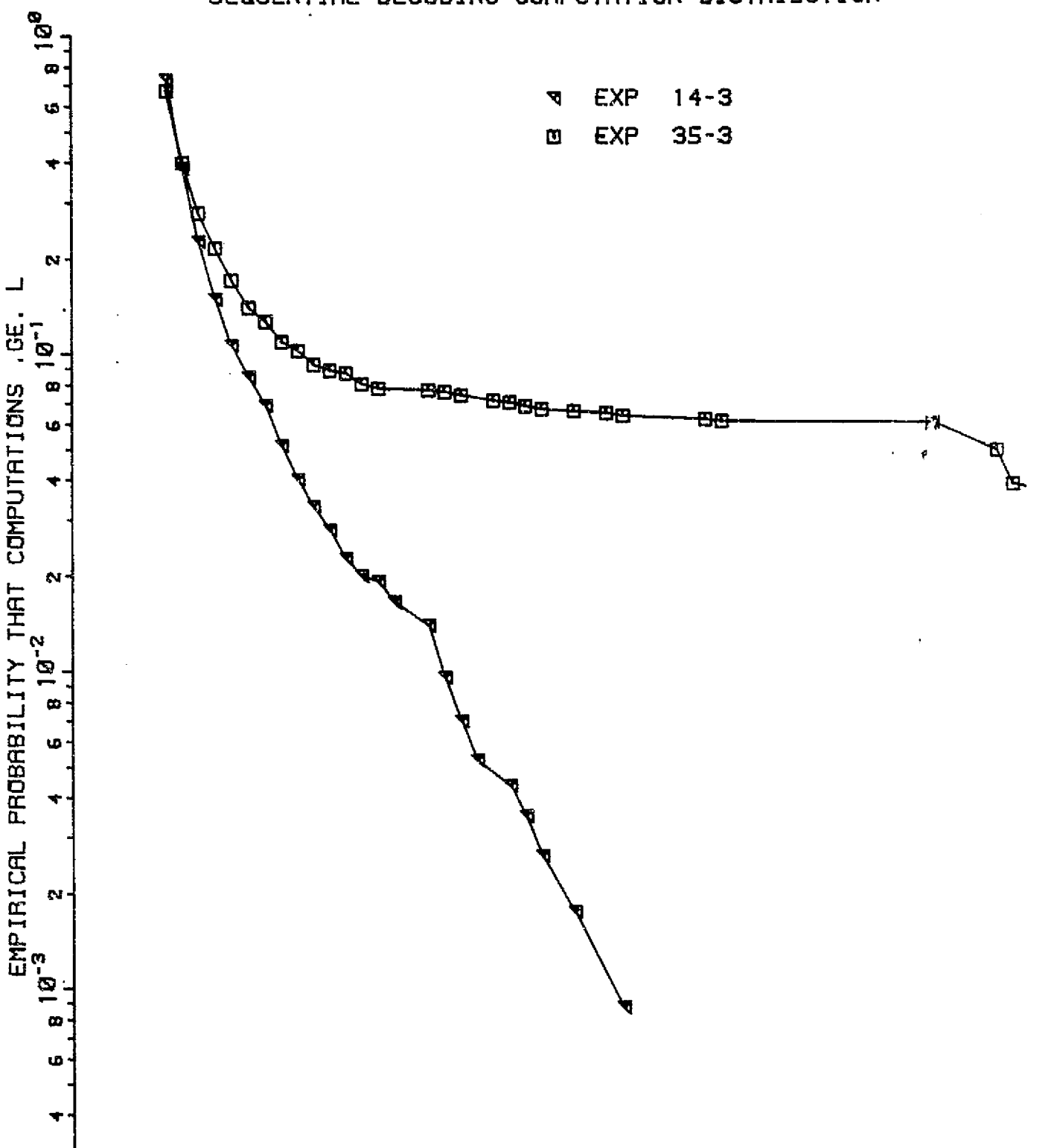

TABLE OF RUN DATA

Rate (BPS)	ID	MI	PE	E_s/N_o	$\frac{P_c}{N_o 2B_{LO}}$
1024	32-1	53	5.11	1.25	22.04
	19-1	53	5.15	1.25	21.58
32	38-2	42	4.07	1.85	11.18
	38-1	45	4.08	1.85	10.32
8	14-3	45	2.92	2.49	7.03
	35-3	45	2.99	2.45	7.03

REFERENCES

Blake, I.F., and Linsey, W.C., "Communications System Development Effects of Phase-Locked Loop Dynamics on Phase-Coherent Communications," JPL Space Programs Summary, 37-54, Vol. 3, pp. 192-5, 1968.

Brockman, M.H., "Analysis of the Subcarrier Demodulator," JPL Space Programs Summary, 37-48, Vol. II, pp. 124-9, 1967.

Brockman, M.H., "MMTS: Performance of Subcarrier Demodulator," JPL Space Programs Summary, 37-52, Vol. II, pp. 127-43, 1968.

Edelson, R.E., Telecommunication Systems Design Techniques Handbook (33-571), Pasadena: JPL, 1972.

Heller, J.A., and Jacobs, I.M., "Viterbi Decoding for Satellite and Space Communications," IEEE Trans. Comm. Tech., Vol. COM-19, pp. 835-48, 1971.

Hofman, L.B., and Lumb, D.R., "Comparison of Viterbi and Sequential Decoding with a Noisy Carrier Reference," International Telemetering Conference Proceedings, Vol. X, p. 152, 1974.

Jacobs, I.M., "Sequential Decoding for Efficient Communication from Deep Space," IEEE Trans. Comm. Tech., Vol. COM-15, pp. 492-501, 1967.

JPL Spec. DOR-1076-DSN

Layland, J.W., "A Model for Sequential Decoding Overflow Due to a Noisy Carrier Reference," International Telemetering Conference Proceedings, Vol. X, pp. 153-161, 1974.

Linsey, W.C., "Error Rates in Phase Coherent Systems with Bandpass Limiters," JPL Space Programs Summary 37-45, Vol. IV, pp. 276-83, 1964.

Linsey, W.C., "Performance of Phase Coherent Receivers Preceded by Bandpass Limiters," IEEE Trans. Comm. Tech., Vol. COM-10, pp. 245-51, 1968.

Lumb, D.R., "A Study of Codes for Deep Space Telemetry," 1967 IEEE Intl. Conv. Rec. pp. 130-6.

Taurworthe, R.C., Theory and Practical Design of Phase-Locked Receivers, Volume I, Pasadena, JPL, 1966.

Viterbi, A.J., Principles of Coherent Communications, New York: McGraw-Hill, 1966.

Wozencraft, J.M., and Jacobs, I.M., Principles of Communication Engineering, New York: Wiley, 1965.

810-5 DSN STANDARD PRACTICE, Pasadena: JPL, Rev. C, 1972, Rev. D, 1975.